Kafirin extracted via large scale production: microparticle formation, morphology and film formation

MF Da Silva

Kafirin extracted via large scale production: microparticle formation, morphology and film formation

Marcio Faria Da Silva

A thesis submitted as partial fulfilment of requirements for the degree

Master of Engineering (Chemical Engineering)

In the

Department of Chemical Engineering
Faculty of Engineering, the Built Environment and Information Technology

University of Pretoria
Pretoria

June 2016

Supervisor: Prof FJWJ Labuschagne

Kafirin extracted via large scale production: microparticle formation, morphology and film formation

Synopsis

A laboratory process exists for the extraction of kafirin protein from sorghum grain in order to form kafirin encapsulating microparticles. This laboratory process extracts approximately 2 g of protein and takes in excess of 60 hours from start to finish. A scaled-up extraction process based on the current laboratory process, consisting of a 100 L extraction vessel, was established in order to extract large volumes of kafirin protein from sorghum grain. Approximately 2.5 kg of kafirin protein, which contained approximately 80 % protein after defatting, was extracted from red sorghum grain. This blended kafirin protein, which was the product of combining 9 batches done on the up-scaled process, was needed in order to obtain a consistent base raw material for further experimentation.

The blended kafirin was used to investigate the formation of kafirin encapsulating microparticles. This was achieved by means of the solvent phase separation technique with acetic acid as the solvent phase. A series of experiments, selected from a partial factorial design, were used to screen how the formation of microparticles was affected by various parameters. The parameters investigated were solvent to protein ratio, stirring speed, water addition rate and number of water droplets. The morphology of the various microparticles produced was analysed by means of light microscopy, FTIR and particle size analysis, and the different formed microparticles characterised.

From the screening partial factorial experimental design, it was determined that the acetic acid concentration was crucial for the formation of microparticles. Microparticles did not form at a low mass ratio (2.3) of glacial acetic acid solvent to protein. Water

addition rate and stirring rate also affected microparticle formation while the number of water droplets was insignificant. Therefore, using a high solvent to protein mass ratio (6.8), additional refined partial factorial experiments were conducted. These experiments focused on the effect of water addition rate and stirring speed on the final kafirin microparticle size.

Ultimately, a polynomial model was developed to predict the final kafirin microparticle size using only the water addition rate and stirring speed as inputs. The model had an R^2 value of 0.986 and was found to relatively accurate during validation. The model also identified that three distinct regions existed within the workspace:

- A region containing large particles due to protein mass agglomeration and crosslinking, which occurs at low stirring speeds (< 400 rpm) and high water addition rates (> 5 mL/min)
- A region where only small individual microparticles exist, which occurs at high stirring speeds (< 800 rpm) and low water addition rates (> 2 mL/min)
- A region where moderate particles existed as uniform agglomerates of the microparticles, which occurs at moderate stirring speeds (± 600 rpm) and moderate water addition rates (± 3.5 mL/min)

Ultimately these kafirin microparticles, prepared from protein extracted in an up scaled process, were used to form qualitative microparticle films. The microparticle films were made without plasticiser and without dewatering the microparticles. Furthermore these films were made from microparticles in the regions identified in the model. This qualitative film formation showed that agglomerated microparticles can form films. This could be beneficial for the feasibility of a commercialised process for kafirin microparticle films since the production time would be shorter and less energy intensive.

KEYWORDS: kafirin, microparticles, particle size, polynomial model, films

Acknowledgements

I would like to thank my supervisor, Prof FJWJ Labuschagne, for his useful guidance, patience and friendship through the duration of my postgraduate studies.

I would also like to thank the Department of Food Science in the Faculty of Natural and Agricultural Sciences at the University of Pretoria for sharing your expert knowledge of kafirin with me. Specifically, to Prof John Taylor, Dr Janet Taylor, Dr Joseph Anyango and Alexandra Sly for all your effort, time and guidance.

I am thankful to Antoinette Buys from the Laboratory of Microscopy and Microanalysis at the University of Pretoria for her help with the microscopy work.

I am grateful to The National Research Foundation (NRF) for their support by means of funding.

And above all else I am grateful to my wife and family for all their love, support, compassion and encouragement.

Contents

List of Figures

List of Tables

Nomenclature

A	Generic variable example	
A_A	Absorbance at α-kafirin peak	-
A_B	Absorbance at β-kafirin peak	-
a_n	Generic constant of the nth term	
B	Generic variable example	
C	Generic variable example	
C_{AA}	Acetic acid ratio	-
C_E	Ethanol solvent ratio	-
D	Generic variable example	
DF-Red	Defatted kafirin extracted from red sorghum	
DF-White	Defatted kafirin extracted from white sorghum	
d_{10}	Particle size at 10% cumulative distribution	μm
d_{50}	Particle size at 50% cumulative distribution	μm
d_{90}	Particle size at 90% cumulative distribution	μm
ε	Relative error	μm
H	Upper limit value for partial factorial design	
L	Lower limit value for partial factorial design	
NDF-Red	Non-defatted kafirin extracted from red sorghum	
N_{PS}	Peristaltic pump setting number	-
N_{WD}	Number of water droplets	-
R_{AB}	Ratio of absorbance at the α and β peaks	-
R_{WA}	Water addition rate	mL/min
T_F	Average time taken to fill 20 mL	s
x_n	Generic parameter of the nth variable	
V_{SS}	Stirrer speed	rpm

1. Introduction

Protein microparticles are attracting a lot of interest, as they are finding potential new applications in the food and pharmaceutical industries. Kafirin is the prolamin storage protein found in sorghum and has been used to form microparticles. A novel process for the extraction and subsequent formation of kafirin microparticles has been developed by Taylor *et al* (2009$_a$). It was also shown by Taylor *et al* (2009$_b$) that these kafirin microparticles have a unique porous nature, which could potentially be exploited for the purpose of encapsulating compounds in the microparticles. The kafirin encapsulating microparticles (KEMS) are of interest for the formation of biodegradable biofilms as discussed by Gao *et al* (2005) and could potentially be a valuable product.

The current lab scale process is not only time consuming but also yields very small amounts of protein per batch. Furthermore, the consistency of this protein can vary significantly from batch to batch due to the natural variations within sorghum grain. While research exists regarding the lab scale production of kafirin microparticles and biofilms, further research into the potential up scaling of the process is required. Specifically, when considering an up scaled process, it is necessary to investigate the parameters for microparticle formation which could affect time, energy and cost. Furthermore, a consistent source of kafirin raw material is required which can be used as a basis for experimentation. Additionally, it is desirable to use any insights obtained to expand the viability of an up scaled process to subsequently consider the formation of biopolymer films.

The purpose of this study was to extract large quantities of kafirin by means of an up-scaled extraction process in order to obtain a blended raw material to be used as a basis for further investigations. The parameters for the formation of kafirin microparticles were investigated, on a lab-scale, to derive a relationship between characteristics of the final kafirin microparticle and the critical parameters identified. Ultimately, these microparticles were evaluated for the qualitative ability to form biopolymer films also on a lab-scale. The lab-scale experiments were done while

keeping the viability of a potential commercial process in mind for the production of kafirin microparticles and biofilms due to the potentially high value applications.

Thus the experiments conducted initially on an up-scaled set up are:
- ➢ The extraction of kafirin protein starting material from sorghum grain.

Subsequently the experiments conducted on a lab-scale set up are:
- ➢ The investigation of parameters for kafirin microparticle formation,
- ➢ The validation of the model derived for kafirin microparticle formation,
- ➢ The qualitative formation of biopolymer films.

The relationships derived from the subsequent experiments are limited to the lab-scale set up and should not be explicitly valid for an up-scaled set up. However, the insight obtained from these subsequent experiments could assist in developing the ultimate up-scaled process for both kafirin extraction and microparticle formation.

2. Theory

2.1. Sorghum Structure and Composition

2.1.1. Sorghum Grain

Sorghum is a type of grain (like wheat, maize and oats) which is relatively common worldwide, but is an important staple food in warmer climates and in particular in Africa. Sorghum consists predominantly of starch in addition to protein, fat, polyphenols and tannins. The sorghum grain is spherical in shape and consists of several parts as shown in Figure 1.
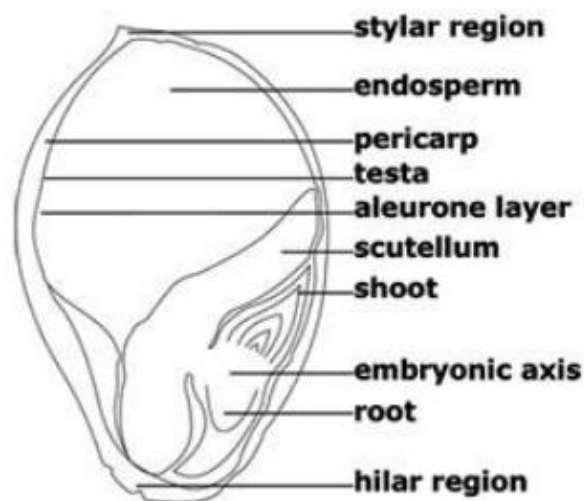
Figure 1: Sorghum grain structure (Sorghum SA, 2015)

The three major parts contributing to the sorghum grain are the pericarp, the endosperm and the germ. All of these main parts contain starch protein and fat. The endosperm contains most of the protein in the grain. The germ consists of approximately equal amounts of protein, starch and fat (Taylor, 2003).

The composition of the grain can vary substantially due to genetics (variations in cultivars) and the environment in which the crops were grown (FAO, 1995). The sorghum grain composition can be approximated for low tannin sorghum cultivars sorted by grain colour, as shown in Table 1 below (Grain SA, 2012).

Table 1: Approximate composition of various sorghum grains

Composition	Red/Brown	White	Pale Yellow
Protein (%)	9.95	9.42	10.06
Starch (%)	60.93	63.4	63.32
Fat (%)	3.32	2.82	3.35
Tannin (%)	0.35	0.16	0.23

It is important to note that as shown in the above table there are different types of sorghum grain (red, white and yellow). In this study the focus was predominantly on red sorghum and to a lesser extent white sorghum. The yellow varietal was not considered.

2.1.2. Kafirin

Kafirin is a unique type of prolamin protein specially found in sorghum grain. It is spherical in shape (similar to the grain) but the size varies depending on the specific type of sorghum cultivar (FAO, 1995). The kafirin protein is located within the starchy endosperm which, makes up about 70 % of the sorghum grain protein (Paulis & Wall, 1979 and Lending *et al*, 1988). Kafirin loses its functional properties when it denatures, which has been found to occur at a temperature of 94 °C (Mishra *et al*, 2008).

2.1.3. Protein Secondary Structure

The kafirin polypeptides are classified into three groups (α-kafirin, β-kafirin and γ-kafirin) and each group differs in solubility, molecular weight and amino acid composition (Hamaker, Mertz & Axtell, 1994). Typically, the sorghum grain is mainly comprised of the α-kafirin class (Belton *et al*, 2006). The structure of α-kafirin is a helical structure whereas the β-kafirin has a sheet like conformation. The α-kafirin and β-kafirin can be identified using Fourier transform infrared (FTIR) by means of two distinguishing peaks in the amide I and amide II bands respectively. The α-kafirin bands are located between 1650 cm^{-1} and 1658 cm^{-1} in the amide I region or between 1545 cm^{-1} and 1547 cm^{-1} in the amide II region. The β-kafirin bands are located between 1620 cm^{-1} and 1640 cm^{-1} in the amide I region or at 1524 cm^{-1} in the amide II region (Duodu *et al*, 2001). Figure 2 below shows the amide I and amide II regions as well as the peaks associated with α and β structures.
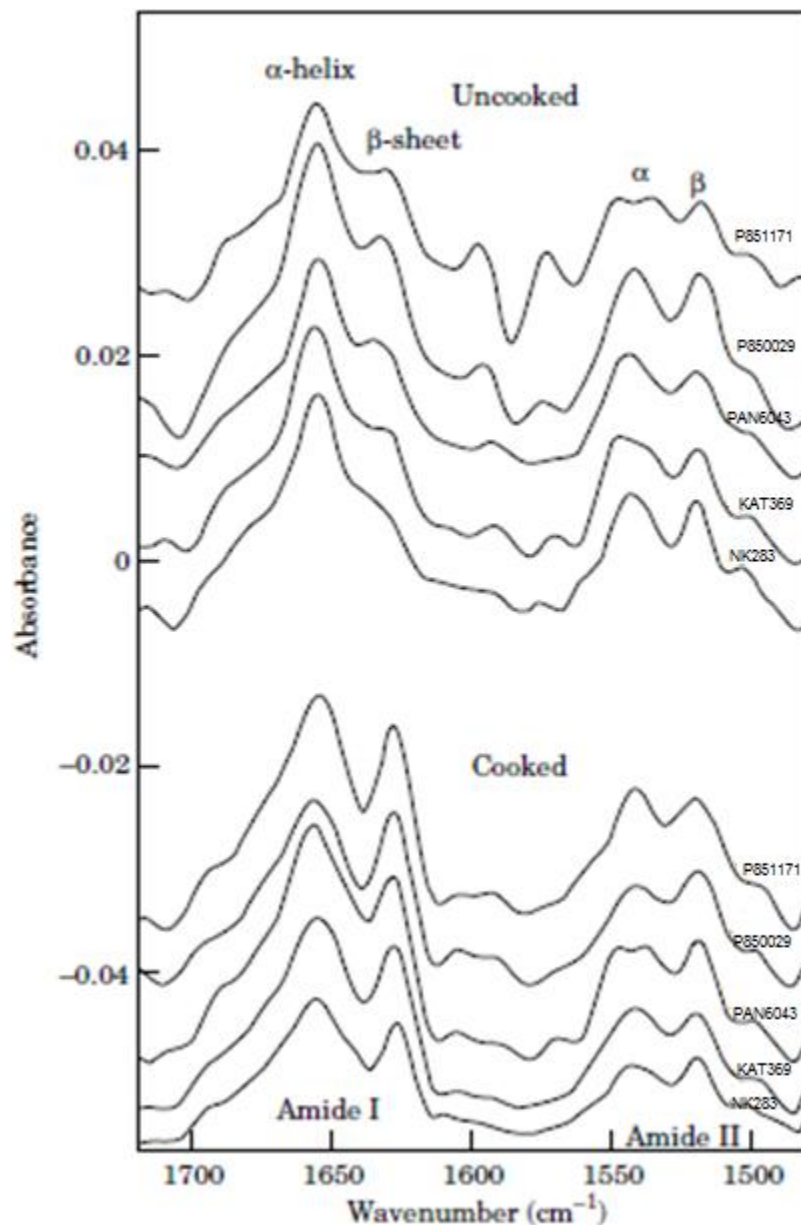
Figure 2: Fourier deconvoluted FTIR spectra of various sorghum and maize protein body preparations (Duodu et al, 2001)

Large polymer chains can occur due to the β-kafirins, which act as cross-links between the α-kafirins and γ-kafirins (El Nour, Peruffo & Curioni, 1998). Additionally, it is believed that the protein cross-linking patterns resulting from the various kafirin protein strains can be expected to impact the overall properties of the kafirin protein during processing (Belton *et al*, 2006).

The kafirin protein can contain small amounts of fat, also known as triglycerides. It is known that fats are esters comprised of fatty acid chains connected by a glycerol molecule. Thus, a convenient method of identification is to observe the strong C=O absorption frequency associated with an ester group, between 1750 cm^{-1} and 1725 cm^{-1}, in the course of FTIR analysis (Coates, 2000).

2.2. Kafirin Extraction and Microparticle Formation Process

2.2.1. Protein Extraction

Extraction involves the entire process of solubilisation, separation, isolation and recovery of a specific component from the other constituents with which it is chemically or physically in close contact (Taylor, 2003). Prolamin proteins, such as kafirin, were found to be soluble in aqueous alcohol mixtures (Osborne, 1924). Furthermore, it has been shown that absolute ethanol in the presence of sodium hydroxide and sodium metabisulfite is a particularly effective kafirin solvent (Gao *et al*, 2005). However, a study was conducted which determined the solubility of kafirin in various solvents. Nine different solvents were investigated at various temperatures and it was found that kafirin was most soluble in glacial acetic acid (25 °C - 70 °C) and lactic acid (25 °C - 70 °C) as primary solvents (Taylor *et al*, 2005). Although it is known that prolamin proteins are soluble in glacial acetic acid (Taylor *et al*, 2005), parallel studies provided significant insight into the optimisation of the kafirin extraction. It was found that that with respect to the commercialisation of the process aqueous ethanol is the preferred choice of solvent (Pienaar, 2015).

The sorghum grain is mixed well overnight with an aqueous sodium metabisulphite solution in a vessel which breaks down disulphide bonds which will improve the protein extraction from the grain. After the metabisulphite soak the mixture is filtered and the solvent (glacial acetic acid in this case) is added to the filter cake and mixed well for 48 hours in order to fully solubilise the protein from the grain. The mixture is filtered once again and the supernatant containing the solubilised protein is retained. The kafirin protein can be recovered at this point by evaporation of the solvent which causes the protein to precipitate out of solution. However, the supernatant can also be stored for the purpose of KEMS formation later (Taylor & Taylor, 2011).

2.2.2. KEM Formation Process

A novel process for formation of kafirin microparticles by phase separation from glacial acetic acid was developed (Taylor *et al*, 2009a). Thus the glacial acetic acid route has the convenience of using the same solvent for the prolamin protein extraction as well as for the formation of microparticles.

The KEMS is precipitated out of solution by slowly adding water in excess to the supernatant containing the solubilised kafirin protein. Historically the laboratory preparation of the KEMS was done using a water addition rate of 1.4 mL per minute with ample mixing. However, this laboratory process was then later progressed to use water addition rates of 100 mL per minute with 300 rpm stirring in a 20 L plastic drum set up in an attempt to speed up the process. It is important to note that the addition of water to the solution at a slow, constant rate causes the formation and precipitation of kafirin microparticles from the solution. During the course of this work the water addition rate and stirring rate were identified as critical factors in the formation of kafirin microparticles (Taylor & Taylor, 2011). Furthermore, the solvent to protein ratio used was also identified as a critical factor for the formation of kafirin encapsulating microparticles (Taylor *et al*, 2009a).

2.2.3. Dewatering of KEMS

After the KEMS are formed it may be required that these microparticles are separated (dewatered) before being used for other applications such as film forming. The current laboratory method separates the precipitated KEMS from the dilute solution by centrifugation for 5 minutes. After which the supernatant is discarded and the KEMS are washed with equal volumes of distilled water before freeze drying to obtain a dried kafirin microparticle powder (Taylor & Taylor, 2011). This dewatering process was deemed to be very intensive and not practical for large scaled production. Therefore, alternative dewatering methods were considered namely; membrane, hydrocyclone, supercritical spray tower and vacuum centrifuge techniques (Da Silva, 2012). The study found that all the alternative methods considered could be considered an improvement compared to the current centrifuge dewatering method in the context of a large scale process. The highest rated alternative method was the vacuum

centrifuge technique which should therefore be considered as the most favourable method of dewatering kafirin microparticles for commercialisation (Da Silva, 2012).

2.2.4. Summary of Extraction and KEM Formation Process

To summarise it is important to note that there are several related time consuming processes which are taken into consideration in this section. The first process is the extraction of the prolamin kafirin protein from the grain. This kafirin protein can be stored as solubilised protein in solution or it can be recovered as precipitated solid after evaporation of the solvent. The second process is the re-solubilisation of this kafirin protein and subsequent formation of kafirin encapsulating microparticles which is achieved by means of water addition to precipitate the KEMS from solution. Depending on the desired final product and intended application it may also be necessary to dewater the KEMS which have been formed. For the purpose of this work the final process is the solubilisation of kafirin encapsulating microparticles in order to form protein films.

The laboratory method of extracting kafirin and the subsequent preparation of KEMS is an extremely time consuming process which can easily take in excess of 60 hours from start to finish. Furthermore the absolute quantity of protein extracted from the lab scale process is very low, typically less than 2 g per batch. The process flow for the glacial acetic acid extraction and microparticle formation route is outlined in Figure 3 below (Taylor & Taylor, 2011). Please note that the actual quantities shown in the figure can be variable depending not only on the intended batch size but also the moisture content in the grain.
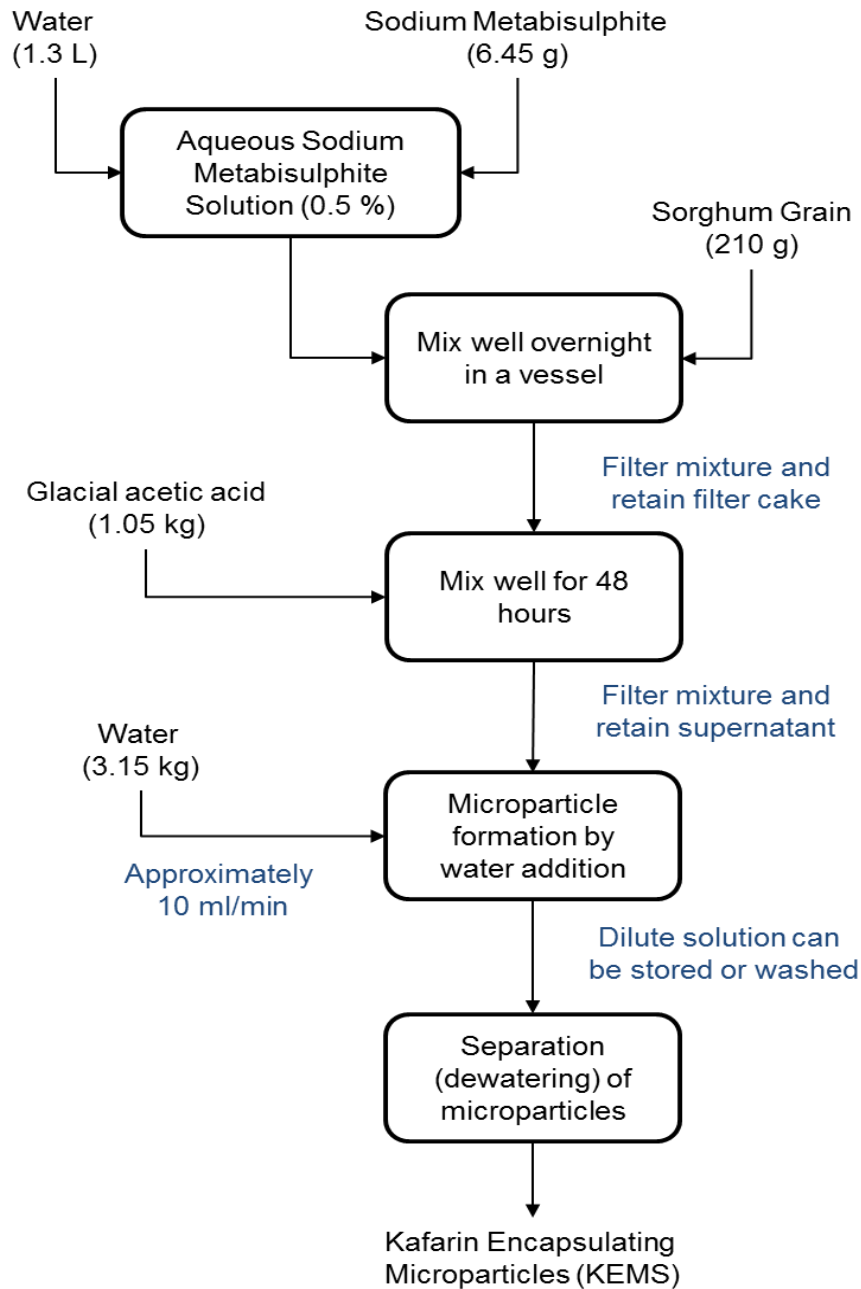
Figure 3: Overview of the kafirin microparticle formation process
(Taylor & Taylor, 2011)

2.3. Film Formation Mechanics

The process for the preparation of kafirin protein microparticle films by phase separation from glacial acetic acid is described thoroughly by Taylor *et al* (2009c). Although an intricate relation exists between protein and acetic acid concentration, it

was found that in general films seem to improve with higher acetic acid concentration. Below a critical concentration no films formed. (Taylor *et al,* 2009c)

The protein secondary structure can be indicative of a change in the protein particle formation. For example, the presence of the β-sheet structure can be indicative of protein agglomeration (Mizutani *et al,* 2003). A number of different structures (spheres, sponges and lamellae) have been identified while studying the amphiphilic nature of another similar prolamin protein zein (Wang, Yin & Padua, 2008). Additional studies concluded that the sphere structures were the base of all other microphases and the formation of these occurs by means of evaporation induced self-assembly as a result of β-sheet orientation as shown in Figure 4 (Wang & Padua, 2012).
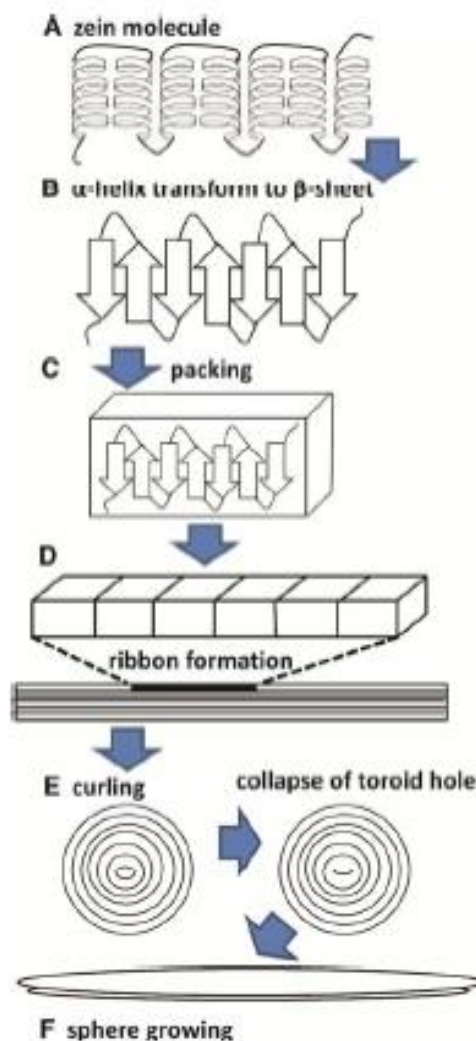
Figure 4: Model for the self-assembly of zein molecules into nanostructures (redrawn by Taylor, Anyango and Taylor 2013).

2.4. Design of Experiments

Experiments containing multiple parameters can be inherently complex and time consuming to investigate thoroughly. Therefore, a strategic approach must be followed in order to fully understand and learn how systems and processes work (Montgomery, 2013).

2.4.1. Full and Partial Factorial Design

A full factorial design experiment evaluates all possible combinations of each parameter at all the levels being considered. Therefore, if parameters at two levels (high and low) are considered, the total amount of experiments required to fully describe the system would be 2^n, where n is the number of parameters. Thus, considering three parameters at two levels would require a total of eight experiments. (Montgomery, 2013)

The effect of a factor is defined to be the change in response produced by a change in the level of the factor. Therefore, the main effect is considered to be the average of the responses obtained at the high level subtracted from the average of the responses obtained at a low level. Figure 5 below illustrates the results of an example of a two level experiment with two parameters, *A* and *B*, respectively. The average response for *A* and *B* is shown below in Equation 1 and 2. (Montgomery, 2013)
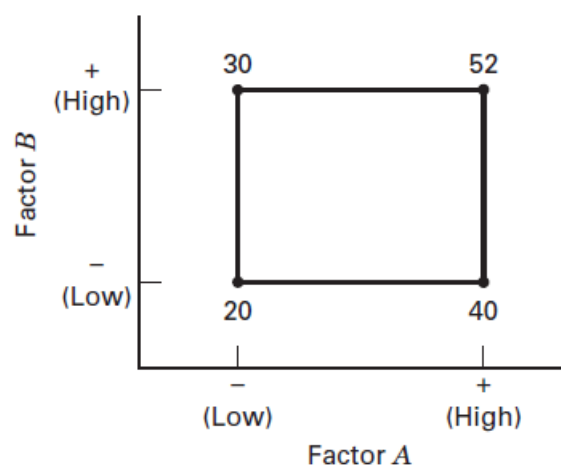
Figure 5: Two-factor factorial experiment, with response shown (Montgomery, 2013)

$$A = \frac{40 + 52}{2} - \frac{20 + 30}{2} = 21 \qquad (1)$$

$$B = \frac{30 + 52}{2} - \frac{20 + 40}{2} = 11 \qquad (2)$$

In complex systems containing numerous parameters a fractional or partial factorial design approach can be used instead of using the full factorial design. Only a fraction of the full factorial experiments is required if it can reasonably be assumed that high order interactions between the variables are negligible. These partial factorial designs are used vastly for product and process design, process improvements and industrial experimentation. This is particularly true for screening experiments in which many factors are considered and the objective is to identify factors which have large effects. The successful use of partial factorial designs is reliant on three key ideas namely; the sparsity of effects principle, the projection property and sequential experimentation. (Montgomery, 2013)

The one-half partial factorial design implies that only half the amount of experiments in a full factorial design are required. Thus, for four parameters considered at two levels only 8 experiments are required instead of 16 experiments. This can be accomplished by means of a 4 x 8 orthogonal array, as shown below in Table 2. The *H* and *L* indicate a high and low parameter value respectively. (Montgomery, 2013)

Table 2: Generic partial factorial design orthogonal (4 x 8) array

Experiment	A	B	C	D
1	L	L	L	L
2	L	L	L	H
3	L	H	H	L
4	L	H	H	H
5	H	L	H	L
6	H	L	H	H
7	H	H	L	L
8	H	H	L	H

2.4.2. Design Space Determination

The design space or workspace is the region falling within the experimental points chosen as shown in Figure 5. Therefore, it is crucial to choose experimental points such that these points define the boundary as well as the centre point of the desired model. A particular approach of determining the workspace is called the central composite design and can be seen in Figure 6 for an experimental space containing two factors. (Montgomery, 2013)
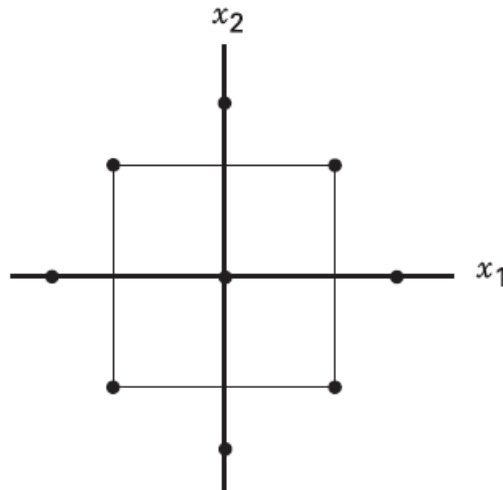
Figure 6: Two factor central composite design (Montgomery, 2013)

2.4.3. Regression Model Analysis

The parameters identified in the partial factorial design can be fitted to a model, subject to the boundary conditions chosen, by means of polynomial regression. A general polynomial expression will form the basis of the mathematical model which will undergo scrutiny by means of the ANOVA statistical analysis technique. Polynomial terms can be added or removed based on the results of the ANOVA analysis of the mathematical model. The general two variable polynomial equation, as shown in Equation 3 below, takes into account possible interaction between various core parameters. The expression can be expanded for as many variables as deemed necessary during the course of the investigations. (Montgomery, 2013)

$$f(x_1, x_2) = a_0 + a_1 x_1 + a_2 x_2 + a_3 x_1 x_2$$
$$+ a_4 x_1^2 + a_5 x_2^2 + a_6 x_1^2 x_2^2 + a_7 x_1 x_2^2 + a_8 x_1^2 x_2 \dots + \varepsilon \qquad (3)$$

When dealing with a multiple parameters repeating experiments for repeatability can become cumbersome. Thus, to reduce the amount of experiments required it can be assumed that the average error about the centre of the workspace can be used to approximate the average error for the entire workspace. This assumption can then be validated during the model validation stage. (Montgomery, 2013)

2.5. Relevant Analytical Methods

2.5.1. Protein Analysis Method

The Dumas method is used for determining the protein content in samples by determining the nitrogen content in the sample. The method entails combusting a sample of known mass in the presence of oxygen and copper (II) oxide at high temperatures. The combustion products are then passed over hot copper which converts nitrogen oxides to nitrogen dioxide. Similarly, the carbon oxides are converted to carbon dioxide. This is followed by columns containing a potassium hydroxide aqueous solution which absorb the carbon dioxide and water. Finally, a column containing a thermal conductivity detector is then used to separate the nitrogen from any residual carbon dioxide and water such that the nitrogen content can be measured and related to the protein content of the sample. (Page, 1982)

2.5.2. Particle Size Analysis Method

The laser diffraction analysis method is used to determine the particle size distribution of a sample. A laser beam is used to pass light through an object and the resulting diffraction pattern can then be related to the particle size (McCave *et al,* 1986). The relevant international governing standard for particle size analysis by means of laser diffraction methods for particle sizes ranging from approximately 0.1 µm to 3 mm is the ISO 13320:2009. This standard assumes a spherical particle shape. However, for non-spherical particles a size distribution is reported.

3. Experimental

3.1. Apparatus

3.1.1. Up-Scaled Kafirin Extraction

The purpose of protein extraction for this study is simply to obtain kafirin protein which can then be used for the microparticle investigations and film formation. Therefore, an up-scaled extraction vessel was designed and constructed based on the process, discussed in Section 2.2, in order to extract kafirin protein from sorghum grains. A schematic of the reaction vessel set can be seen below in Figure 7.
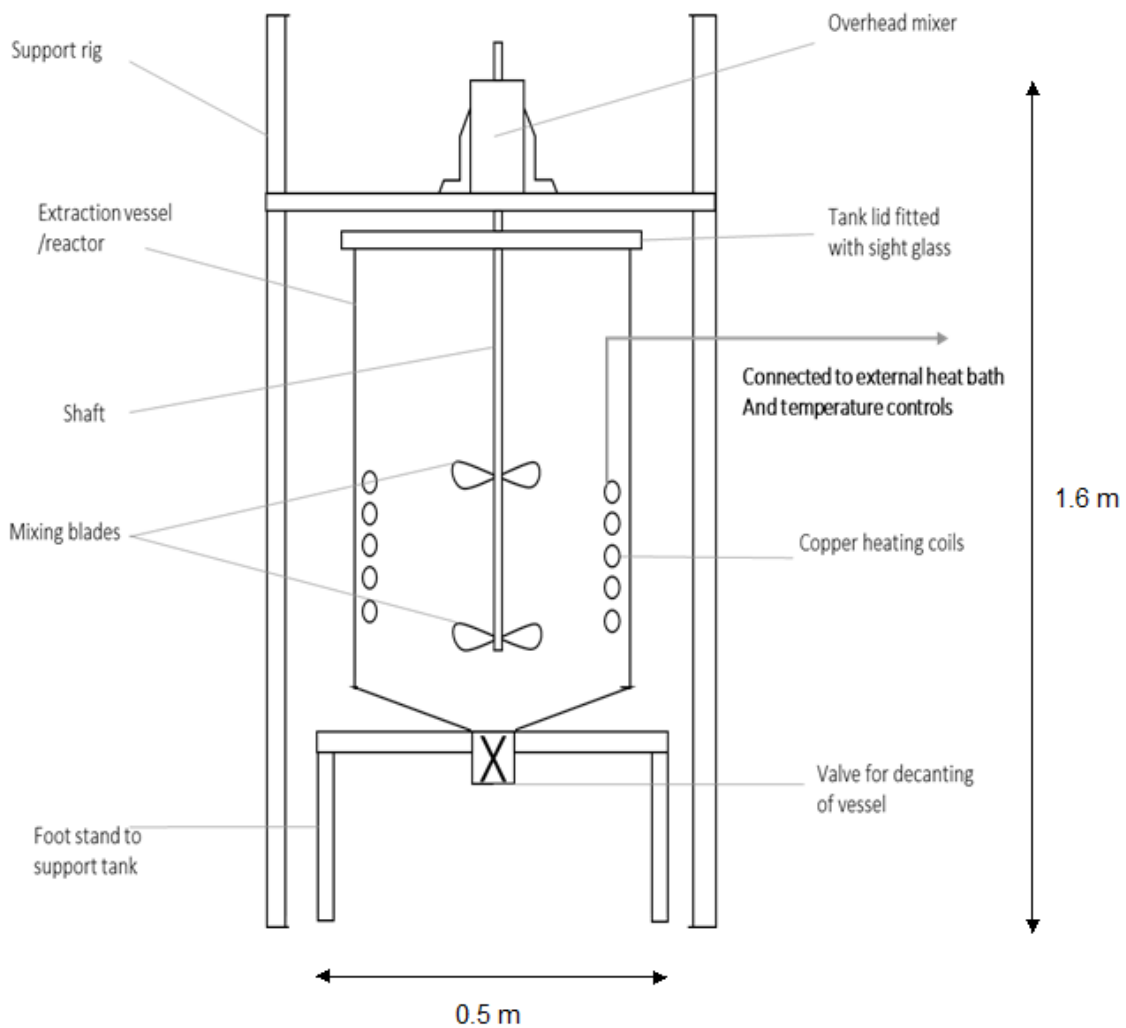
Figure 7: Schematic diagram of protein extraction vessel

This large scale set up comprised of a 100 L plastic vessel (approximately 75 L operational volume). The vessel had a sealed lid to prevent potentially harmful vapours (ethanol or acetic acid fumes) escaping the setup. Since the solvent and grain mixture results in a slurry, an overhead mixer was installed. The mixer was fitted with two mixing blades chosen to ensure good mixing conditions within the vessel namely; an impeller (mid shaft) and a high shear diffuser (shaft end). A copper heating coil (linked to a hot water bath) was fitted inside the reactor to ensure optimal temperature control, which is critical to improve the solubility of the protein while not raising the temperature to high and risk denaturing the kafirin protein.

The warm extraction slurry was then decanted out of the extraction vessel to be filtered. A Stewart and Brierley 20 L pressure filter (bomb filter) was used to separate the sorghum spent grain after extraction from the supernatant containing solubilised protein. Multiple 25 L plastic buckets with lids were used for the storage and transportation of the warm extraction slurry, filter cake and supernatant from pressure filter.

The multiple supernatant batches were combined since it was desirable to obtain a uniform singular large quantity of kafirin protein which can be blended to form a consistent raw material. The supernatant was evaporated rather than stored (Section 2.2.1) to obtain a solid kafirin raw material which could then be used for various purposes. The evaporation vessel was placed in a water bath in a room with extraction fans. A Julabo VC temperature controller was used in the water bath to keep the temperature constant at 40 °C in order to avoid the denaturation of the protein. A copper pipe air bubbler was purposefully built and inserted into the evaporation vessel to assist with speeding up the evaporation process. A schematic overview of the evaporation vessel set up can be seen below in Figure 8.
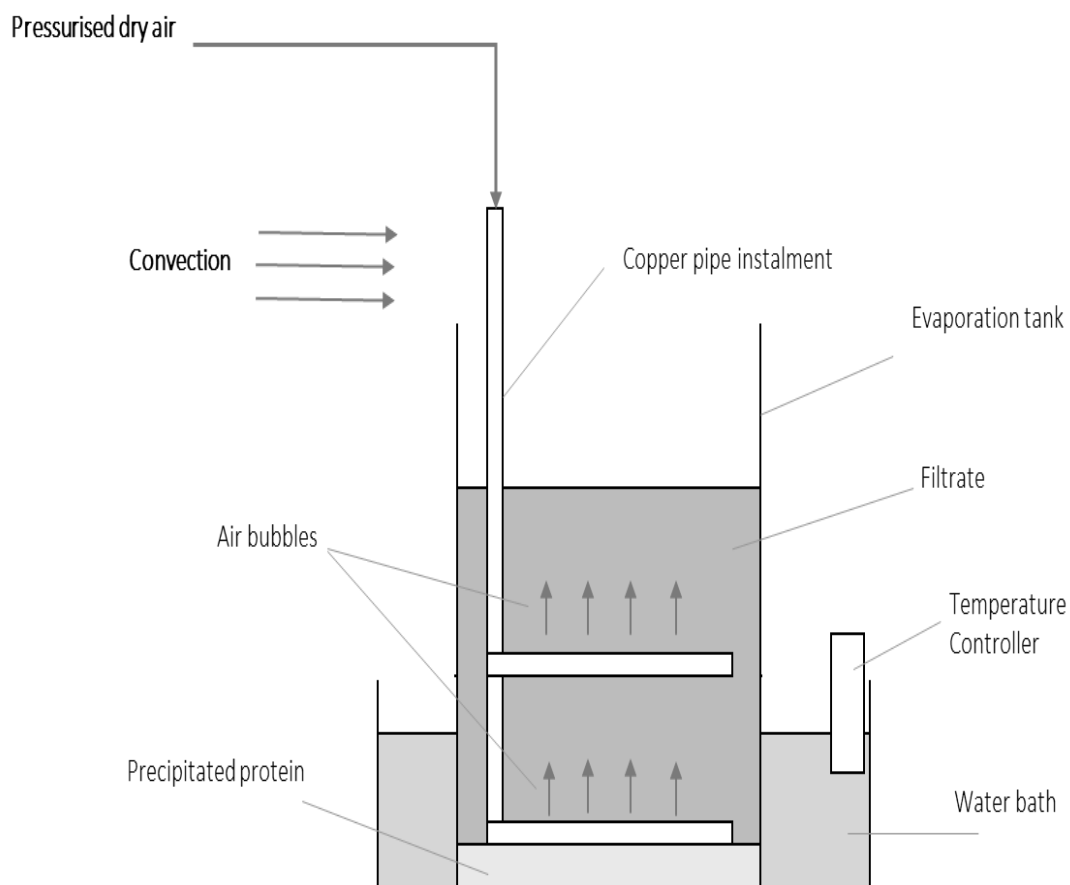
Figure 8: Schematic diagram of evaporation set up

A closed system setup of the above example was also investigated as an attempt to recover the ethanol by means of condensing the filtrate fumes in a separate unit during the evaporation process. The recovery of ethanol starting solvent could have crucial cost and sustainability implications for the large scale extraction of kafirin protein. However, the recovery system was not successful and was therefore discarded.

The extracted protein was first crushed using an IKA A11 basic electric hand mill. Before being passed through a 0.5 mm sieve on a laboratory hammer mill (falling number 3100, Hudding, Sweden), rendering a fine kafirin protein powder.

3.1.2. KEMS Investigations

The protein and solvent used for the formation of KEMS was accurately weighed using a Mettler Toledo laboratory scale. This solvent and protein mixture was then stirred in a 50 mL beaker using a magnetic stirrer rod with MS-H280- Pro Lab smart stirring plate. The water addition rate was controlled by using a laboratory Watson Marlow

peristaltic pump. The number of water droplets was achieved by attaching simple connectors to the pipe in order to provide the number of desired outlets. Samples were taken from each experiment and stored in 24 mL poly top glass vial before being analysed by means of the various analytical methods.

3.1.3. Film Formations

The film casting solutions were prepared from the same 50 mL beakers used during the KEMS investigation. The casting solution contained approximately 2.5 % kafirin, 25 % glacial acetic acid and the remainder was made up from distilled water. The solution did not contain any plasticizer however plasticizer can be added to solution if desired. Mainly, glass petri dishes (80 mm diameter) were used as the moulds for the film casting solution. However, a silicone baking tray was also occasionally used in order to obtain varying sizes and shapes. These film casting moulds were placed inside a Labotec drying oven overnight to produce films.

3.2. Analytical Methods

3.2.1. Particle Size Analysis

The particle size of the kafirin microparticles formed is a desired characteristic and therefore, particle size analysis (PSA) was done after the microparticle forming water addition step. All samples were tested wet. The particle size distributions, including the mean d_{10}, d_{50} and d_{90} sizes, for each sample were obtained using a Malvern Mastersizer 3000, with the large volume wet unit attachment. Since the apparatus can run wet samples, it was not necessary to dewater the microparticle solution. However, the solution was carefully washed with water to dilute the acetic acid concentration and prevent any potential corrosion to the equipment. In order to obtain the optimal operating conditions, of the Mastersizer 3000, test measurements were done at lower and higher rpm, with and without ultrasound as well as with and without surfactant to determine the accuracy of the readings. It was found that the ideal operating conditions for these samples are with stirrer speed set to 2000 rpm with no surfactant and no ultrasound required.

Since the particle size will be a critical characteristic for the model output, three samples were measured per experimental point in accordance with the ISO 13320 for particle size analysis. The mean particle size, d_{50}, is the most representative of the sample and therefore this value was chosen to characterise the microparticles formed.

3.2.2. Light Microscopy

Light microscopy was done on the kafirin microparticles to better understand the microparticle morphology and to confirm the particle size results obtained by means of particle size analysis. In order to ensure a representative sample was taken, each stored kafirin microparticle solution was vigorously shaken to re-suspend any larger particles. A representative sample of the solution was then extracted using a pipette and smeared onto a microscope slide. The slide was then analysed with the Zeiss V20 Discovery Stereo Microscope. The images were viewed at various magnifications; however, images of relative samples were compared at the same magnification.

3.2.3. Fourier Transform Infrared Spectroscopy (FTIR)

FTIR spectroscopy was performed to investigate the secondary structure of the kafirin protein. The analysis was performed on the initial kafirin protein samples, both non-defatted and defatted kafirin. The kafirin protein extracted from both red and white sorghum grain were both encompassed and analysed independently. Additionally, the analysis was conducted on the microparticles and agglomerated proteins corresponding to the initial kafirin protein extracted from red and white sorghum respectively. Samples were scanned in a Perkin Elmer Spectrum 100, fitted with a diamond window attenuated total reflectance (ATR) cell. The collection parameters for the apparatus were set with 32 scans from a range of 550 cm^{-1} to 4000 cm^{-1} at a resolution of 2 cm^{-1}. As described in literature, the α-kafirin and β-kafirin peaks were inspected at the relevant wavelengths (~ 1650 cm^{-1} and ~ 1620 cm^{-1} respectively). The ratio, R_{AB}, of the transmittance of these α-kafirin and β-kafirin peaks, A_A and A_B respectively, was considered (Equation 4).

$$R_{AB} = \frac{A_A}{A_B}$$

(4)

3.2.4. Dumatherm Analysis

The extracted kafirin protein was uniformly milled and dried for both defatted and non-defatted protein samples. These uniform samples were then sent for protein content and fat content analysis. The Gerdardt Dumatherm apparatus was used to determine the protein content and fat content of the extracted kafirin samples by means of the Dumas method. The method determines the nitrogen content by combusting the sample in the presence of oxygen at high temperatures and then separating the non-nitrogen based products (Page, 1982).

3.3. Experimental Planning

3.3.1. Up-Scaled Kafirin Extraction

The yield of kafirin protein extracted from sorghum grain is expected to be low. Therefore, even on an up-scaled 100 L batch process multiple batches will need to be done. For the purpose of these investigations it is estimated that approximately 1 kg of combined extracted kafirin protein will be sufficient. The average protein content in the sorghum grain is around 10 %, with a yield of 30 % on a lab scale. Therefore, it is expected that multiple batches, at least 6, will need to be done.

Ethanol is a cheaper solvent than glacial acetic acid. Thus, ethanol will be used as the extraction solvent for the up-scaled process rather than glacial acetic acid due to the volume of solvent which will be required for all the batches. Furthermore, it is not necessary to use glacial acetic acid at this point since the kafirin microparticles will only be formed at a later stage after all the kafirin raw material necessary for the experiments has been extracted.

The extraction vessel and the evaporation vessel are the same volume. However, the supernatant recovered during the filtration step is less than the total liquid volume charged to the vessel due to loss of liquids during processing. Therefore, it is expected that the supernatant from several extraction batches will be combined in the evaporation vessel before the evaporation vessel is full.

3.3.2. Preliminary KEMS Formation Investigations

To form microparticles, the extracted kafirin protein must be re-solubilised and then water addition can be done to precipitate microparticles (Section 2.2). However, the ratio of protein to solvent during extraction is low and makes a viscous mixture which is difficult to stir well. It was therefore decided to investigate if increasing the acetic acid solvent to protein ratio would assist with mixing and the resulting effect on microparticles formed.

The microparticle formation process, shown previously in Figure 3 (Section 2.2), describes that the kafirin protein must be mixed well overnight in order to fully solubilise the protein. It was therefore decided to investigate the solubility of kafirin. An attempt to determine the exact amount of time required to fully solubilise the protein is desired for considerations regarding commercialisation.

During the course of the preliminary investigations it was necessary to calibrate the peristaltic pump used during the water addition step to precipitate out the protein. This was done in order to correlate the number setting of the pump to a desired flow rate.

3.3.3. Screening Partial Factorial Experiments

From literature (Section 2.2), the critical parameters for microparticle formation were identified. In addition to these parameters, it is suspected that the droplet geometry altered by changing the number of droplets may also be of significance. This denotes that at a given water addition rate adding more droplets splits the flow resulting in smaller droplets, however the nett flow rate remains the same. All the parameters being investigated for the microparticle formation are listed in Table 3.

Table 3: Microparticle formation parameters identified

Parameter	Symbol
Acetic Acid Ratio	C_{AA}
Ethanol Ratio	C_E
Number of Water Droplets	N_{WD}
Stirrer Speed	V_{SS}
Water Addition Rate	R_{WA}

A strategic design of experiments was used to minimise the amount of experiments required to screen the effect of multiple parameters within a system (Section 2.4). Therefore, a two level partial factorial design approach was followed for the parameters shown in Table 3. Each experiment was set up by means of a 4 x 8 orthogonal array, as shown below in Table 4. The *H* and *L* indicate a high and low parameter value respectively and the values were chosen based on the values used in literature and the limitations of the apparatus used. The average response for each parameter was observed at the high and low levels respectively.

Table 4: Partial factorial design orthogonal (4 x 8) array with chosen parameters

Experiment	C_{AA}	V_{SS}	R_{WA}	N_{WD}
1	L	L	L	L
2	L	L	L	H
3	L	H	H	L
4	L	H	H	H
5	H	L	H	L
6	H	L	H	H
7	H	H	L	L
8	H	H	L	H

A reasonable difference in the average response at a high and low level is indicative of the effect of the corresponding parameter. The responses of each parameter can, therefore, be compared to determine the most relevant effects or whether the parameter is in fact relevant. The upper and lower values of each parameter were chosen, while taking into account the limitations and constraints of each individual parameter or the apparatus used. These boundary limits can be seen in Table 5 and in some scenarios when it is applicable to use a third point a reference a medium value was also used. The medium value was always taken as the halfway point between the high and the low value shown in Table 5.

The screening partial factorial set of experiments was repeated using different sources of the starting kafirin protein as well as different choices of solvent. The protein sources were defatted kafirin extracted from red sorghum, non-defatted kafirin extracted from

red sorghum and defatted kafirin extracted from white sorghum. The main solvent was glacial acetic acid however the use of ethanol as a solvent was also considered. The description of these concurrent sets of screening partial factorial experiments can be seen in Table 6 below. Each set of experiments contained their own comparable subset of experiments, defined by the orthogonal (4 x 8) array, and therefore a total of 32 screening experiments were conducted.

Table 5: High and low parameter values for initial partial factorial designs

Symbol	Parameter Description	High Value (*H*)	Low Value (*L*)
C_{AA}	*Acetic Acid Ratio	6.8	2.3
C_E	Ethanol Ratio	6.8	2.3
N_{WD}	Number of Water Droplets	4 droplets	1 droplet
V_{SS}	Stirrer Speed	80 rpm	500 rpm
R_{WA}	Water Addition Rate	2.5 mL/min	66.7 mL/min

Solvent to protein ratio. The value prescribed in literature is the low value

Table 6: Sets of screening partial factorial experiments

Set	Protein Source Description	Solvent
1	Defatted kafirin extracted from red sorghum (*DF-Red*)	Glacial Acetic Acid
2	Non-defatted kafirin extracted from red sorghum (*NDF-Red*)	Glacial Acetic Acid
3	Defatted kafirin extracted from white sorghum (*DF-White*)	Glacial Acetic Acid
4	Defatted kafirin extracted from red sorghum (*DF-Red*)	Ethanol

3.3.3. Protein Secondary Structure Experiments

The secondary structure of kafirin protein can play a crucial role in microparticle and film formation (Section 2.3). It was therefore decided to investigate the protein secondary structure of the three main protein starting materials, namely; defatted

protein extracted from red sorghum, non-defatted protein extracted from red sorghum and defatted protein extracted from white sorghum by means of FTIR.

The secondary structure of the processed protein which had been precipitated after the water addition step for each of these protein sources was also investigated in order to determine if the protein secondary had changed during processing.

3.3.4. Model Development Experiments

Ideally, the design of experiments approach was used to develop a model based on the relevant input parameters which had been identified during the screening partial factorial experiments (Section 2.4). Depending on the outcome of the screening partial factorial experiments some parameters which are deemed to play a relatively insignificant role may be discarded and further factorial experiments done which are focused on the actual relevant parameters. Ultimately, the refined factorial experiments can be used to develop a model which will be able to predict the final microparticle size as a function the actual relevant parameters.

Any potential iterations will, therefore, be highlighted and the parameters will be adjusted accordingly. The boundary conditions will be re-evaluated and the partial factorial design repeated (as necessary) to obtain a practical relationship by means of ANOVA statistical analysis and a regression model described by Equation 3.

It is important to choose experimental points such that the points define the boundary as well as the centre point of the desired model workspace. It was therefore necessary to investigate the boundary conditions in order to ensure that the actual model workspace is for a valid region where microparticles are being formed and protein mass agglomeration is not occurring. Therefore, the boundary points are determined by starting at the most favourable conditions for microparticle formation and varying only one parameter at a time to determine where protein mass agglomeration occurs.

Since the nature of the model is expected to be complex and may contain curvature, additional experimental points were necessary for the purpose of model development. The first set of supplementary points were chosen approximately halfway between the

respective boundary limits and, thus, help to outline the boundary conditions. The subsequent set of points were to help identify if any curvature may be present and were chosen approximately in the middle of the quadrants formed by the boundary conditions and the centre point. Choosing the experimental points in this manner means that there are three points keeping first parameter constant, while the second parameter varies. Similarly, there were three points keeping parameter two constant while parameter one varies. The graphical interpretation of the points will be able to determine if curvature is present and thus guide the choice of parameters used in the regression model for fitting.

The protein microparticles were precipitated out of solution based on the experimental points identified. The resulting microparticle size were determined by means of laser diffraction and light microscopy. As per the literature (Section 2.4) each experimental point was conducted once and only the centre point experiment was repeated three times in order to determine an average error for the entire workspace.

Ultimately, a final model was fitted using the resulting data from the series of experiments identified in the workspace. This was done using ANOVA statistical analysis in conjunction with the regression model described by Equation 3. An iteration procedure was necessary whereby the terms in the regression model were altered depending on the statistical relevance determined from the ANOVA analysis.

3.3.5. Model Validation Experiments

Once the final model was developed it was necessary to validate the model. The validation process can verify if the assumption to use only the average standard error about the centre point, was sufficient (Section 2.5). Therefore, for the purpose of model validation, additional experimental points were chosen within the workspace which were not the same as the experimental points used for the development of the model. The kafirin microparticles are the intended product of interest while mass protein agglomeration is an undesirable product. Thus, only relevant validation points were chosen predominantly in the microparticle region taking care to avoid areas where mass protein agglomeration may be present.

If the model could not be validated, the model development would be revisited and the iteration process repeated in order to refine the model. If necessary additional experimental points for either the model development would be identified in order to reduce error.

3.3.6. Qualitative Film Forming Experiments

Currently, one of the main applications of kafirin microparticles is to form kafirin microparticle based films. The process of film formation requires phase separation from glacial acetic acid, which is present in dilute concentrations in the dewatering solution. It was therefore decided to attempt to make films from the various sizes of microparticles produced from the kafirin extracted from the large scaled process. Further investigation was conducted to determine the necessity of dewatering the kafirin microparticles prior to the film forming process step, while keeping in mind the potential commercialisation of a scaled up process.

It was also decided to attempt to form films from some of the microparticles produced within the model workspace. This was done in order to confirm, qualitatively, that the microparticles produced from protein extracted in a large scale set was capable of forming films. If possible it would be desirable to use the developed model in order to identify benefits for the potential commercialisation of an up scaled process.

3.4. Method

3.4.1. Up-Scaled Kafirin Extraction

An extraction solution was prepared comprising of ethanol (approximately 70 % w/w), glacial acetic acid (0.35 % w/w), and sodium metabisuplhite (0.5 % w/w) with the remainder being water. This solution was preheated in the extraction vessel to 70 ˚C. Once the target temperature had been reached, the sorghum flour (fine Mabelle® sorghum meal) was added in a ratio of 1:5 to the extraction solution. A maximum of 15 kg of sorghum flour was processed at a time, due to constraints of mixing capability and problems encountered later with the filtering process. The protein extraction process was carried out in the reactor vessel at 70 ˚C with strong stirring for 1 h, after which the extraction mixture was decanted into smaller containers. The decanted

solution was then filtered through a filter (under vacuum) and the filtrate was recovered and stored. For the purpose of this study, the filter cake (comprising mostly of starch) was discarded.

The supernatant from 3 batches of kafirin extractions were combined into the evaporation vessel which was placed in a water bath at 30 °C – 35 °C. This was done in order to avoid denaturising the protein. The evaporation caused the kafirin protein to precipitate out of solution. The bubbler also ensured gentle mixing in the tank to prevent a protein film barrier from forming on the liquid surface and hindering evaporation. The evaporation unit was left for several days until most of the solvent had evaporated off.

The precipitated chunks of kafirin protein, recovered after evaporation, were further refined before storage. The solid pieces were broken up by hand and left to dry in drying trays. All the kafirin protein extracted on the up-scaled process was ultimately combined in order to have a single consistent raw material. The dried blended protein was then further crushed into smaller more uniform particles using an electric hand mill in order to make the defatting process more efficient.

A non-polar solvent, hexane, was used to defat the kafirin protein using a 3:1 solvent to protein ratio. The defatting process was carried out at ambient temperatures for 1 h after which the hexane was removed. The defatting procedure was repeated a total of three times. After the third repetition of the defatting process, the hexane was removed and the kafirin protein was vacuum filtered and air dried overnight in a fume hood. The resultant defatted protein was then milled using a laboratory hammer mill rendering a fine kafirin protein powder. The defatting procedure was repeated as required for kafirin samples which had an unsatisfactorily high fat content. However, not all the extracted protein was defatted in order to have some non-defatted samples for investigation.

3.4.2. Sample Preparation for KEMS Formation

In order to make microparticles, the blended kafirin protein, must be completely re-solubilised in the solvent. Thus, 1.9 g of kafirin was dissolved in 4.3 g of glacial acetic acid and mixed well overnight, in order to ensure the protein was fully solubilised.

Generally, the water addition rate was set at 2 mL/min and controlled by a laboratory Watson Marlow peristaltic pump. It was necessary to calibrate the pump in order to accurately correlate the number setting on the pump to a desired flow rate.

The method for microparticle formation discussed above, was altered in accordance with the described experimental planning by changing the various parameters identified.

3.4.3. Protein Solubility Factors for KEMS Formation

As described above, re-solubilisation of the protein was left to occur overnight, ensuring that the protein was completely solubilised. However, the time taken for the protein to solubilise was also investigated to determine if processing times could be shortened. Four samples were prepared using the same general sample preparation as above while varying the solubilisation times from 1 h, 2 h, 3 h and 16 h respectively.

These mixtures of solvent with protein were highly viscous, low volume mixtures. These subsequent mixtures could be undesirable as it is difficult to mix well. Therefore, increasing the amount of solvent (acetic acid) was also investigated. It is suspected using more solvent may reduce the time required to fully solubilise the protein, taking into account better mixing conditions and more available solvent. Once again four samples were prepared using 12.9 g of glacial acetic acid, while varying the mixing times from 1 h, 2 h, 3 h and 16 h respectively.

The samples were visually inspected to determine the extent of protein solubilisation. Kafirin microparticles were formed from the above samples and analysed to determine the effect of solubilisation on kafirin microparticle characteristics.

3.4.4. Solvent Type for KEMS Formation

The primary solvent used for the sample preparations to form KEMS was glacial acetic acid. However, attempts to form microparticles from an ethanol solvent were also made. The sample preparation for microparticles formed from ethanol was carried out the same manner as the process for the glacial acetic acid solvent. The solvent to protein ratio used was the same for both the acetic acid and ethanol sample preparations.

3.4.5. Protein Type for KEMS Formation

When preparing samples, the kafirin protein source was occasionally altered. Principally, the protein used for the sample preparations was the defatted kafirin protein obtained in the up scaled extraction process from red sorghum grain (*DF*-Red). However, samples were also prepared from non-defatted kafirin extracted from the same red sorghum grain (*NDF-Red*) or defatted kafirin which was extracted from white sorghum grain (*DF-White*).

3.4.6. KEMS Film Formation

The KEMS formed using the method described can be used in order to form kafirin microparticle films. The KEMS must be completely re-solubilised in acetic acid solvent, with the remainder of the solution made up of water such that the acetic concentration in solution is above the critical point (Taylor *et al,* 2009c). Therefore 4 g of KEMS was added to 39.4 g of glacial acetic acid and 116.9 g of distilled water. Plasticiser can be added during the protein solubilisation step for improved film flexibility, if desired, however it was not added in this case (Anyango, 2013). The solution was then poured into a casting mould and left in an oven at 50 °C overnight. Once the solvent was evaporated, the film was removed from the mould carefully to avoid tearing or breaking of the film. The films were analysed qualitatively by visual inspection merely to determine if a film had been formed or not.

4. Results and Discussion

4.1. Up-Scaled Kafirin Extraction

The red sorghum flour (fine Mabelle® meal) used for the extraction of kafirin was more difficult to process when compared to the white sorghum meal tested. Duratherm analysis of the red sorghum flour, found that the raw material was of low quality and had a high fat content. It was noted that several bags of the sorghum flour showed signs of microbial infections and were discarded. However, it may be possible that some of the bags did not show such clear signs of infection and were unintentionally processed contributing to the initial low quality protein extracted. The overall yield when considering all the combined batches was 25 %.

In order to fill the evaporation tank, it was necessary to combine the filtrate from three independent kafirin extractions. The precipitated kafirin protein was then analysed and found to have a very high fat content, which was as high as 50 %. The poor protein quality was a direct consequence of using inferior quality starting material. However, this protein content varied considerably from batch to batch, due to the inconsistency of the sorghum flour used. The final purity of the blended kafirin protein was considerably increased to at least 80 %, by defatting.

The large scale extraction process was successful at extracting large quantities of prolamin proteins from sorghum grain starting material. The blended protein was the combined product from 9 extraction batches. Approximately 2.5 kg of kafirin protein, which contained approximately 80 % protein after defatting, was extracted from red sorghum grain. Approximately 0.5 kg of this kafirin protein was not defatted. The average protein content before defatting was approximately 35%.

During the protein drying step, the moist protein is typically vulnerable to microbial infections if the drying environment is not ideal. However, the kafirin protein extracted on the large scale process proved to be rather resistant to microbial infections. This may be due to the copper pipes and fittings used in the large scale process, which are not present in the laboratory-scale extractions and may act as an antimicrobial.

4.2. Initial Investigation Findings for KEMS Formation

4.2.1. KEMS Formation from Glacial Acetic Acid

The glacial acetic acid solvent to protein ratio played a significant role in the solution viscosity and thus the ease of mixing required during the protein re-solubilisation prior to the precipitation of kafirin microparticles. When more solvent was present the mixture was considerably easier to stir. Thus, an attempt to form microparticles, while varying the acetic acid ratio and using a constant stirring speed and water addition rate, was done and the resulting particle size analysis can be seen in Figure 9. The acetic acid to protein ratio for the low, medium and high values were 2.3, 4.6 and 6.8 respectively.
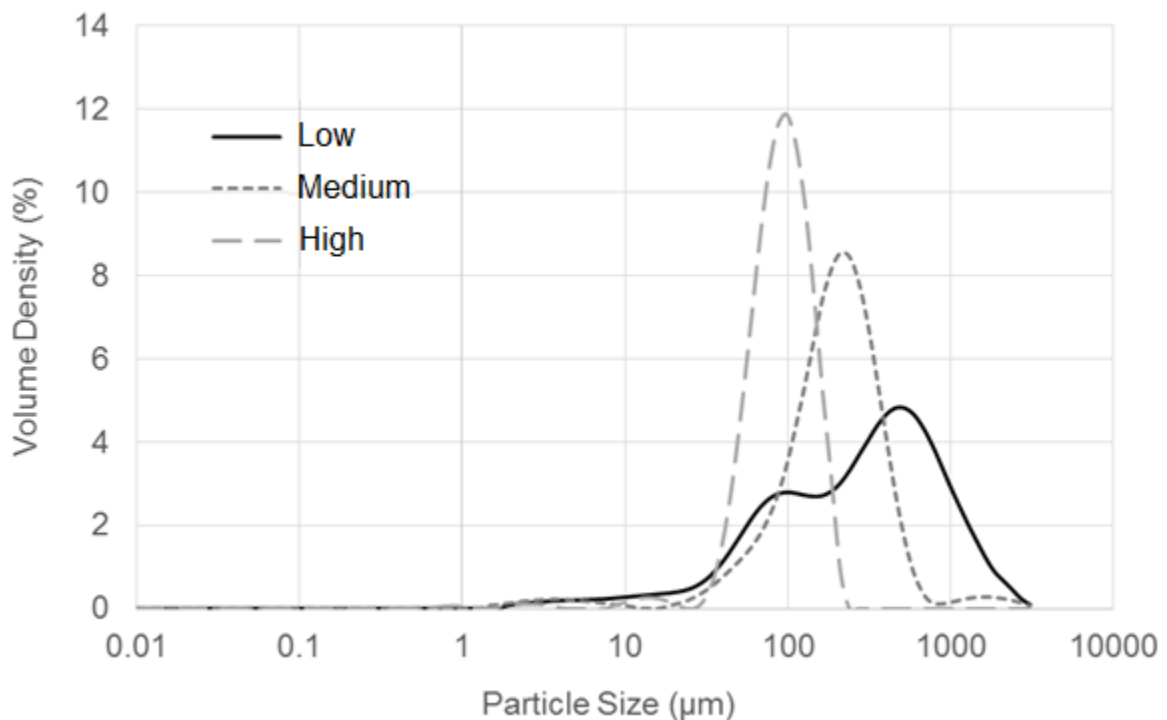
Figure 9: PSA analysis of varying acetic acid ratios

Upon inspection, it was seen that the significantly larger particle sizes were due to mass protein agglomeration and cross linking occurring at very low glacial acetic acid solvent ratios. As can be seen in Figure 9, there are very large particles (around 1 mm in size) at low and medium glacial acetic acid ratios. It was confirmed using light microscopy that these particles are aggregated, crosslinked proteins (Figure 10). As

31

the ratio of acetic acid to protein was increased, the capability to form microparticles improved significantly. Similar results were observed for non-defatted kafirin which can be viewed in Appendix A.

Low
Acetic Acid Ratio
(2.3)

Medium
Acetic Acid Ratio
(4.5)

High
Acetic Acid Ratio
(6.8)
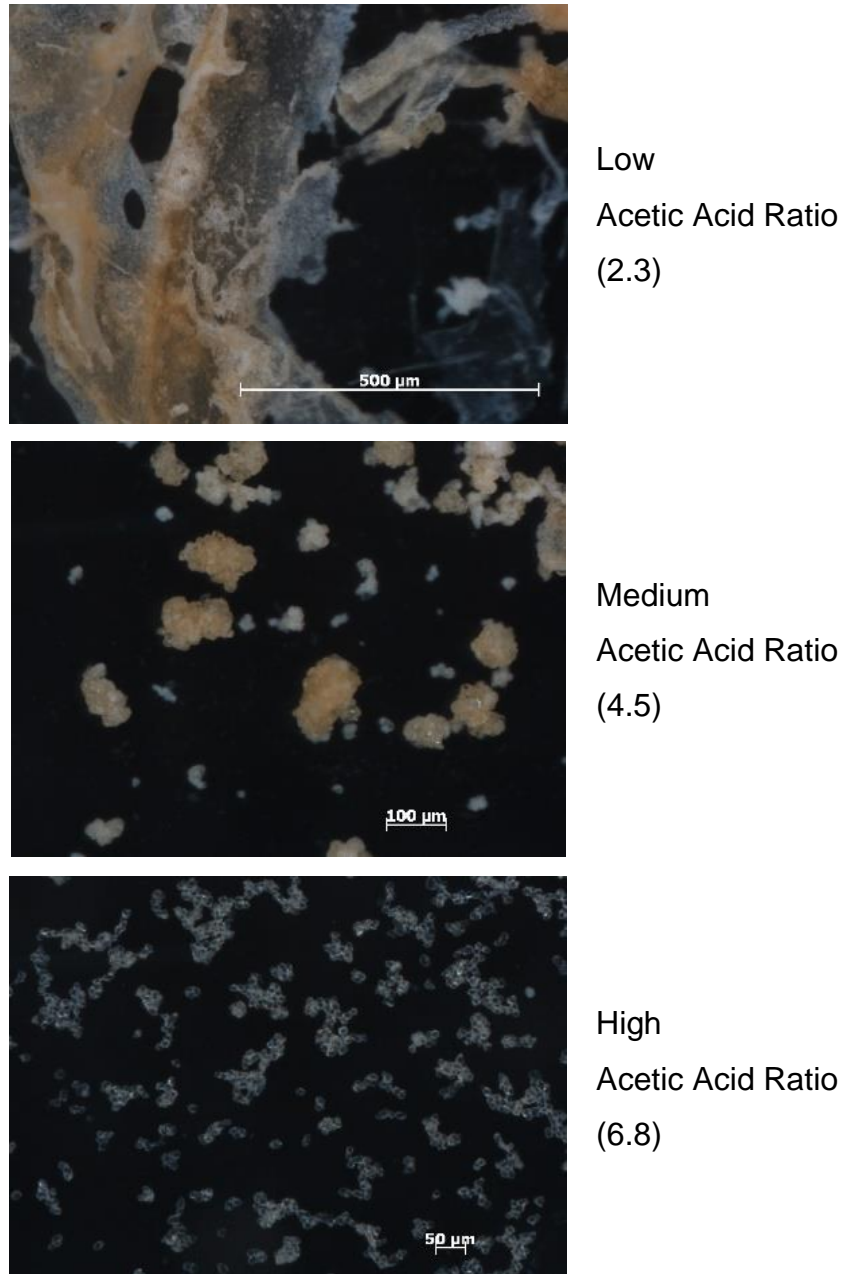
Figure 10: Morphology of precipitated protein as acetic acid ratio increased (constant magnification)

4.2.2. Kafirin Solubility Analysis

Figure 11 below shows the solubility of the kafirin protein at various times at the low acetic acid to protein ratio (2.3) as well as at a high ratio (6.8) (see Table 5)
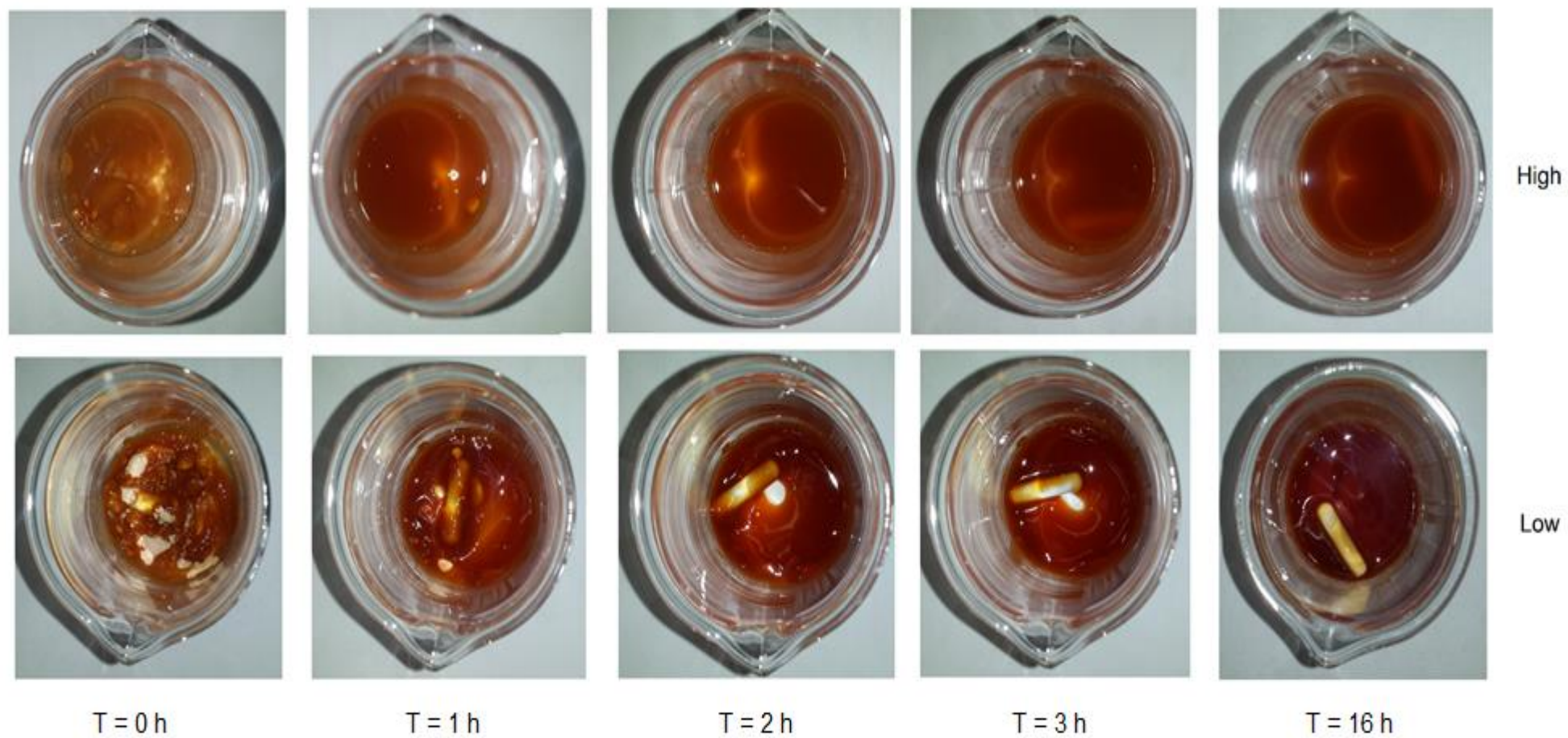
Figure 11: Kafirin protein solubility over time at high and low solvent ratio

33

In Figure 11, clumps of protein can be seen in the solvent after the first hour of mixing. The clumps diminish over time and can vaguely be seen at the 2 h interval and ultimately disappear at the 3 h interval. There is no observable change between the 3 h and 16 h intervals. These observations were noted for both the high and low acetic acid solvent to protein ratios. However, the higher solvent ratio dissolved the protein easier (smaller clumps of protein for the corresponding initial time intervals) in addition to being considerably easier to mix. The low acetic acid solvent ratio proved problematic to mix due to the very viscous nature of the mixture, resulting in the magnetic stirrer often becoming ensnared and requiring intervention.

Figure 12 shows the particle size distribution of the microparticles formed with the low acetic acid concentration after 3 h and 16 h of solubilisation respectively. While, Figure 13 shows the particle size distribution of the microparticles formed at the high acetic acid concentration after 3 h and 16 h of solubilisation respectively. Appendix B directly compares the particle size distributions of the kafirin microparticles prepared using 3 h and 16 h of solubilisation times at high and low acetic acid ratios respectively. All the above kafirin microparticles prepared were also examined under light microscopy and compared, as can be seen in Figure 14 below.

It is clear from the comparison of Figure 12 and Figure *13* that the higher acetic acid concentration yields smaller microparticles. Furthermore, in Figure 12, Figure *13* and Figure *14* it can be seen that the shorter solubilisation times also yield smaller kafirin microparticles. It is believed that the lengthy solubilisation time allows sufficient time for the acetic acid to evaporate resulting in a reasonably lower acetic acid ratio than the initial solution. Hence from the above figures, it is clear that the protein fully solubilises after 3 h and that prolonging the solubilisation time is a futile effort, which negatively impacts kafirin microparticle formation.
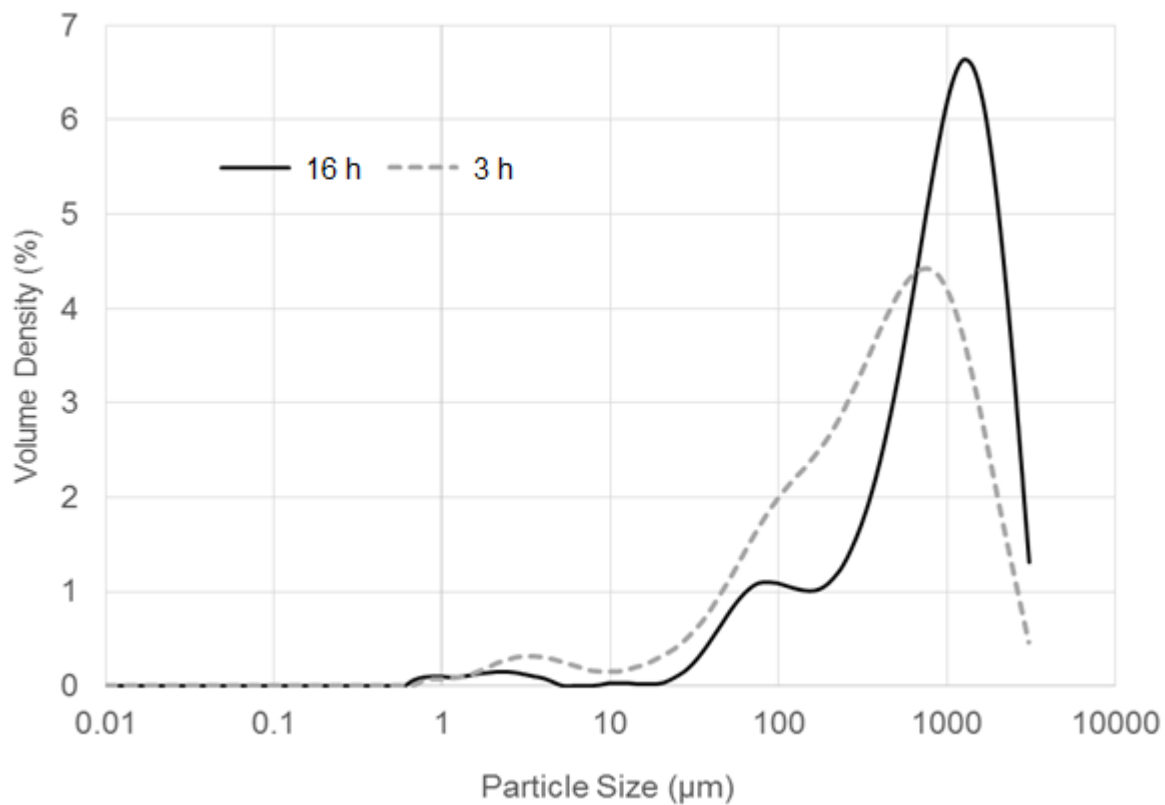
Figure 12: Size distribution of kafirin microparticles formed from low solvent ratio at varying protein solubilisation intervals.
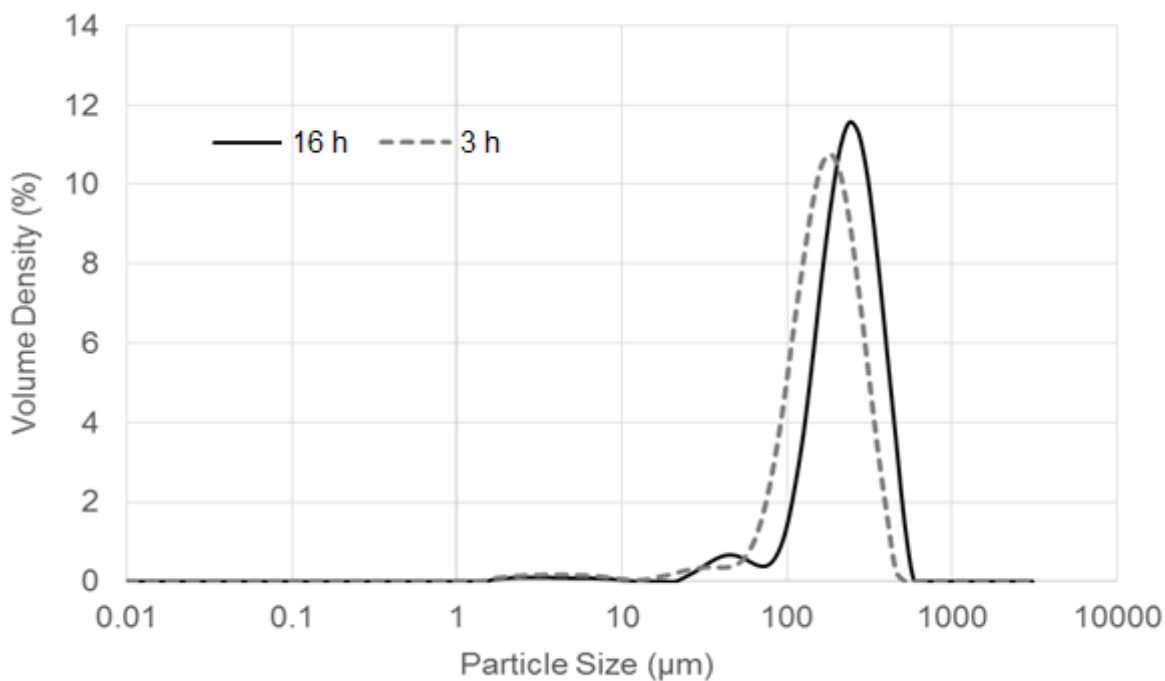
Figure 13: Size distribution of kafirin microparticles formed from high solvent ratio at varying protein solubilisation intervals.

35
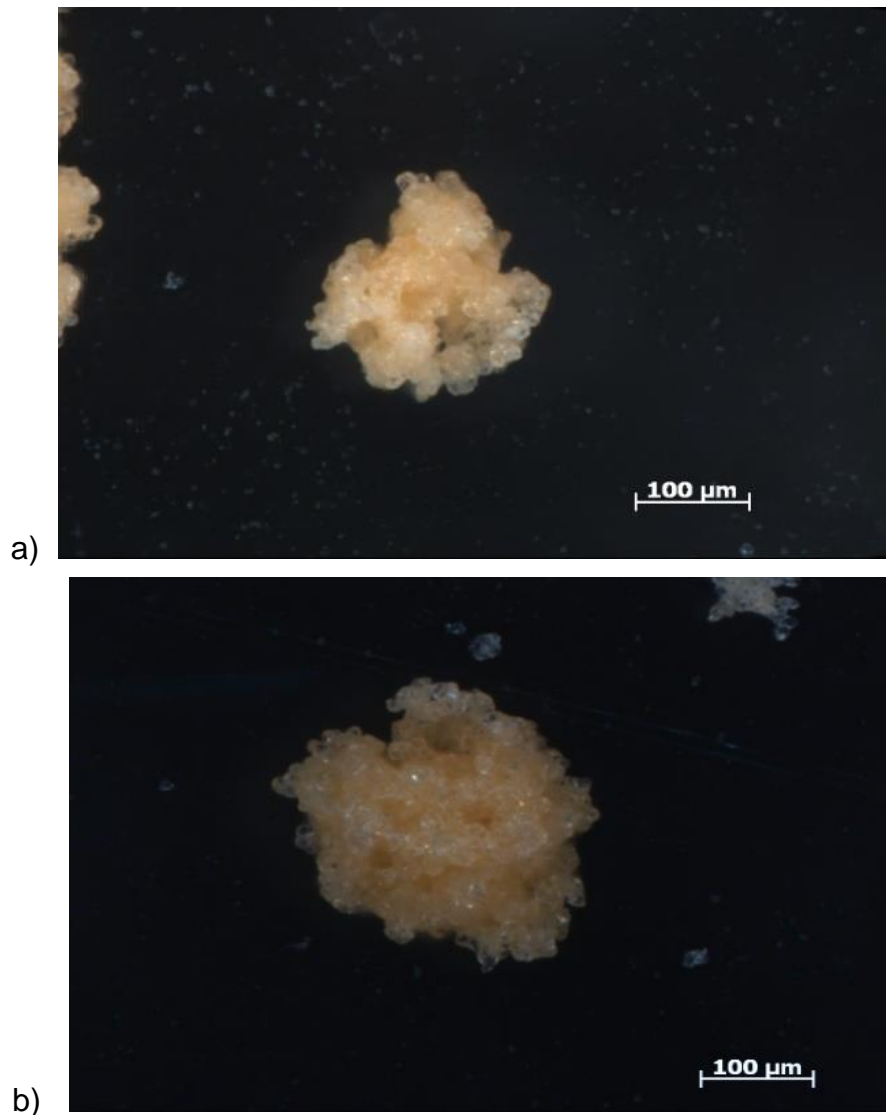
Figure 14: Light microscopy comparison of microparticles formed at a) 3 h and
b) 16 h solubilisation time

4.2.3. Peristaltic Pump Calibration

The peristaltic pump calibration provides an expression relating the actual water addition rate to the settings shown on the pump. This was necessary since this expression can be substituted into the polynomial model developed later. Table 7 shows the calculated pump rate (R_{WA}) based on the average time recorded (T_F) to fill 20 mL volume of water at the corresponding pump setting (N_{PS}).

The relationship between the pump setting and pump rate was linear and by means of linear regression the pump rate can be described by Equation 5 below. The corresponding pump curve can be seen in Appendix C.

Table 7: Water pump rates at corresponding pump settings

N_{PS}	T_F	R_{WA}
	(s)	(mL/min)
5	418.0	2.9
10	223.3	5.4
15	152.0	7.9
20	117.7	10.2
30	69.3	17.3
50	46.7	25.7
60	36.7	32.7
120	18.7	64.3

$$R_{WA} = (0.535 \times N_{PS}) + 0.054 \tag{5}$$

4.3. Screening Partial Factorial Experiments for KEMS Formation

4.3.1. Glacial Acetic Acid Based Screening

The partial factorial experiments, as shown in Table 4, were carried out using the defatted kafirin protein extracted from red sorghum (by means of the large scale extraction setup) and glacial acetic acid as solvent. PSA was done on the resulting precipitated protein, as can be seen in Table 8 below.

Table 8: Particle size of defatted kafirin during screening partial factorial experiments

Experiment	C_{AA}	V_{SS}	R_{WA}	N_{WD}	d_{10} (µm)	d_{50} (µm)	d_{90} (µm)
1	L	L	L	L	61	181	1120
2	L	L	L	H	62	139	1060
3	L	H	H	L	66	164	1070
4	L	H	H	H	61	157	1260
5	H	L	H	L	38	117	351
6	H	L	H	H	29	123	397
7	H	H	L	L	50	87	156
8	H	H	L	H	43	78	144

Figure 15, Figure *16* and Figure *17* show the corresponding average high and low d_{10}, d_{50} and d_{90} responses for each parameter. From these figures the glacial acetic acid ratio has the biggest impact on the final microparticle size compared to the other variables.

Similarly, the same screening partial factorial experiments were repeated for microparticles precipitated from non-defatted kafirin extracted from red sorghum, as well as kafirin extracted from white sorghum. The results agreed with the results for defatted kafirin samples, and can be seen in Appendix D1 and D2.

Regardless of the type of kafirin protein used the ratio of glacial acetic acid consistently had the biggest impact. The stirring speed and water addition rate consistently had a relatively mild impact while the number of water droplets consistently had an almost insignificant impact.

More detailed graphs, indicating the response for each parameter across all relevant particle sizes, can be seen in Appendix D3 for all the kafirin protein types tested. While the complete particle size analyses for each starting material are directly compared for each partial factorial experiment in Appendix D4. The results for the ethanol based experiments are also contained in Appendix D4 which is discussed in the next section.
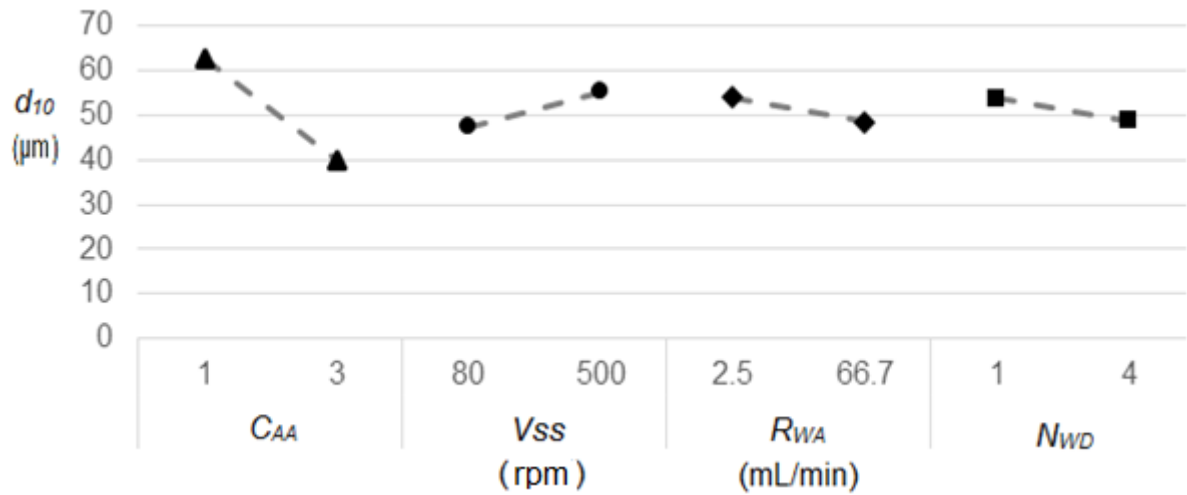
Figure 15: Screening partial factorial results (d_{10}) for *DF-Red* kafirin
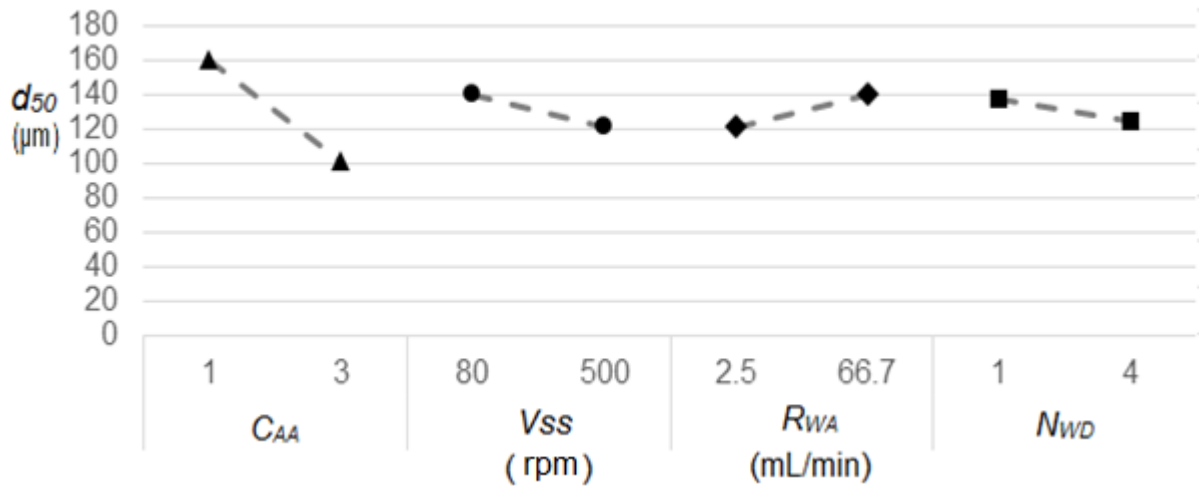
Figure 16: Screening partial factorial results (d_{50}) for *DF-Red* kafirin
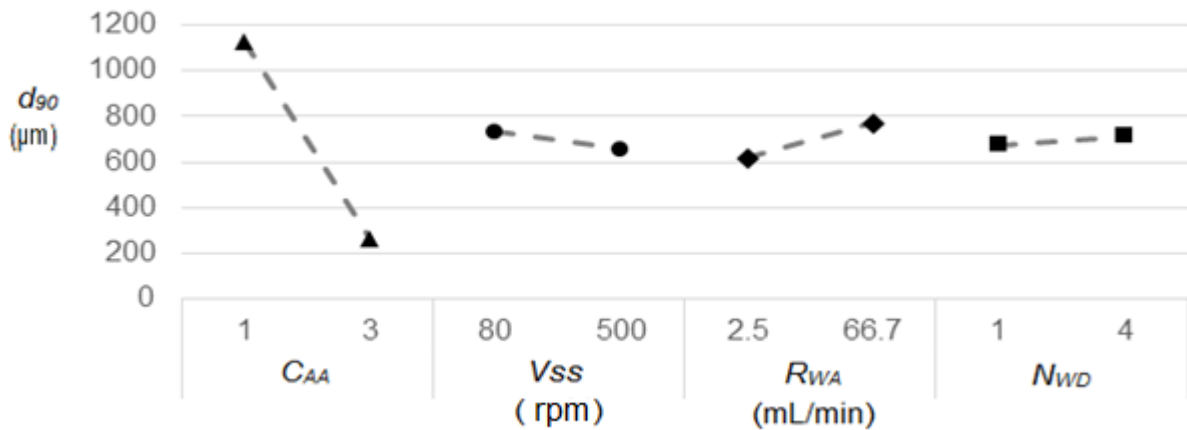
Figure 17: Screening partial factorial results (d_{90}) for *DF-Red* kafirin

4.3.2. Ethanol-Based Screening

The partial factorial experiments were repeated as in section 4.2.1 with ethanol as solvent. The PSA for the resulting precipitated particles can be seen in Table 9 below.

Table 9: Particle size using ethanol solvent for screening partial factorial experiments

Experiment	C_E	V_{SS}	R_{WA}	N_{WD}	d_{10} (µm)	d_{50} (µm)	d_{90} (µm)
1	L	L	L	L	23	62	161
2	L	L	L	H	20	58	150
3	L	H	H	L	25	57	143
4	L	H	H	H	19	52	122
5	H	L	H	L	21	72	168
6	H	L	H	H	19	55	147
7	H	H	L	L	22	69	176
8	H	H	L	H	27	81	195

Figure 18, Figure *19* and Figure *20* show the corresponding average high and low d_{10}, d_{50} and d_{90} values respectively when using ethanol solvent to solubilise the kafirin protein.

From the figures it appears that most of the parameters had very little to no influence in the formation of microparticles when ethanol solvent was used. This was a contradiction since the solvent ratio was a significant parameter when glacial acetic acid was used as solvent. This contradiction was resolved during the comparison of the solvents in the following section.
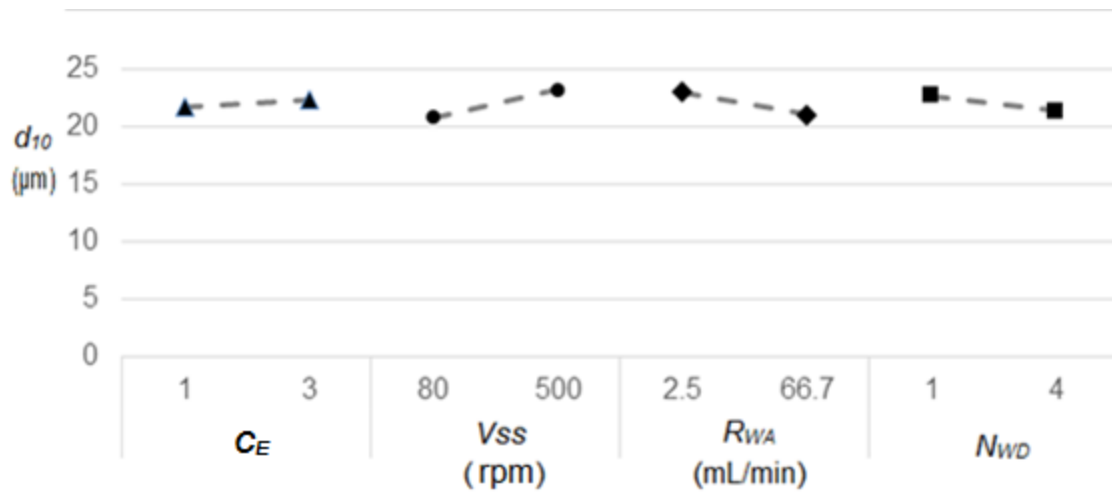
Figure 18: Partial factorial results (d_{10}) for defatted protein solubilised in ethanol
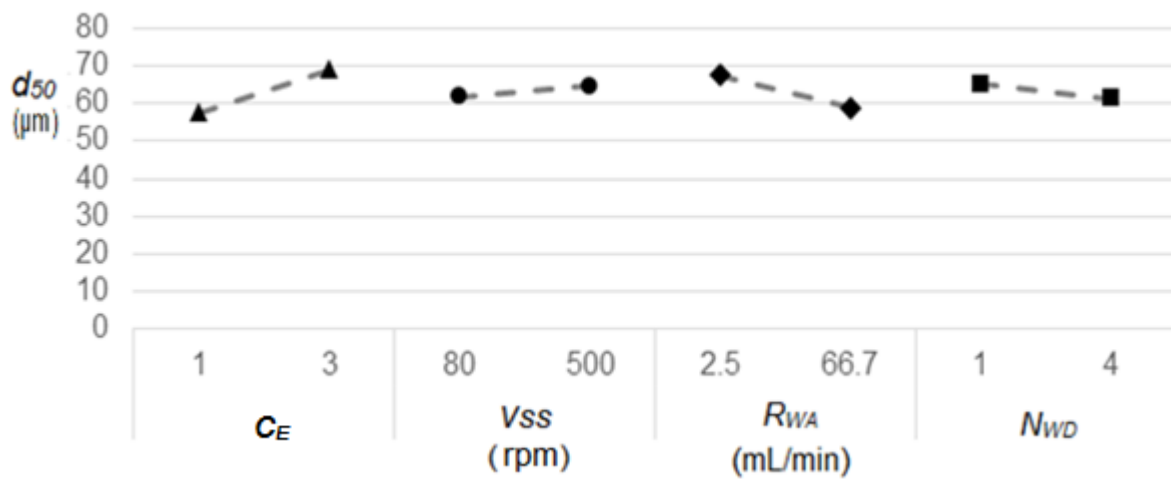
Figure 19: Partial factorial results (d_{50}) for defatted protein solubilised in ethanol
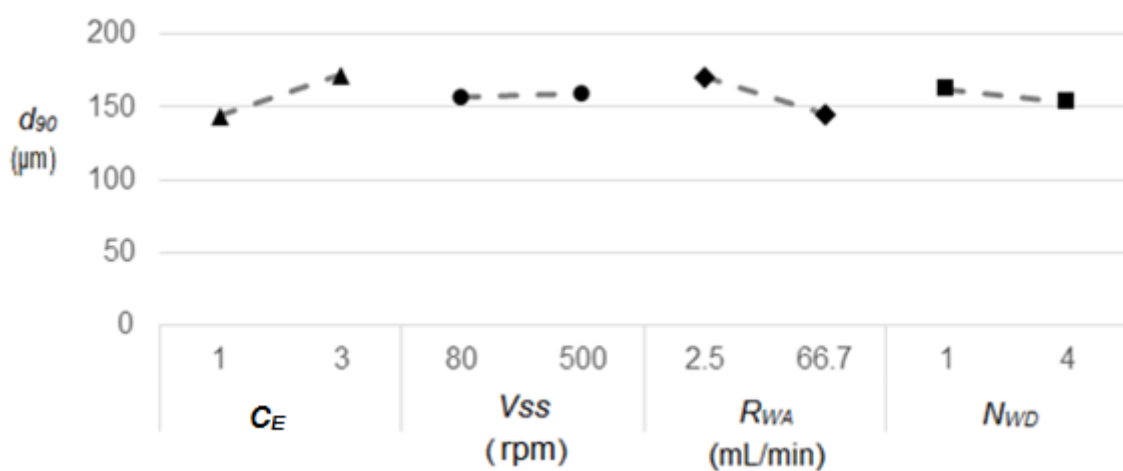
Figure 20: Partial factorial results (d_{90}) for defatted protein solubilised in ethanol

4.3.3. Comparison of Acetic Acid and Ethanol Solvent during Screening

The comparison of ethanol and acetic acid solutions after the solubilisation phase indicated that only the kafirin in the acetic acid solvent had successfully solubilised. As can be seen in Figure 21 below the acetic acid solution has a deep rich colour while the ethanol solution has a dull opaque colour after a 16 h solubilisation stage. The dark colour indicates protein solubilisation while the dull opaque resembles that of the initial dry kafirin protein. All of the protein was solubilised for the glacial acetic acid solvent however this was not the case for the ethanol based solvent.

a)   b)
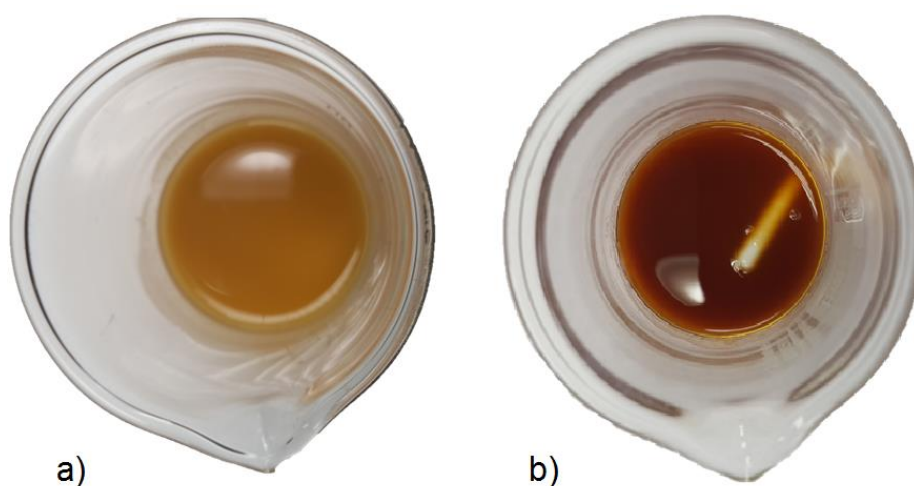
Figure 21: Comparison of a) ethanol and b) glacial acetic acid protein solutions

The particle size distributions of the various ethanol based experiments as compared to the initial starting material can be seen in Appendix D5. These distributions further show the uniformity of the ethanol-based experiments results with only a minor change from the initial starting kafirin. This reaffirms the suspicion that the ethanol based solubilisation of kafirin protein was only partially achieved.

This result and due to the potential to form films downstream when using acetic acid as solvent, the glacial acetic acid preparation was considered as the preferred method keeping commercialisation in mind. Therefore, from this point onwards the results were only focused on the experiments where glacial acetic acid was used as solvent.

4.4. Analysis of Protein Secondary Structure

4.4.1. Analysis of Starting Materials

The three main protein starting materials, namely; defatted protein extracted from red sorghum (*DF-red*), non-defatted protein extracted from red sorghum (*NDF-red*) and defatted protein extracted from white sorghum (*DF-white*) were analysed by means of FTIR. Figure 22 and Figure *23* below focus on the amide I and II regions, respectively. The complete scans can be seen in Appendix E1.
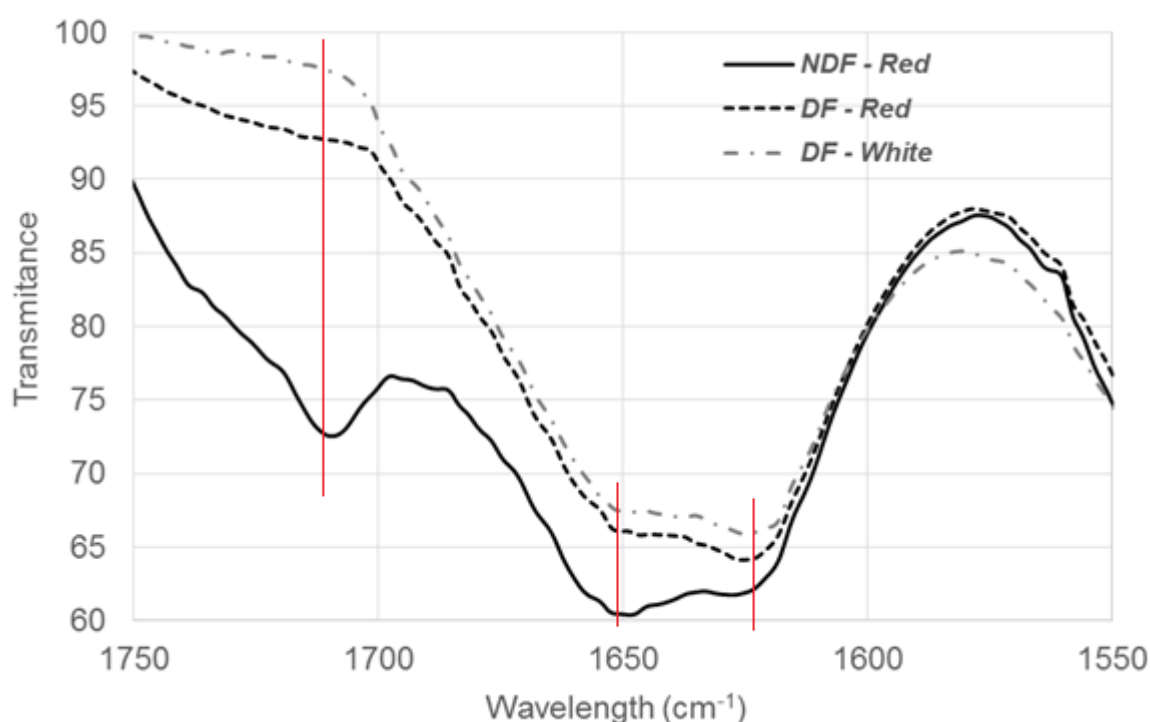
Figure 22: Starting proteins FTIR scan in the amide I region

As seen from Figure 22, the normal defatted kafirin extracted from red sorghum and the defatted kafirin extracted from the white sorghum are very similar in nature. Both display a lower β-kafirin than α-kafirin transmittance at 1620 cm^{-1} and 1650 cm^{-1}, respectively. However, the non-defatted kafirin showed a lower α-kafirin than β-kafirin transmittance. Additionally, it can be seen in the region of 1750 cm^{-1} to 1720 cm^{-1}, the C=O bond frequency for esters, that the non-defatted sample has a significantly higher fat content than both the defatted and white kafirin. The white kafirin had the lowest fat content and was considered to be the highest quality protein.
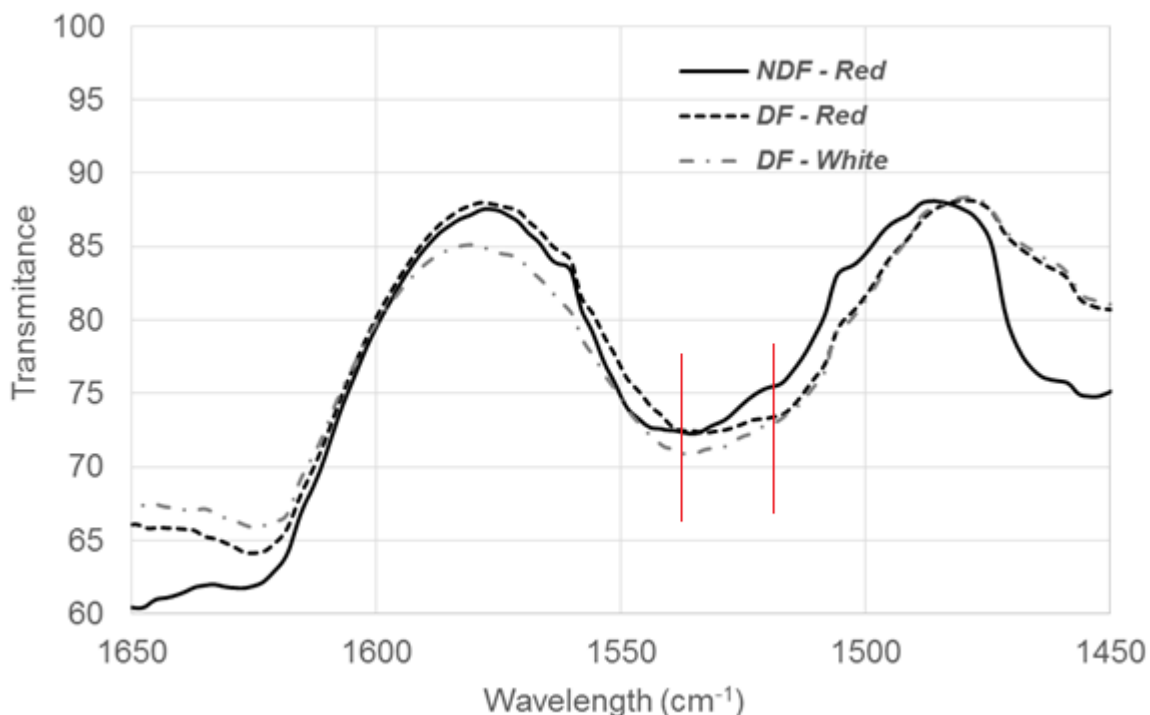
Figure 23: Starting proteins FTIR scan in the amide II region

Similarly, from Figure 23, it can be seen that the defatted kafirin extracted from red sorghum has a lower β-kafirin than α-kafirin transmittance at 1516 cm^{-1} and 1545 cm^{-1} respectively. While the converse is true for the non-defatted kafirin extracted from red sorghum. The ratios of the α-kafirin and β-kafirin transmittances were calculated using Equation 4. A ratio above 1 indicates that the sample contained more β-kafirin, while a ratio below 1 indicates that more α-kafirin was present. From the comparison of defatted and non-defatted kafirin, as shown in Table 10 below, the defatting process has altered the secondary structure of the protein. This could have a negative effect, since α-kafirin is more favourable with regards to microparticle formation.

Table 10: Transmittance ratios for the various protein starting materials

Sample	R_{AB} at amide I	R_{AB} at amide II
DF-Red	1.016	1.011
NDF-Red	0.956	0.958
DF-White	1.017	0.984

4.4.2. Analysis of Processed Protein

Processed protein here refers to the protein which has undergone the water addition step during KEMS formation. Defatted kafirin, extracted from both red and white sorghum grain respectively, was solubilised and processed. It was noted that not all processed proteins formed microparticles. Depending on the formation parameters used, either microparticles or crosslinked mass agglomerated protein precipitated out of the solvent as shown in Figure 24 for defatted red kafirin. It was noted that crosslinked mass agglomerated protein tended to occur at low solvent to protein ratios, high water addition rates or low stirring speeds.

These products were further analysed by means of FTIR, as shown in Figure 25 and Figure *26* below, which focused on the amide I and II regions, respectively. The complete FTIR scan for the products formed from *DF-Red* and *DF-White* kafirin can be seen in Appendix E2 and E3, respectively.

As can be seen from Figure 25, the starting *DF-Red* kafirin displayed the lowest β-kafirin dip at 1620 cm^{-1} which becomes less pronounced during processing when the microparticles or agglomerated crosslinked protein are formed. This flattening of the dip as the protein is processed can also be observed in Figure 26, which focuses on the amide II region. The corresponding figures for white kafirin showed the same trends and can be viewed in Appendix E4.

The ratios of the α-kafirin and β-kafirin transmittances for *DF-Red* and *DF-White* kafirin were, once again, calculated using Equation 4 and the values can be seen in Table 11 below.
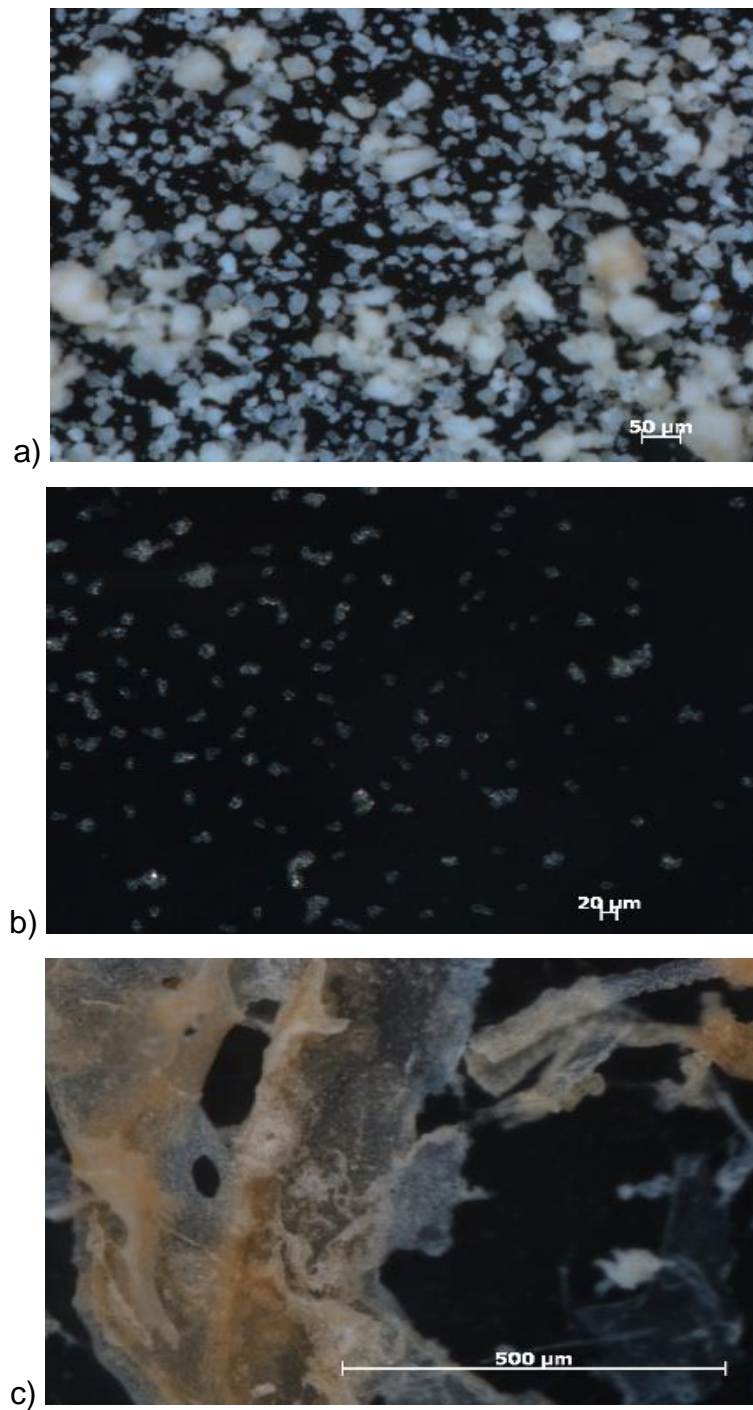
Figure 24: Light microscopy of protein types produced from *DF-Red* kafirin. The samples are a) starting kafirin, b) microparticles and c) crosslinked protein
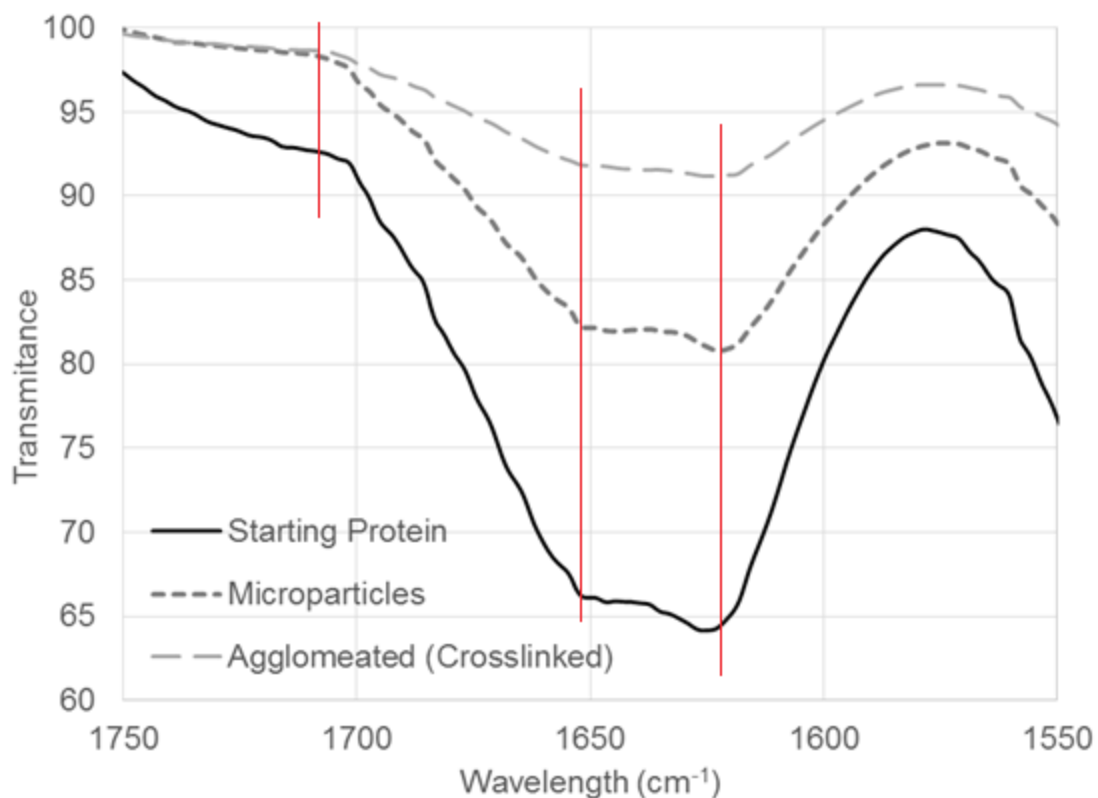
Figure 25: Processed *DF-Red* kafirin FTIR scan in the amide I region
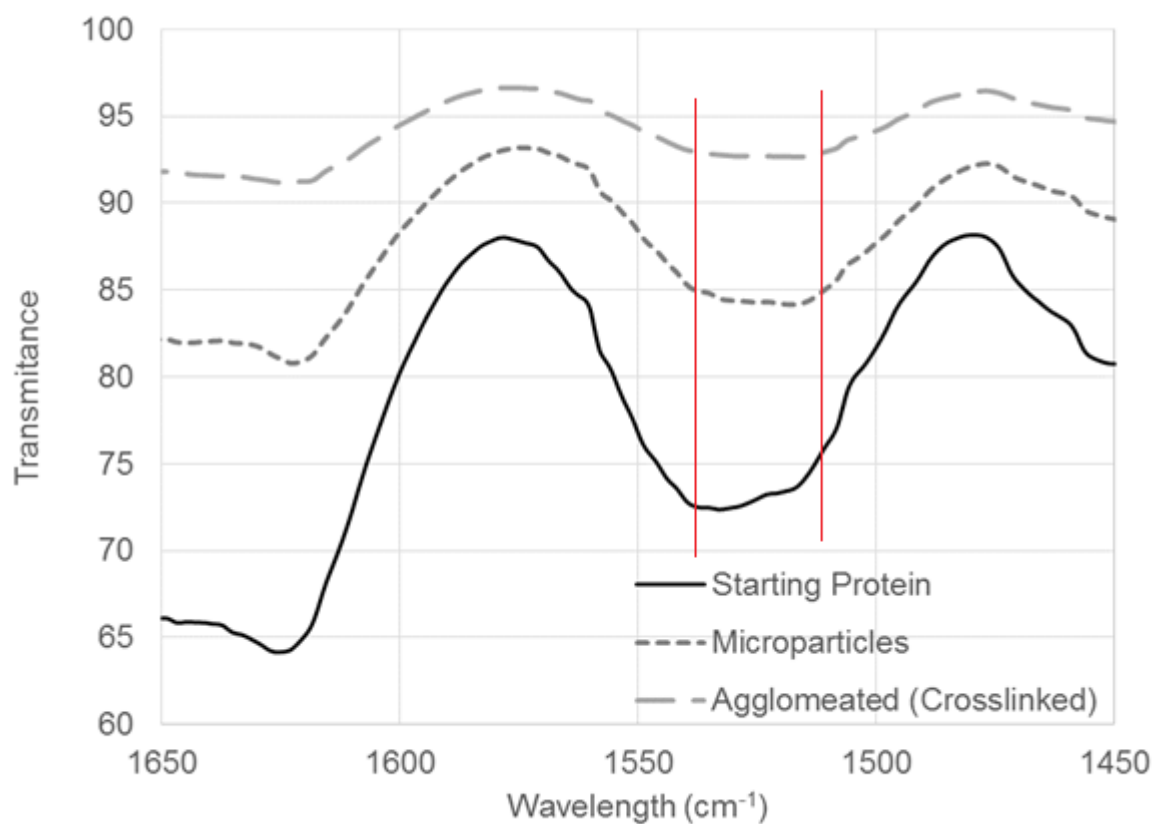
Figure 26: Processed *DF-Red* kafirin FTIR scan in the amide II region

Table 11: Transmittance ratios for the processed defatted kafirin samples extracted from both red and white sorghum

Sample	R_{AB} at amide I	R_{AB} at amide II
DF Kafirin - Red		
Starting Protein	1.016	1.011
Microparticles	1.015	1.032
Agglomerated	1.006	1.011
DF Kafirin - White		
Starting Protein	1.017	0.984
Microparticles	1.020	1.046
Agglomerated	1.008	1.022

As can be seen from the above tables and figures, the microparticle secondary structure generally resembles that of the starting material (occasionally with a slightly higher amount of α-kafirin present). However, when the protein crosslinks and mass agglomeration was present, the β-kafirin structure becomes more prominent and the peaks tend to flatten out as the ratio approaches 1. Additionally, from Figure 25, inspection of the dip between 1750 cm^{-1} and 1720 cm^{-1} indicates that the fat present in the starting protein is hardly present in the processed materials. This is most likely due to the fat not precipitating out of the solvent with the protein during the water addition step and, thus, remains in solution when solid protein is separated.

Therefore, the precipitation of the protein by means of water addition has altered the secondary structure of the protein. When microparticles are formed, the α-kafirin structure is more noticeable; however, when crosslinking occurs, the β-kafirin structure becomes more prominent. Since the α-kafirin structure is strongly associated with microparticle formation, care should be taken to avoid encouraging the formation of the β-kafirin structure, which can occur during the defatting process, as highlighted in the previous section. Furthermore, the defatting of the protein occurs irrespectively during the water addition step through protein precipitation.

4.5. Model Fitting

4.5.1. Boundary Determination

It was found in the initial KEMS formation from glacial acetic acid investigations (Section 4.2.1) and the screening partial factorial experiments (Section 4.3.1) that the glacial acetic acid to protein ratio played the most significant role in forming good microparticles. The screening experiments also found that stirring speed and water addition rate played a moderate role, while the number of droplets was relatively irrelevant. Subsequent to the outcome of these experiments it was determined that the glacial acetic acid ratio to protein ratio was kept constant at the high level ($C_{AA} = 3$). Furthermore, for the purpose of forming microparticles, it was decided to focus on the water addition rate and stirring speed variables, as they showed some effect during the first experiments.

In order to determine the boundary point where mass protein agglomeration occurs, particle size analysis was conducted on samples at constant low water addition rates ($N_{PS} = 5$), while the stirring speed was gradually increased. The particle size distributions for these samples can be seen in Figure 27.
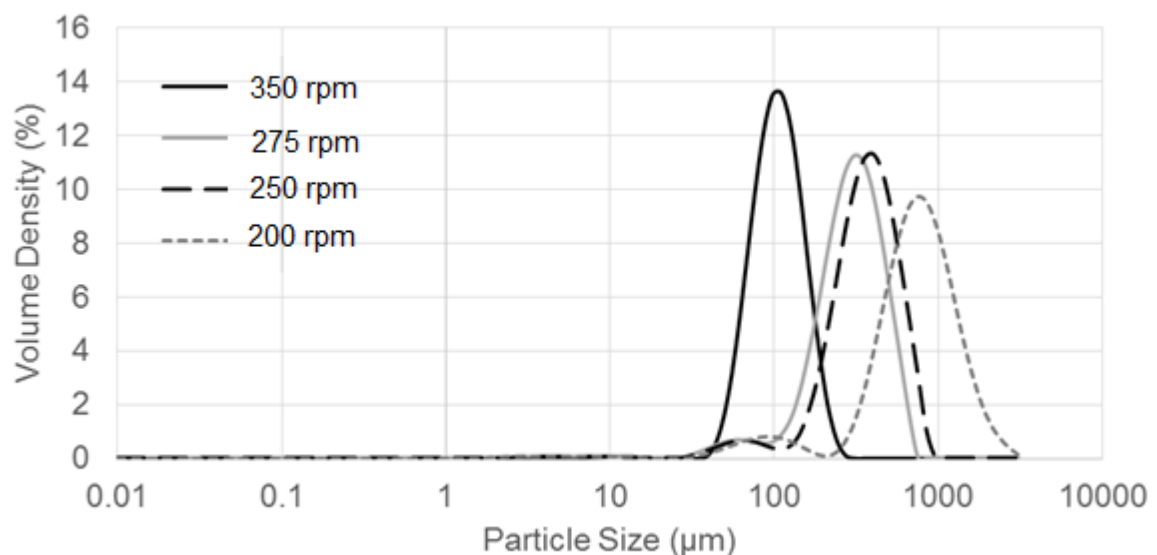
Figure 27: PSA of samples at low water addition rates while increasing stirring speed

As can be seen in Figure 27, the lowest acceptable stirring speed that ensures satisfactory microparticles (mean particles around 100 µm in size) was identified as 350 rpm. This outlines one of the limits of the workspace since we now know that we are inside the microparticle forming region. The other boundary limit was found by increasing water addition rate until protein mass agglomeration was observed. At 350 rpm, the highest water addition rate where notable agglomeration started occurring was at 5.4 mL/min (N_{PS} = 10). The remaining workspace boundaries were determined by the limits of the apparatus. That is the lowest water addition rate used was 2.7 mL/min (N_{PS} = 5) and the highest stirring speed achievable with the apparatus was 900 rpm. The boundary conditions for the model workspace can be seen in Table 12 below. The model will make use of peristaltic pump number. However, this number can be related back to a water addition rate, using Equation 5.

Table 12: Parameter values for boundary conditions and centre point

Boundary	V_{SS}	N_{PS}	R_{WA}
	rpm	-	mL/min
Upper Limit	900	10	5.4
Lower Limit	350	5	2.7
Centre Point	625	7	3.8

These boundary points were used in conjunction with a centre point and supplementary points for model fitting. Hence the entire model workspace chosen can be seen below in Figure 28 indicating the experimental points used for the model determination.
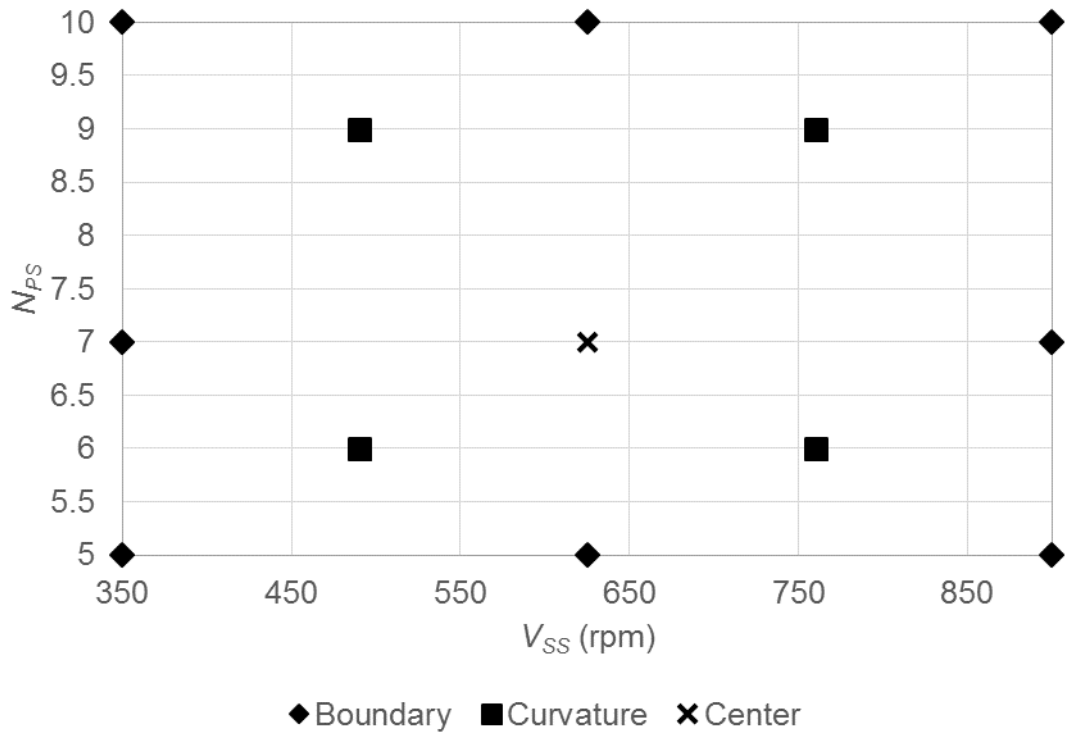
Figure 28: Model workspace with chosen experimental points

4.5.2. Model Curvature Analysis

From the experimental points chosen there are three points of constant water addition rate, while the stirring speed varies. Similarly, there are three clear lines of constant stirring speed while water addition rate varies. That is at N_{PS} equal to 5, 7 and 10 respectively while V_{SS} varies from 350 rpm, 625 rpm and 900 rpm separately and vice versa. The mean particle size for a constant V_{SS} and N_{PS} can be seen in Figure 29 and Figure 30 respectively.
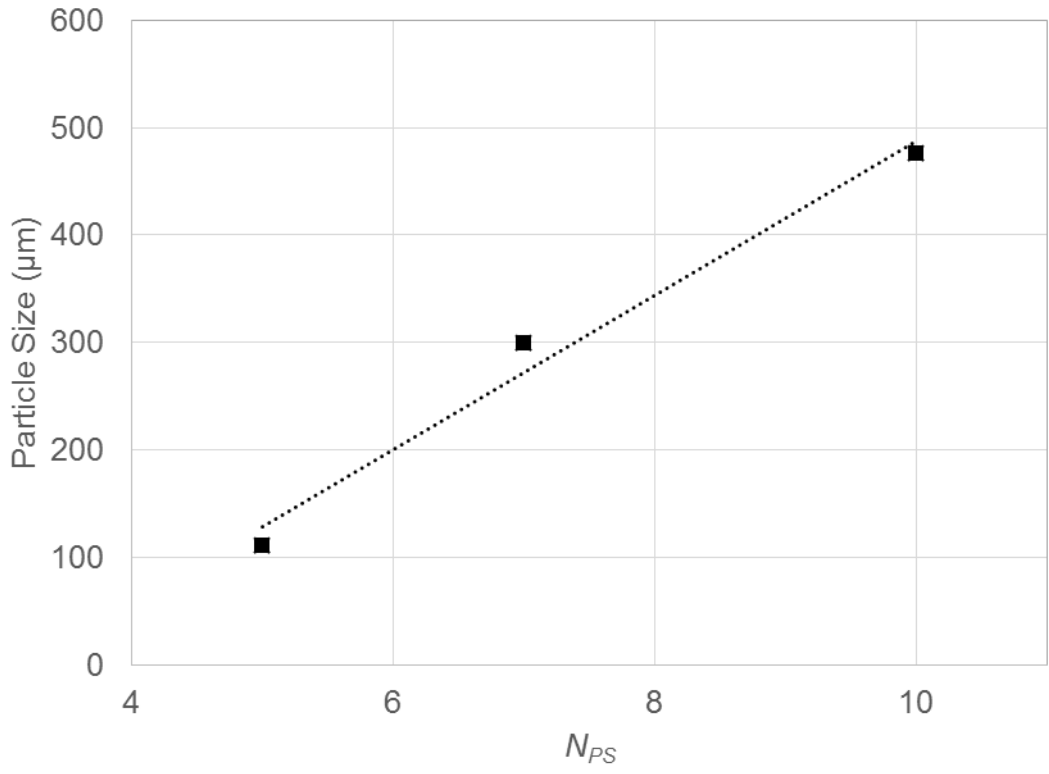
Figure 29: Resulting d_{50} at constant V_{SS} (350 rpm) varying N_{PS}
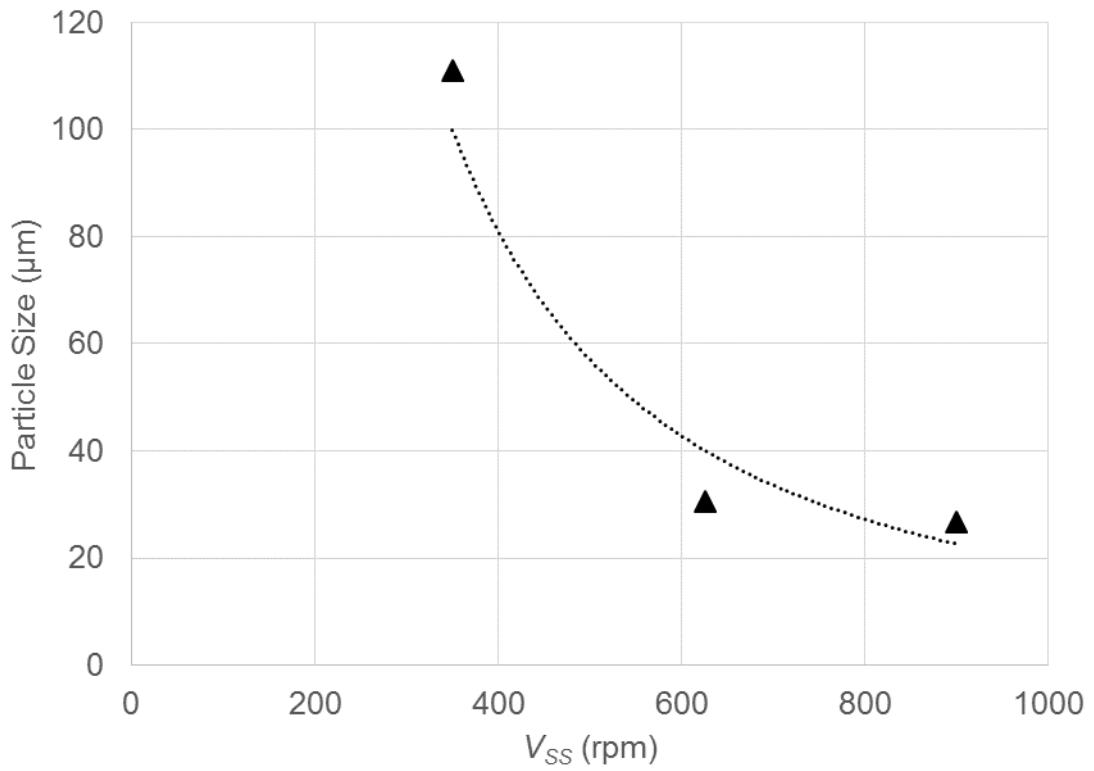
Figure 30: Resulting d_{50} at constant N_{PS} (5) varying V_{SS}

From Figure 29 it can be seen that, as expected, an increase in water addition rate increases the mean particle size. Also from Figure 29 it is shown that the relationship between d_{50} and water addition rate appears to be a linear relationship. The other constant stirring speed lines (for 625 rpm and 900 rpm) are similar to Figure 29 and also suggest a linear relationship, as and can be seen in Appendix F1.

From Figure 30, it can be seen that an increase in stirring speed radically decreases the mean particle size. More importantly, the relationship between mean particle size and stirring speed appears to be a nonlinear relationship (possibly exponential in form with an asymptote). The other constant water addition rate lines ($N_{PS} = 7$ and 10) are similar to Figure 30 and also suggest a nonlinear relationship, as shown in Appendix F2.

The comprehensive particle size distributions for the constant stirring speed experiments discussed above (350 rpm, 625 rpm and 900 rpm) resemble the same trends discussed above and can be viewed in Appendix F3. Similarly the comprehensive particle size distributions for the constant water addition rate experiments ($N_{PS} = 5$, 7 and 10) can be viewed in Appendix F4.

4.5.3. Final Model

A comprehensive particle size analysis was done on the experimental points as indicated in Figure 28. A total of three particle size measurements were done per experimental point, and the average of the mean particle size (d_{50}) can be seen in Table 13 below. The experiment about the centre point of the workspace was repeated three times to determining the average error. The particle size distribution analysis for the centre point repeats can be seen in Figure 31 below. The complete particle size distributions for every experimental point, including the d_{10}, d_{50} and d_{90} values, can be seen in Appendix G. For model fitting only the d_{50} was considered since it was determined to be the most representative of the particles formed.

Table 13: Particle size (d_{50}) analysis of model fitting experimental points

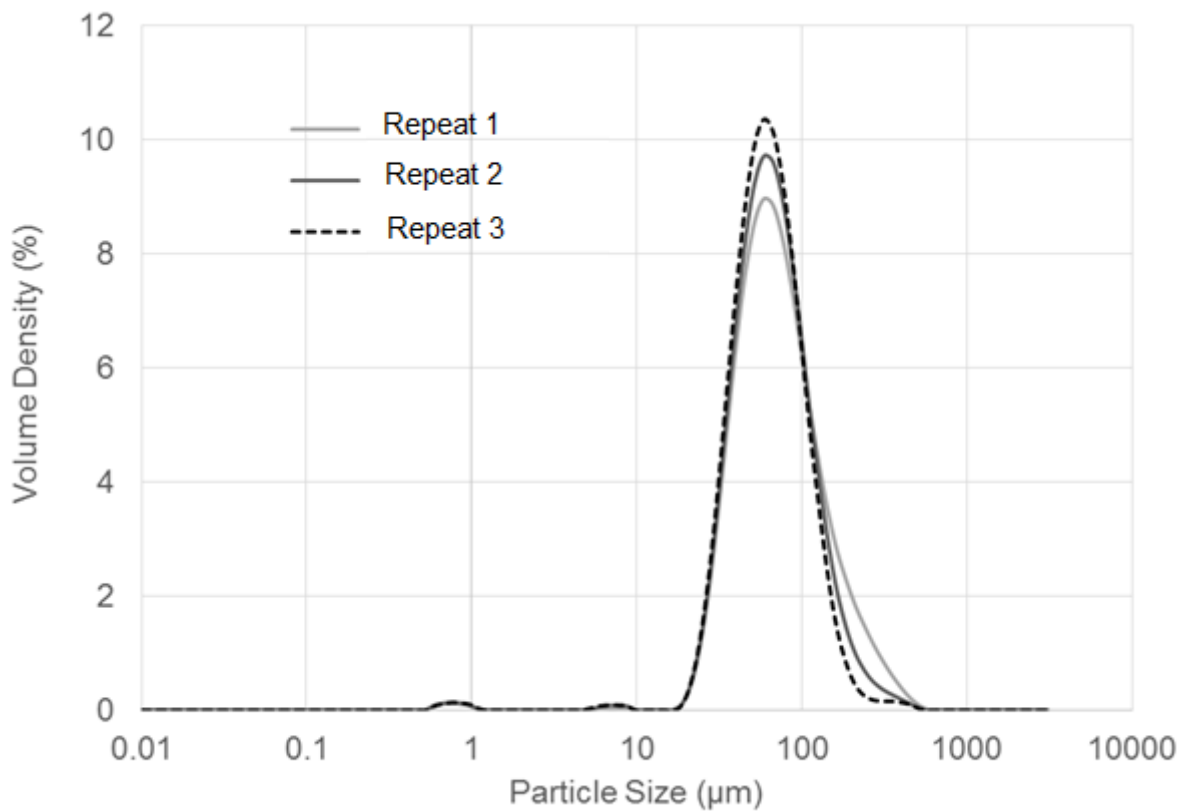| Exp	V_{SS}	N_{PS}	R_{WA}	d_{50}
	rpm		mL/min	µm
1	900	10	5.4	43
2	900	5	2.7	27
3	350	5	2.7	111
4	350	10	5.4	476
5	900	7	3.8	33
6	350	7	3.8	300
7	760	6	3.3	57
8	760	9	4.8	83
9	625	5	2.7	31
10	625	10	5.4	88
11	625	7	3.8	60
12	490	6	3.3	109
13	490	9	4.8	139

Figure 31: Particle size distribution for experimental repeats about the centre point

54

From Table 13, it can be seen that the mean microparticle size covers a large range. The smallest microparticles (26.7 µm) were observed at high stirring speed and low water addition rates, while the largest microparticles (476 µm) were observed at low stirring speeds and high water addition rates. As can be seen from Figure 31 the experiments about the centre point proved to be repeatable with a relatively small standard deviation calculated to be 1.7 µm.

A combination of polynomial terms based on Equation 3 were evaluated using the ANOVA statistical analysis method to fit a model to the experimental points shown above. The analysis of the explorative models can be seen in Appendix H. This was a trial an error method of adding and removing terms which seemed statistically viable. Some of these trial models may have seemed to be better fit statistically, however, plotting the expression showed a wave like section in the middle of the workspace which was unrealistic. The final model, which is represented by Equation 6 and Figure 32 below, was statistically a good fit and seemed realistic based on the experimental observations. The regression statistics and ANOVA statistical summary of the final model is shown below in Table 14 and Table *15* respectively.

$$
\begin{aligned}
d_{50} = {}& -809 + 2.2\,V_{SS} - (1.4 \times 10^{-3})\,V_{SS}^2 \\
& + N_{PS}[377 - 1.4\,V_{SS} + (1.7 \times 10^{-3})\,V_{SS}^2 - (7 \times 10^{-4})\,V_{SS}^3]
\end{aligned} \tag{6}
$$

The expression can be related directly to the stirring speed and water addition rates by combining Equation 6 and 5 to yield Equation 7 below.

$$
\begin{aligned}
d_{50} = {}& -809 + 2.2\,V_{SS} - (1.4 \times 10^{-3})\,V_{SS}^2 \\
& + \frac{(R_{WA} - 0.054)}{(0.535)}[377 - 1.4\,V_{SS} + (1.7 \times 10^{-3})\,V_{SS}^2 - (7 \times 10^{-4})\,V_{SS}^3]
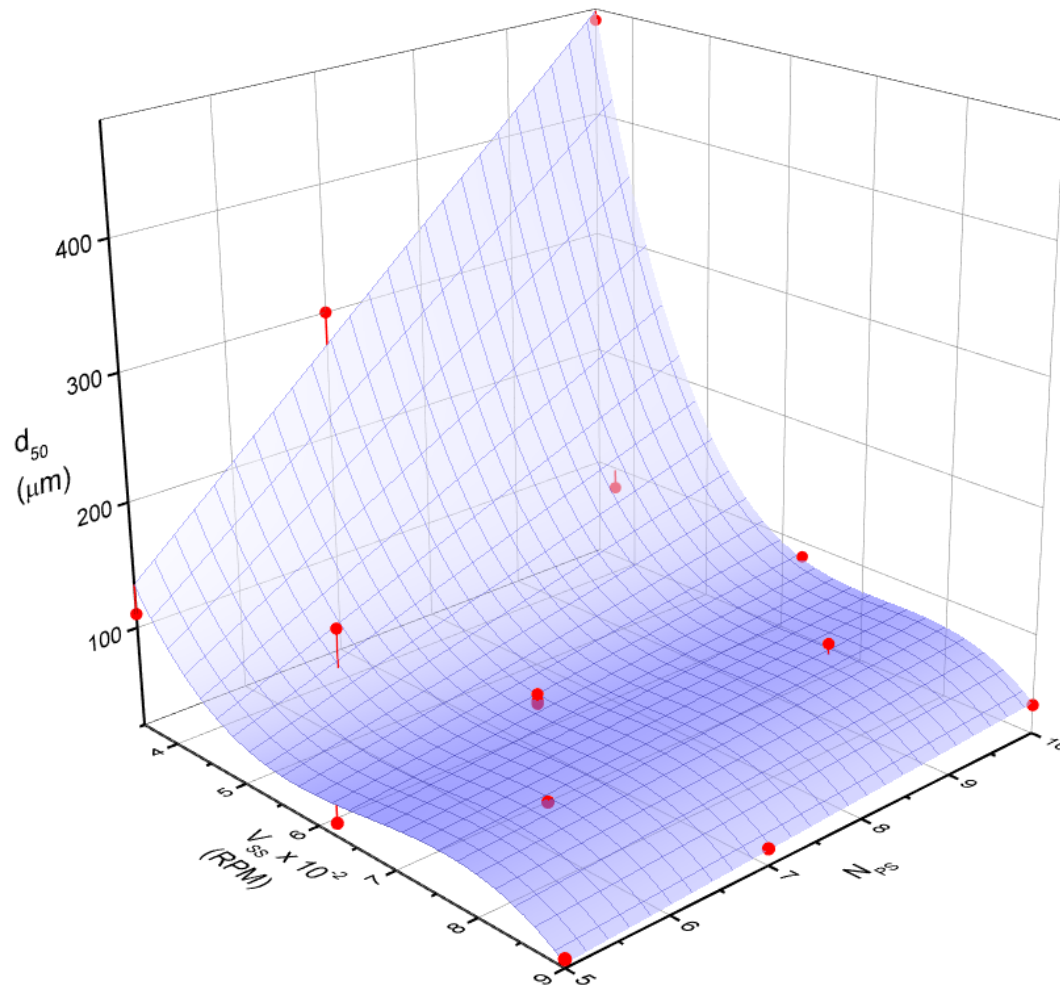\end{aligned}
$$

$$\tag{7}$$

Figure 32: Final model surface and experimental points

Table 14: Summary output of regression statistics for final model

Description	Value
Multiple R	0.993
R Square	0.986
Adjusted R Square	0.976
Standard Error	18.86
Observations	15

Table 15: ANOVA summary for the final model terms

Model Term	Coefficients	P-value
Intercept	-809	0.0059
V_{SS}	2.208	0.0189
N_{PS}	377.4	0.000003
$(V_{SS})^2$	-1.4×10^{-3}	0.0410
$V_{SS}.N_{PS}$	-1.408	0.0002
$(V_{SS})^2.N_{PS}$	1.7×10^{-3}	0.0007
$(V_{SS})^3.N_{PS}$	-7.4×10^{-4}	0.0025

The final model is a good fit for the experimental points as shown by Figure 32, which is further confirmed from Table 14. Not only are the R values close to 1 but also the standard error is relatively small. All the terms in Equation 6 are relevant, since a P-value smaller than 0.05 indicates that a term is significant, as confirmed in Table 15.

As expected, the particle size can be altered by changing the stirring speed and water addition rates during the protein precipitation step. From Figure 32, it appears as though three regions of various protein particle sizes exist. The first region consists of large particles (above 200 µm) at low stirring speeds and high water addition rates. The particle sizes decrease drastically and plateau into the second region which consists of moderate particles (around 100 µm) at moderate stirring speeds and moderate water addition rates. Finally, the particle sizes decrease again into the third region, which consists of small particles (around 20 µm) at high stirring speeds and low water addition rates.

The microparticles formed during the experiments were analysed further by means of light microscopy, in order to understand the regions identified above. Figure 33 below shows the morphology of the protein particles precipitated, which corresponds to the model and experimental points previously shown in Figure 32.
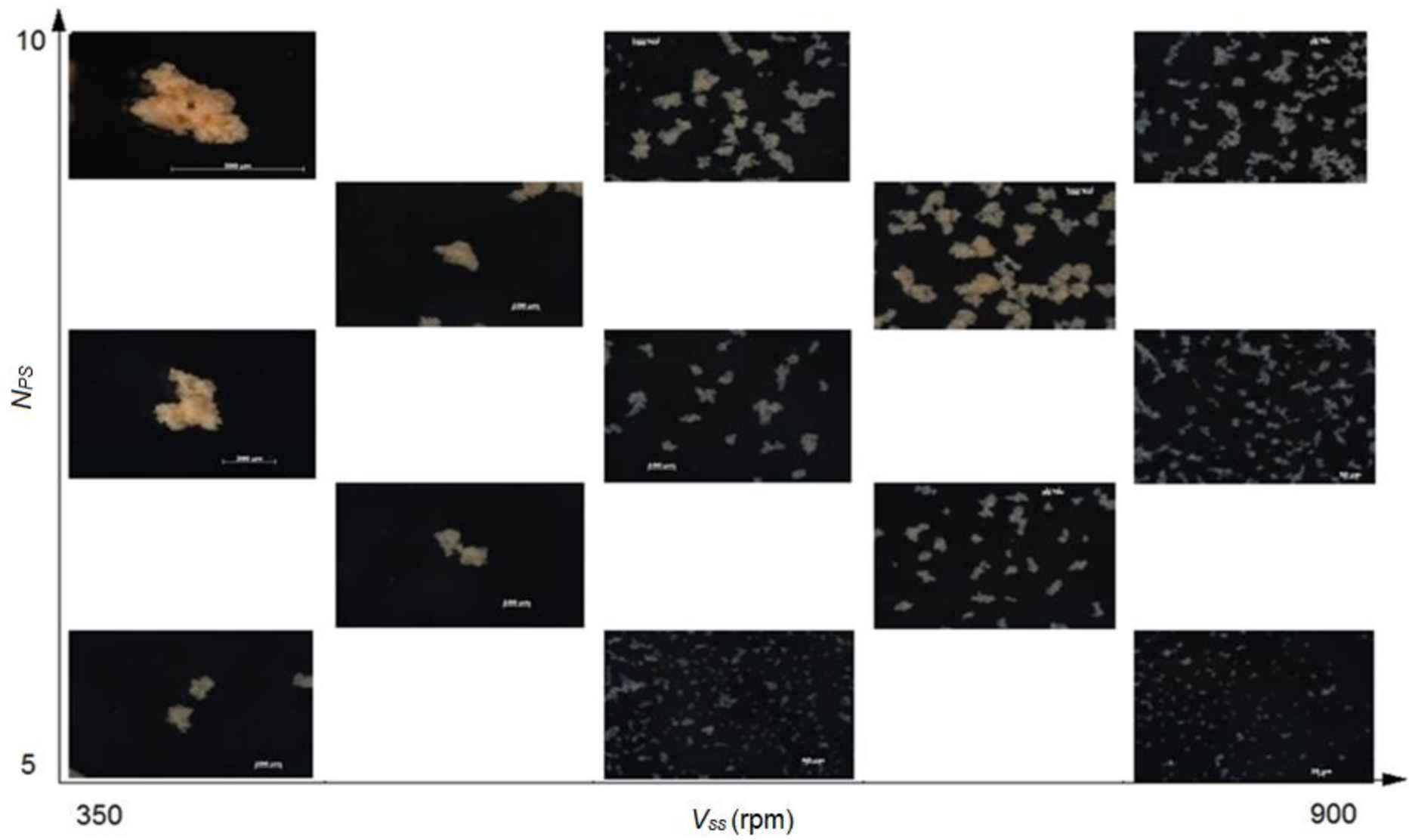
Figure 33: Particle morphology corresponding to the model workspace

The particle morphology, as shown in Figure 33, confirms that increasing stirring speed and decreasing the water addition rate leads to the formation of smaller particles. Furthermore, from Figure 33 we can understand the three regions previously mentioned and summarised below in Table 16 for convenience.

The first region, which consists of large particles (above 200 µm), at low stirring speeds and high water addition rates is crosslinked protein, which has begun to mass agglomerate. The second region, which consists of moderate particles (around 100 µm), at moderate stirring speeds and moderate water addition rates, appears to be agglomerated microparticles. The use of strong sonication, as well as high stirring speeds during the particle size analysis, did not break down the agglomerates; therefore, it is believed that these agglomerates are the result of protein covalent bonding and not due to secondary Van der Waals forces. Finally, the microparticles in the third region which consists of small particles (around 20 µm) at high stirring speeds and low water addition rates are the singular microparticles, as identified by the singular small round particles in Figure 33.

Table 16: Summarised description of particles formed in the various model regions

Region	Particle type	Parameter description
Primary	*Crosslinked protein*	*Low stirring speeds* *High water addition rates*
Secondary	*Agglomerated microparticles*	*Moderate stirring speeds* *Moderate water addition rates*
Tertiary	*Individual microparticles*	*High stirring speeds* *Low water addition rates*

Although it is implied that the kafirin microparticle size is altered by changing the stirring speed and water addition rate during the protein precipitation step, it is clear from the morphology that the primary protein microparticle remains approximately 20 µm and the variance in particle size is attributed to the size of the agglomerated microparticles. Ultimately, microparticles cease to form and mass crosslinked protein agglomeration begins to occur.

The agglomerated microparticles in the secondary region have not previously been identified. As identified from light microscopy the primary particle size of these microparticles, making up the agglomerates, resembles that of the individual microparticles. Therefore, it is hypothesised that the agglomerated microparticles could share similar properties as the isolated microparticles. This is significant since the singular microparticles require considerably more effort to form.

4.6. Model Validation

Additional experimental points were chosen within the microparticle region, to validate the model as described by Equation 6. The first region was avoided, since the crosslinked mass protein agglomeration is an undesirable product. The experimental points chosen are shown in Table 17 below.

Table 17: Experimental points chosen for validation of model

V_{SS}	N_{PS}	R_{WA}
rpm		mL/min
500	6	3.3
500	8	4.3
760	7	3.8
700	6	3.3
700	9	4.8
850	6	3.3
850	9	4.8

Kafirin microparticles were formed using the parameters shown in Table 17. The actual mean particle size (d_{50}) as well as the values predicted by Equation 6 for the experiments are shown below in Table 18. The standard error expected when using Equation 6 is ± 18 µm, as shown in Table 14. The upper range and lower range for the predicted values are also shown in Table 18.

Table 18: Model validation – actual and predicted results

V_{SS}	N_{PS}	Actual d_{50}	Predicted d_{50}	Upper Limit	Lower Limit	Error
rpm		μm	μm	μm	μm	%
500	6	77.8	72.9	90.9	54.9	6.3
500	8	126.0	119.9	137.9	101.9	4.9
760	7	66.8	64.2	82.2	46.2	3.9
700	6	40.5	57.0	75.0	39.0	40.7
700	9	85.1	73.1	91.1	55.1	14.2
850	6	32.3	47.9	65.9	29.9	48.2
850	9	61.9	62.6	80.6	44.6	1.1

In order to put these results into perspective, the actual mean particle size results relative to the predicted model surface are shown in Figure 34 below. The complete particle size analysis of all the experimental validation points can be seen in Appendix I.
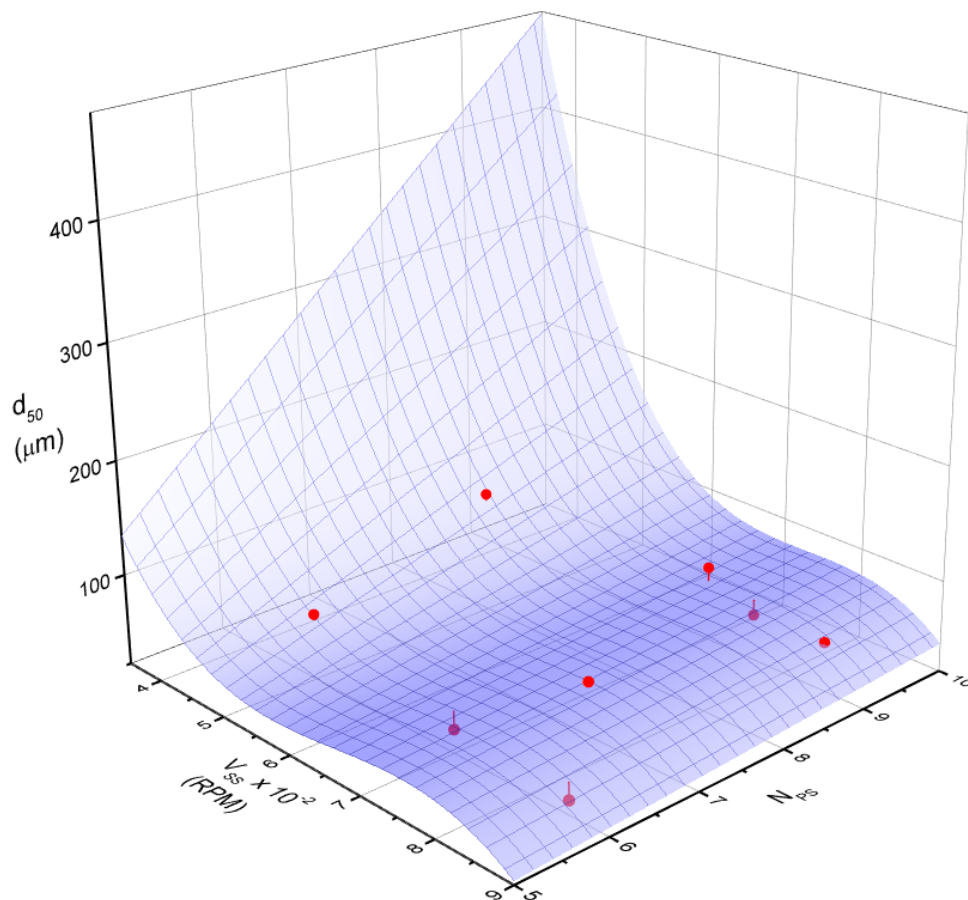

Figure 34: Validation experimental points plotted with predicted model

From Table 18 and Figure 34, it can be seen that the model predicts the mean microparticle size (d_{50}) very well. All the actual mean particle sizes fall within the predicted upper and lower boundaries. The model slightly over estimated the particle size for the microparticles formed at lower water addition rates with a calculated error of 40.7 % and 48.2 %, respectively. The reason for the error being so large is due the very small size of the microparticles in question; however, relative to the model as a whole, these points are still acceptable, as shown by Figure 34.

Therefore, the model described by Equation 6 can be used as a guide in terms of the formation of microparticles of a desired final mean microparticle size (d_{50}). The model can be used as an accurate guide to determine which parameters to use in order to achieve a specific region of kafirin microparticle formation. Specifically, the model regions as described in Table 16.

It is also important to note that the model is only valid within the set boundary conditions (Table 12). Namely for the range 350 rpm < V_{SS} < 900 rpm and 2.7 mL/min < R_{WA} < 5.4 mL/min at an acetic acid to kafirin ratio of above 6.8.

4.7. Qualitative Film Formation and Commercialisation Prospects

Some of the films produced can be seen in Figure 35 below. These films were made without dewatering the precipitated microparticles prior to the film formation step. No plasticiser was used for the production of these films however using plasticiser is possible if desired. The films below were the best quality films produced. All films made are shown in Appendix J.

Figure 35: Qualitative films produced without dewatering microparticles

As can be seen from Figure 35, kafirin microparticle based films can be made from solution after the water addition step, without requiring the dewatering step. It was indicated in literature that the glacial acetic acid concentration plays a vital role in the formation of kafirin microparticle films. Since the films were successfully formed it can be concluded that there was sufficient acetic acid in solution post microparticle precipitation for the films to be cast directly from the solution.

Thus, for the purpose of film forming, it is not necessary to dewater the kafirin microparticles prior to the film formation step. Removing the dewatering step in the large scale production of kafirin microparticles could not only have significant economic implications but also considerably reduce production times.

As discussed in Section 2.3, the kafirin microparticle films have been formed using individual microparticles as described by the third region in the proposed model. Since the model found different regions of microparticles, it was decided to investigate whether the agglomerated microparticles (the second region in the model) can also form films. This was done since the primary particle size of the agglomerated microparticles appears similar to that of the isolated microparticles. Figure 36 below shows the film produced from agglomerated kafirin microparticles as described by the second region in the proposed model. The film was not cast in a round petri dish but rather a flat tray. Once again no plasticiser was used.

Figure 36: Qualitative film produced from agglomerated microparticles

As can be seen from Figure 36, the attempt to make films from agglomerated microparticles was also successful. Therefore, for the purpose of producing kafirin microparticle films on a large scale setup, agglomerated kafirin microparticles can also be used. The implication being that moderate stirring speeds and water addition rates can be used for the microparticle precipitation, as opposed to very high stirring speeds and very low water addition rates. This results in even greater reduction in the time and energy requirements required to produce kafirin microparticle films. Ultimately, this could have the effect of reducing not only cost but also production times for a commercialised process.

5. Conclusions

An up-scaled process was established, which was capable of successfully extracting 2.5 kg of the kafirin protein from sorghum grain. This protein had a purity of at least 80 % after defatting and provided a consistent base raw material which could then be used for further study.

Investigation of the solubilisation time required for the blended kafirin protein showed that a 3 h solubilisation time instead of a 16 h solubilisation time produced better quality microparticles. Furthermore, it was concluded that a higher acetic acid to kafirin ratio enhanced the mixing efficiency of the solution, which, in turn considerably improved the quality of microparticles formed.

The partial factorial experiments emphatically confirmed that the greatest contributing factor determining the final precipitated protein particle size is the ratio of glacial acetic acid to kafirin. This was found to be true for defatted and non-defatted kafirin extracted from red sorghum, as well as kafirin extracted from white sorghum. The use of ethanol to solubilise the protein failed under regular conditions and was deemed extraneous for the purpose of an up scaled process.

The analysis of the protein secondary structure concluded that the precipitation of the protein by means of water addition altered the secondary structure of the protein. When kafirin microparticles are formed, the α-kafirin structure is noticeable, however, when mass protein agglomeration occurs the β-kafirin structure becomes more prominent. Additionally, it was noted that the defatting process undesirably altered the protein secondary structure by increasing the amount of β-kafirin present.

In order to form high quality microparticles, it was concluded to only use a high mass ratio of acetic acid to kafirin protein (three times higher than the prescribed ratio) due to the substantial role of the ratio. At this higher ratio of acetic acid to kafirin protein, the mean particle size of the kafirin microparticles was notably affected by the stirring speed and water addition rate during precipitation. An increase in stirring speed resulted in a nonlinear decrease in mean particle size, while an increase in water

addition rate resulted in an almost linear increase in particle size. The mean particle size of the precipitated kafirin microparticles can be related to the stirring speed and water addition rates directly by the following expression:

$$d_{50} = -809 + 2.2\,V_{SS} - (1.4 \times 10^{-3})\,V_{SS}^2$$
$$+ \frac{(R_{WA} - 0.054)}{(0.535)}[377 - 1.4\,V_{SS} + (1.7 \times 10^{-3})\,V_{SS}^2 - (7 \times 10^{-4})\,V_{SS}^3]$$

The model realistically predicted mean precipitated particle size (d_{50}) for a given stirring speed (V_{SS}) and water addition rate (R_{WA}). The model was validated by successfully predicting the particle size for a series of points, all of which fell within the expected range of ± 18 µm. However, the model is only valid for the range 350 rpm < V_{SS} < 900 rpm and 2.7 mL/min < R_{WA} < 5.4 mL/min at an acetic acid to kafirin ratio of above 6.8.

Analysis of the kafirin microparticle morphology in conjunction with the above model clearly identifies three distinct regions of precipitated protein particles. The first region which consists of large particles (above 200 µm) at low stirring speeds and high water addition rates is crosslinked protein which has begun to mass agglomerate. The second region which consists of moderate particles (around 100 µm) at moderate stirring speeds and moderate water addition rates appears to be agglomerated microparticles. Finally, the microparticles in the third region which consists of small particles (around 20 µm) at high stirring speeds and low water addition rates are clearly the primary individual kafirin microparticles.

Considering the prospective commercialisation of an up scaled process, it is vital to bear in mind the intended application of the kafirin microparticles. When the intended application is to form microparticle based films the microparticle dewatering step can be disregarded entirely. This notion was confirmed by the qualitative production of films completely disregarding the microparticle dewatering step. Also, when considering the production of kafirin microparticle films, additional qualitative films were made using agglomerated microparticles (identified as region 2) signifying further potential economical and practical process improvements.

6. Recommendations

Although the larger scaled extraction of prolamin protein was successful, it is recommended that a higher quality starting grain be used for future protein extractions. The particular red sorghum flour used as starting material was of poor quality, which resulted in many complications during processing. The high fat content drastically lowered the final protein purity and clogged the filter during processing.

It is further recommended that, for forming microparticles, the defatting of kafirin protein is altogether avoided since the procedure negatively impacts the protein secondary structure. However, if the protein does have an unacceptably high fat content, it is recommended that the fat is naturally separated in the solution from the kafirin during precipitation of the protein.

Finally, for film formation, it is recommended that a quantitative rather than qualitative study of the film properties and morphology be conducted. Specifically focusing on the films produced of varying microparticle size. Using the final model provided, it is recommended to conduct a detailed comparison of microparticle films produced from the various regions identified in the final model. It is suspected that the films made from singular microparticles could yield more flexible and transparent films while those made from the agglomerated microparticles may yield higher strength films.

7. References

Anyango, JO (2013) "Preparation of KEMS films", Personal Communication, Department of Food Sciences, The University of Pretoria.

Belton, PS, Delgadillo, I, Halford, NG. and Shewry, PR. (2006) "Kafirin structure and functionality", *Journal of Cereal Science*, (44), pp.272-286.

Coates, J (2000) "Interpretation of Infrared Spectra, A practical approach", *Encyclopedia of Analytical Chemistry*, R.A. Meyers Ed, John Wiley & Sons Ltd, Chichester, pp 10815-10837.

Da Silva, MF (2012) *Dewatering of Kafirin Microparticles,* CSK 732 Literature review*, University of Pretoria.

Duodu, KG, Tang, H, Grant, A, Wellner, N, Belton, PS and Taylor, JRN (2001) "FTIR and Solid State ^{13}C NMR Spectroscopy of Proteins of Wet and Cooked and Popped Sorghum and Maize" *Journal of Cereal Science,* 33, 261-269.

El Nour, I, Peruffo, A and Curioni, A (1998) "Characterisation of sorghum kafirins in relation to their cross-linking behaviour", *Journal of Cereal Science,* 28, 197-207.

Emami, S, Tabil, LG and Tyler, RT (2010) "Performance comparison of two media during starch-protein separation of chickpea flour using a hydrocyclone", *Journal of Food Process Engineering,* 33(4), 728-744.

FAO (Food and Agriculture Organization of The United Nations), (1995). Sorghum and millets in human nutrition. FAO Food and Nutrition Series. Rome.

Galli, L, Esposito, P, Segale, L, Giovannelli, L, Pattarino, F and Danan, H (2011) "Process for dewatering of product powders and pharmaceutical compositions according to this process", *EP Patent 2 298 286 A1*, assigned to Messer Italia, IT.

Gao, C, Taylor, J, Wellner, N, Byaruhanga, YB, Parker, ML, Clare Mills, EN and Belton, PS (2005) "Effect of Preparation Conditions on Protein Secondary Structure and Biofilm Formation of Kafirin" *Journal of Agricultural and Food Chemistry,* 53, 306-312.

Grain SA, (2012). *Physio-chemical characteristics and nutritional value of sorghum grain.* [online] Grain SA. Available at: http://www.grainsa.co.za/physio-chemical-characteristics-and-nutritional-value-of-sorghum-grain. [Accessed 12 January. 2015].

Guell, C and Davis, RH (1996) "Membrane fouling during microfiltration of protein mixtures" *Journal of Membrane Science,* 119, 269-284.

Guy, JL, Massy, Le Pecq and Serveau, M (1993) "Centrifugal evaporator-concentrator for concentrating specimens by evaporation of the solvent", *US Patent 5,217,572* , assigned to Jouan, Saint-Nazaire, France.

Hamaker, B., Mertz, E. and Axtell, J. (1994). "Effect of extrusion on sorghum kafirin solubility" *Cereal chemistry*, 71, pp.515--515.

ISO 13320:2009 "Particle size analysis – Laser diffraction methods"

Kuberkar, VT and Davis, RH (2001) "Microfiltration of protein-cell mixtures with crossflushing or blackflushing" *Journal of Membrane Science,* 183, 1-14.

Marshall, AD, Munro, PA and Tragardh, G (1993) "The effect of protein fouling in microfiltration and ultrafiltration on permeate flux, protein retention and selectivity" *Desalination,* 91, 65-108.

Mishra, A., Tomar, A., Bansal, S., Khanna, V. and Garg, G. (2008) "Temporal and spatial expression analysis of gamma kafirin promoter from Sorghum" *Molecular biology reports*, 35(2), pp.81--88.

Mizutani, Y, Matsumura, Y, Imamura, K, Nakanishi, K and Mori, T. (2003) "Effects of water activity and lipid addition on secondary structure of zein in powder systems" *Journal of Agricultural and Food Chemistry*, 51, 229-235.

McCave, IN, Bryant, RJ, Cook, HF and Coughanowr, CA. (1986) "Evaluation of a laser-diffraction size analyser for use with natural sediments" *Journal of Sedimentary Research,* 56, 561-564.

Montgomery, DC (2013) *Design and Analysis of Experiments* 8th Ed. John Wiley & Sons Inc, New York.

Osborne, T (1924) *The vegetable proteins* 2nd Ed. London, Longmans, Green, and Co., New York.

Page AL (1982) Methods of soil analysis. Part 2. Chemical and microbiological properties, Soil Science Society of America, Madison

Paulis J.W, J.S Wall Distribution and electrophoretic properties of alcohol-soluble proteins in normal and high-lysine sorghums Cereal Chemistry, 56 (1979), pp. 20–23

Pienaar, SW (2015) *Optimisation of Kafirin Extraction Parameters for Commercial Applications*, Masters dissertation*,* University of Pretoria.

Sorghum SA (available at: http://www.sorghumsa.co.za/sorghum-plant-seed.htm) [Accessed 14 May 2016]

Shevchenko, A, Wilm, M, Vorm, O and Mann, M (1996) "Mass Spectrometric Sequencing of Proteins from Silver-Stained Polyacrylamide Gels" *Analytical Chemistry,* 68, 850-858.

Taylor, J (2003) Master of Technology, Technikon Witwatersrand.

Taylor, J and Taylor JRN (2011) *Project to develop a pilot industrial scale process for the production of kafirin and kafirin encapsulating microstructures (KEMS) from sorghum spent grain,* Report to Intsormil, Department of Food Science, University of Pretoria.

Taylor, J, Anyango, JO, Taylor, JRN (2013) "Developments in the science of zein, kafirin and gluten protein bioplastic materials" *Cereal Chemistry,* 90(4), 344-357.

Taylor, J, Taylor, JRN, Belton, PS and Minnaar, A (2009a) "Formation of kafirin microparticles by phase separation from an organic acid and their characterisation" *Journal of Agricultural and Food Chemistry*, 57, 7523-7528.

Taylor, J, Taylor, JRN, Belton, PS and Minnaar, A (2009b) "Kafirin Microparticle Encapsulation of Catechin and Sorghurm Condensed Tannins" *Journal of Agricultural and Food Chemistry*, 57, 7523-7528.

Taylor, J, Taylor, JRN, Belton, PS and Minnaar, A (2009c) "Preparation of free-standing films from kafirin protein microparticles: Mechanism of formation and functional properties" *Journal of Agricultural and Food Chemistry*, 57, 6729-6735.

Taylor, JRN, Taylor, J, Dutton, MF and De Kock, S (2005) "Identification of kafirin film casting solvents" *Journal of Food Chemistry,* 32, 149-154.

Van Esch, F (1991) "The Efficiency of Hydrocyclones for the Separation of Different Starches" *Starch,* 43 (11), 427-431.

Wang, Q, Yin, L and Padua, GW (2008) "Effect of hydrophilic and lipohilic compounds on zein microstructures" *Food Biophysics,* 3, 174-181.

Wang, Y and Padua, GW (2012) "Nanoscale characterisation of zein self assembly" *Langmuir,* 28, 2429-2435

8. Appendix

Appendix A. Precipitated Protein Morphology Effect of C_{AA}
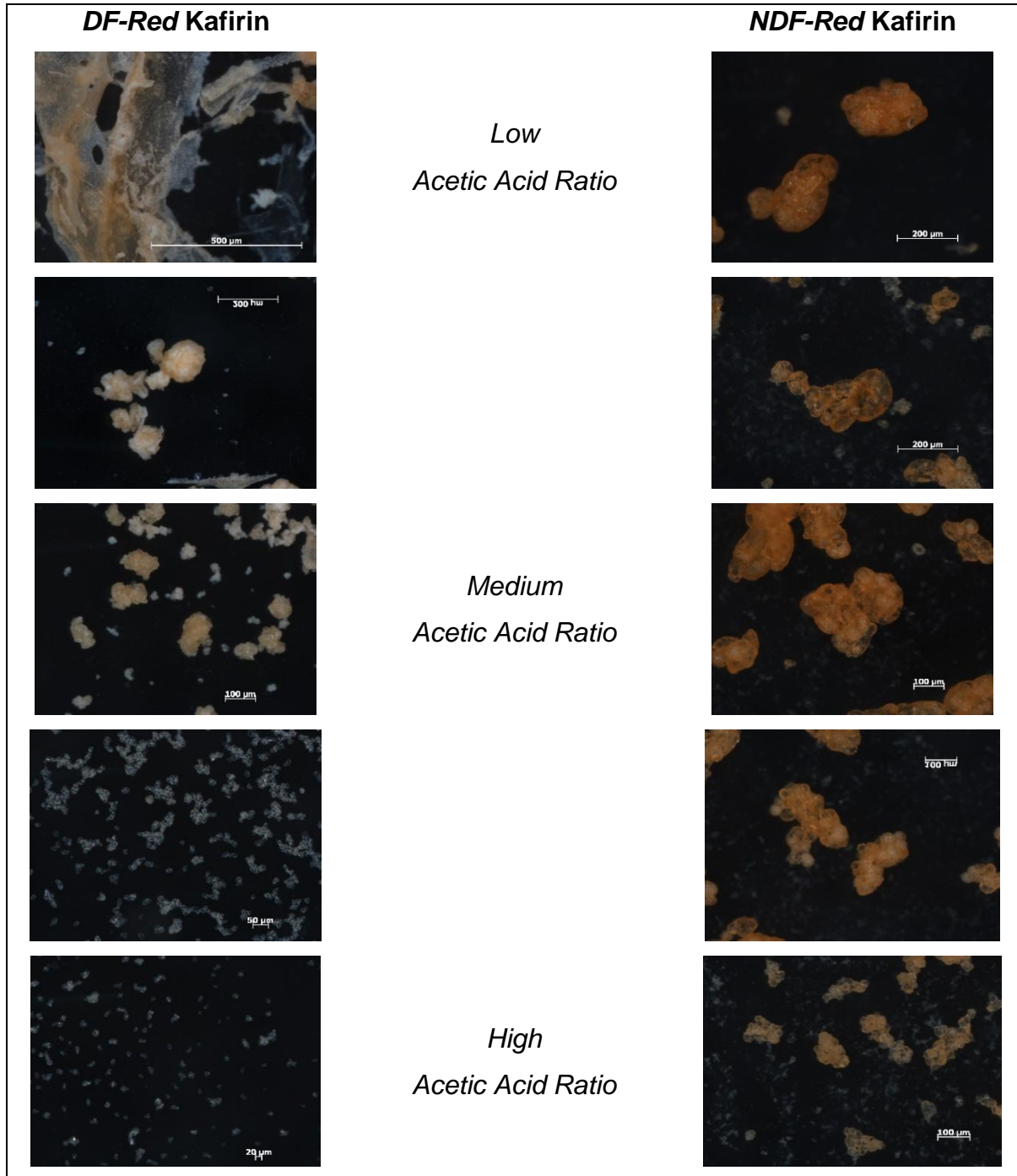
Figure 37: Morphology of starting material and microparticles formed using *DF-Red* and *NDF-Red* kafirin while varying C_{AA}

Appendix B. Solubility Experiments PSA
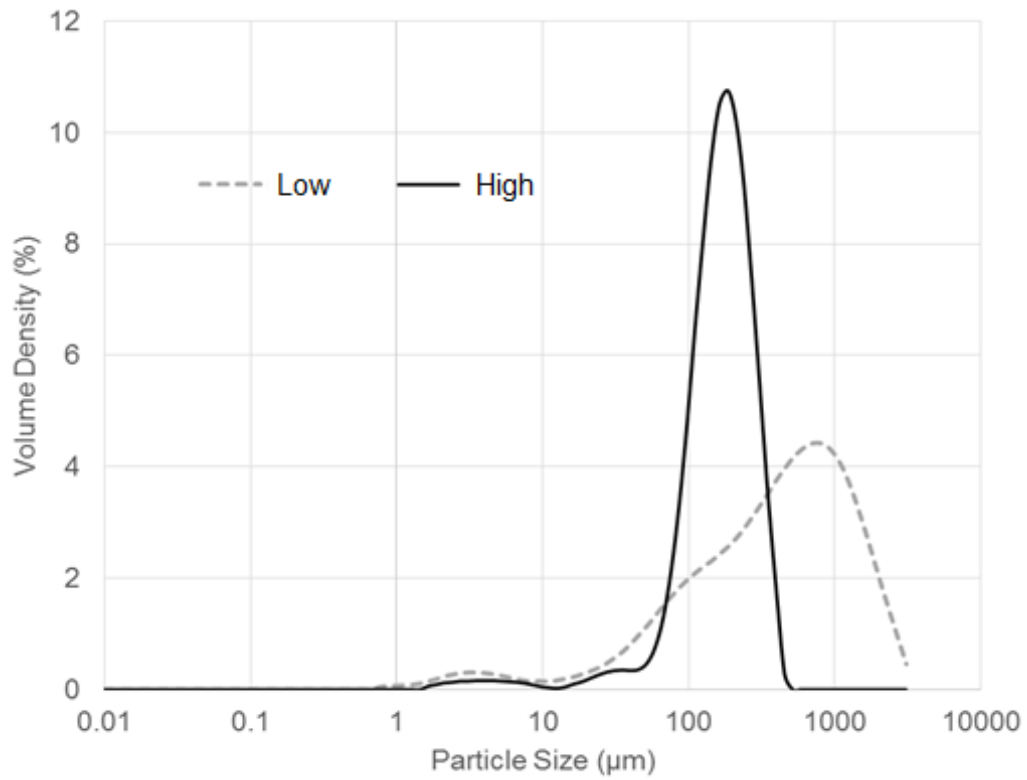
Figure 38: Particle size analysis for solubility PSA at 3 h
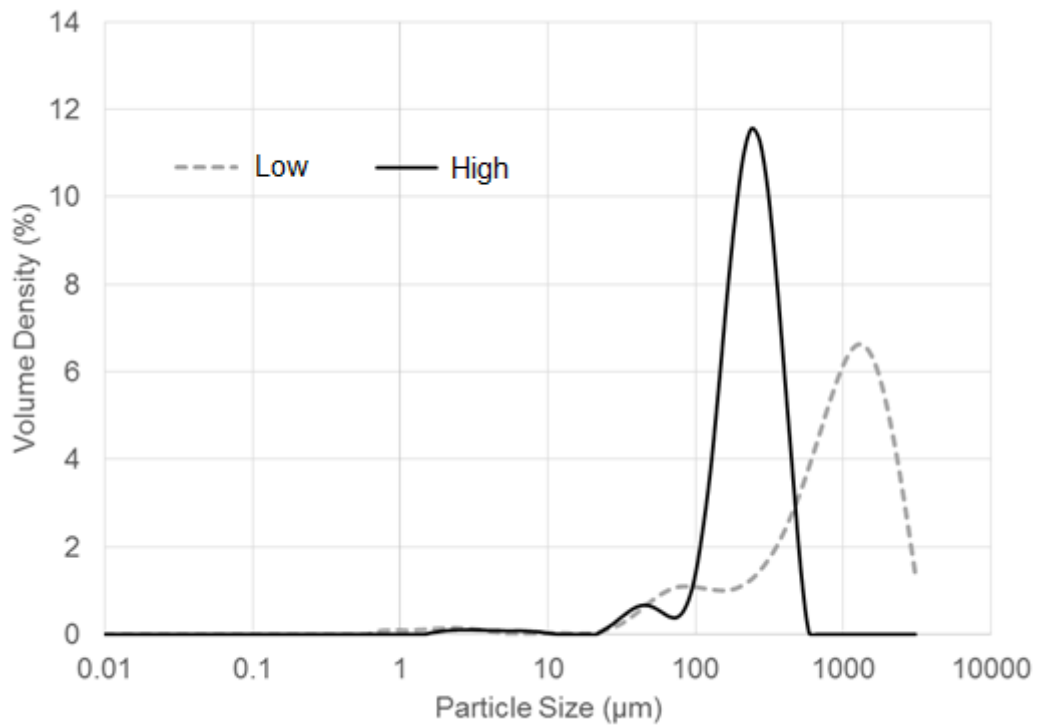
Figure 39: Particle size analysis for solubility PSA at 16 h

Appendix C. Peristaltic Pump Curve
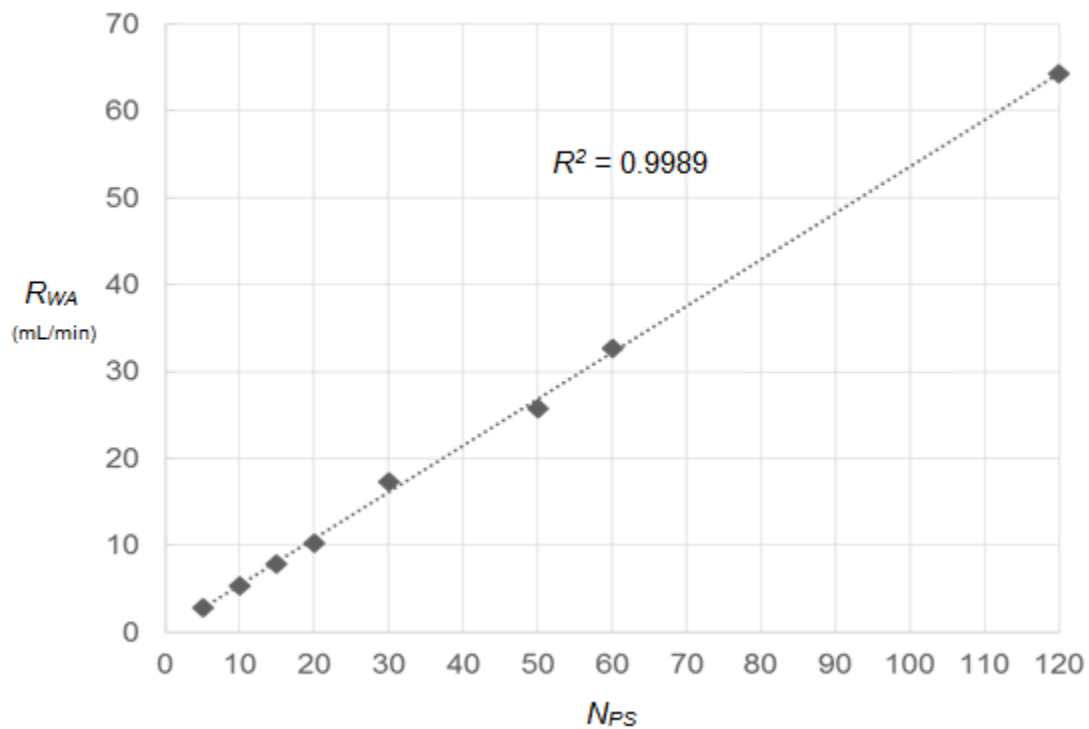
Figure 40: Water pump rate curve for the peristaltic pump

The above pump curve was a result of the calibration of a laboratory Watson Marlow peristaltic pump. Although the manual for the apparatus did have a correlation it was necessary to calibrate the pump since the correlation was no longer accurate. This is most likely due to a combination of factors such as changes of tubing, fouling and general wear and tear of the device. Therefore, it was necessary to perform a calibration in order to accurately correlate the number setting on the pump (N_{PS}) to a desired flow rate (R_{WA}).

The minimum N_{PS} and maximum N_{PS} was 5 and 120 respectively. This correlated to a minimum R_{WA} and maximum R_{WA} of 2.5 mL/min and 66.7 mL/min respectively.

Appendix D. Supplementary Results Screening Partial Factorial

D.1. *NDF-Red* and *DF-White* kafirin partial factorial experimental tables

Table 19: Particle size of *NDF-Red* kafirin during screening partial factorials

Experiment	C_{AA}	V_{SS}	R_{WA}	N_{WD}	d_{10} (µm)	d_{50} (µm)	d_{90} (µm)
1	L	L	L	L	46.0	206.0	877.0
2	L	L	L	H	25.6	152.0	682.0
3	L	H	H	L	34.2	174.0	1560.0
4	L	H	H	H	52.4	409.0	1630.0
5	H	L	H	L	26.7	156.0	870.0
6	H	L	H	H	8.2	85.6	549.0
7	H	H	L	L	7.9	26.5	67.5
8	H	H	L	H	9.2	28.7	101.0

Table 20: Particle size of *DF-White* kafirin during screening partial factorials

Experiment	C_{AA}	V_{SS}	R_{WA}	N_{WD}	d_{10} (µm)	d_{50} (µm)	d_{90} (µm)
1	L	L	L	L	115.0	948.0	2170.0
2	L	L	L	H	84.8	874.0	1980.0
3	L	H	H	L	65.3	936.0	2130.0
4	L	H	H	H	57.7	937.0	2170.0
5	H	L	H	L	1.2	34.1	233.0
6	H	L	H	H	2.4	56.6	375.0
7	H	H	L	L	17.3	30.9	55.2
8	H	H	L	H	18.8	33.3	58.4

D.2. *NDF-Red* and *DF-White* kafirin screening responses
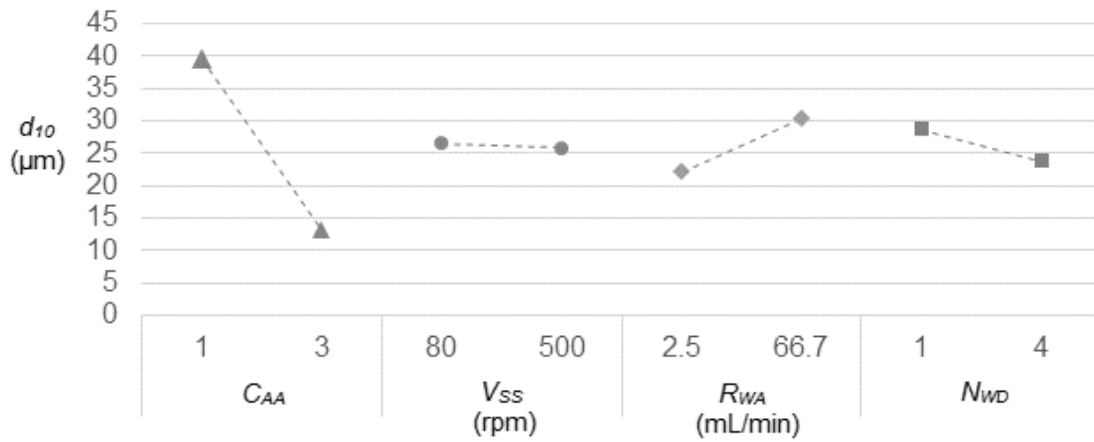
Figure 41: Screening partial factorial results (d_{10}) for *NDF-Red* kafirin
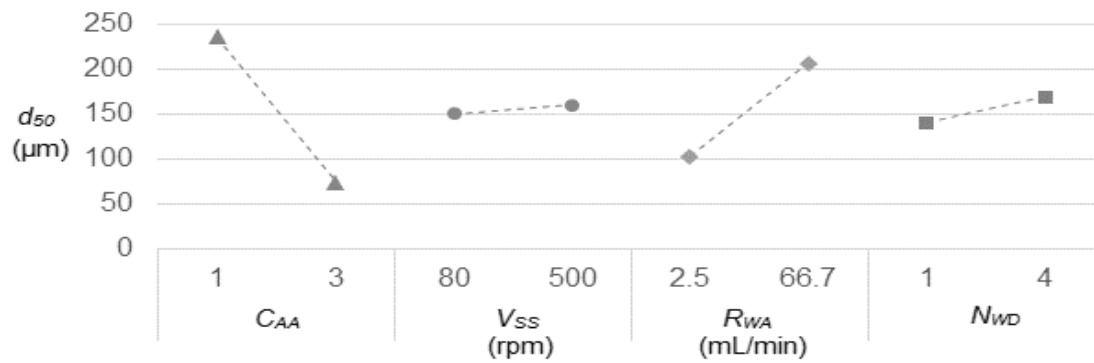
Figure 42: Screening partial factorial results (d_{50}) for *NDF-Red* kafirin
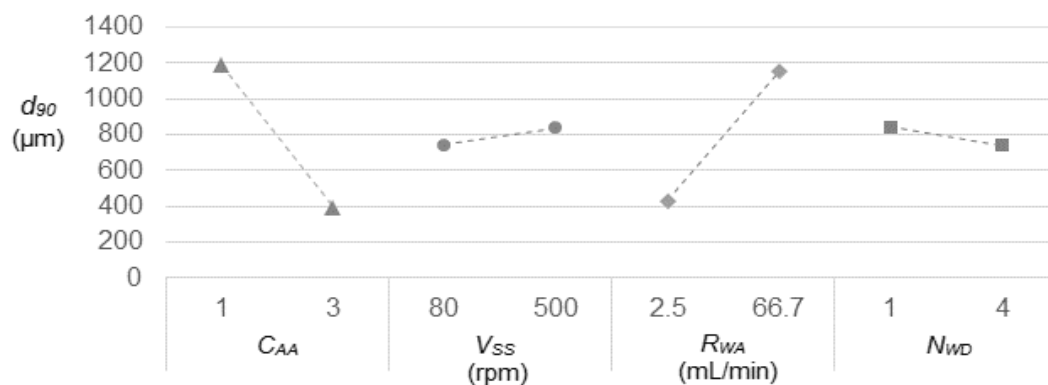
Figure 43: Screening partial factorial results (d_{90}) for *NDF-Red* kafirin
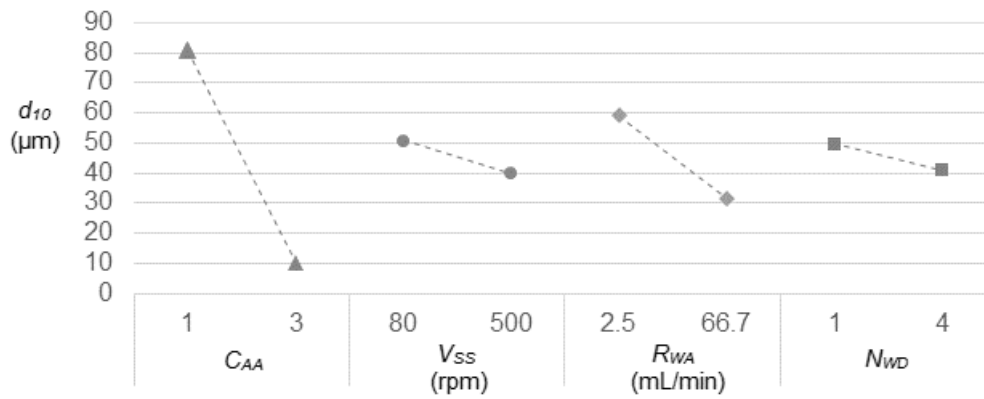
Figure 44: Screening partial factorial results (d_{10}) for *DF-White* kafirin
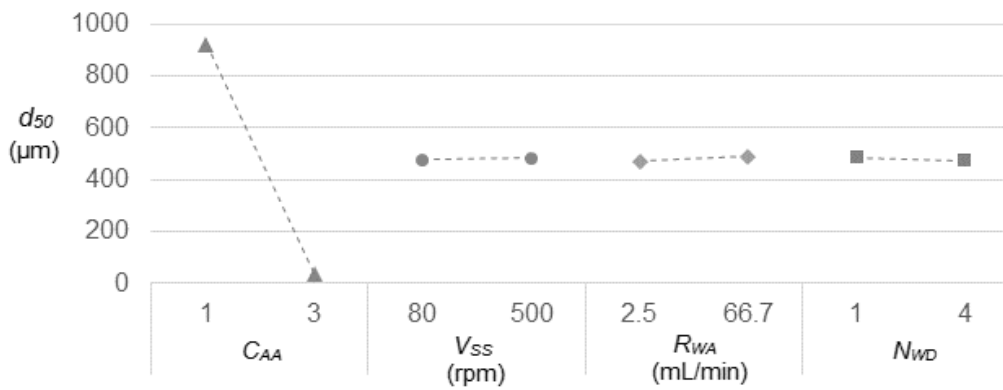
Figure 45: Screening partial factorial results (d_{50}) for *DF-White* kafirin
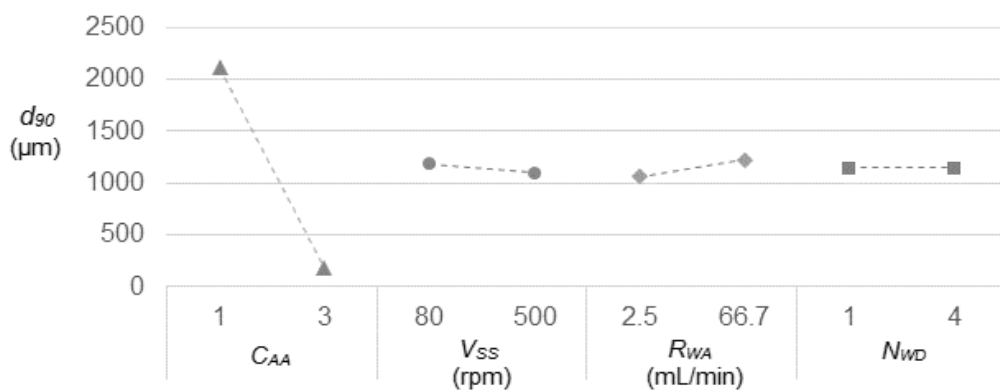
Figure 46: Screening partial factorial results (d_{90}) for *DF-White* kafirin

D.3. Comprehensive graphs for screening partial factorial experiments

D3.1. Solvent to protein ratio (C_{AA}) responses for experimental screening sets
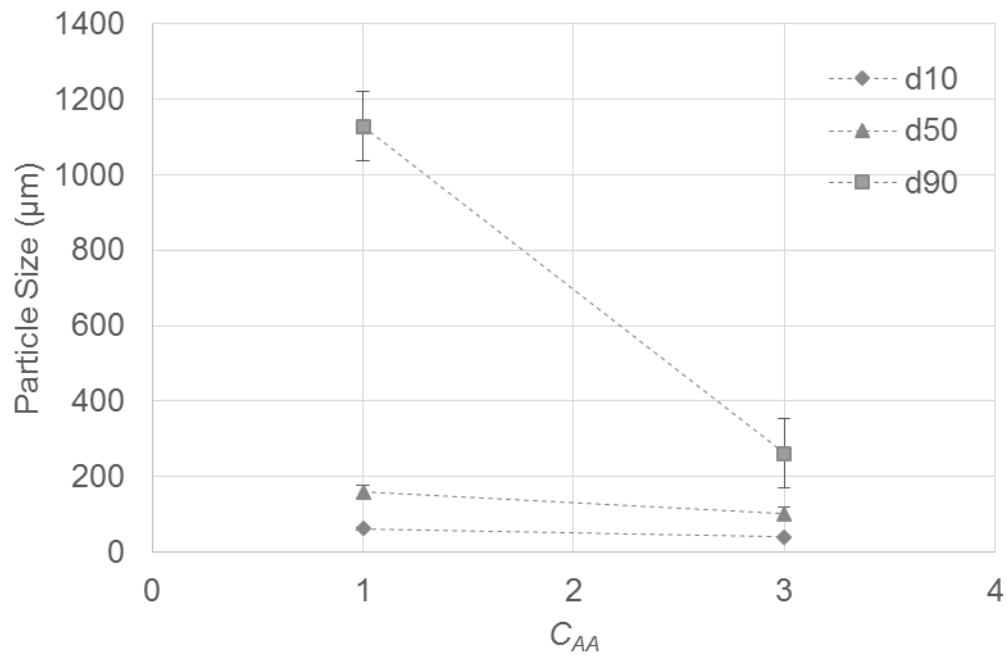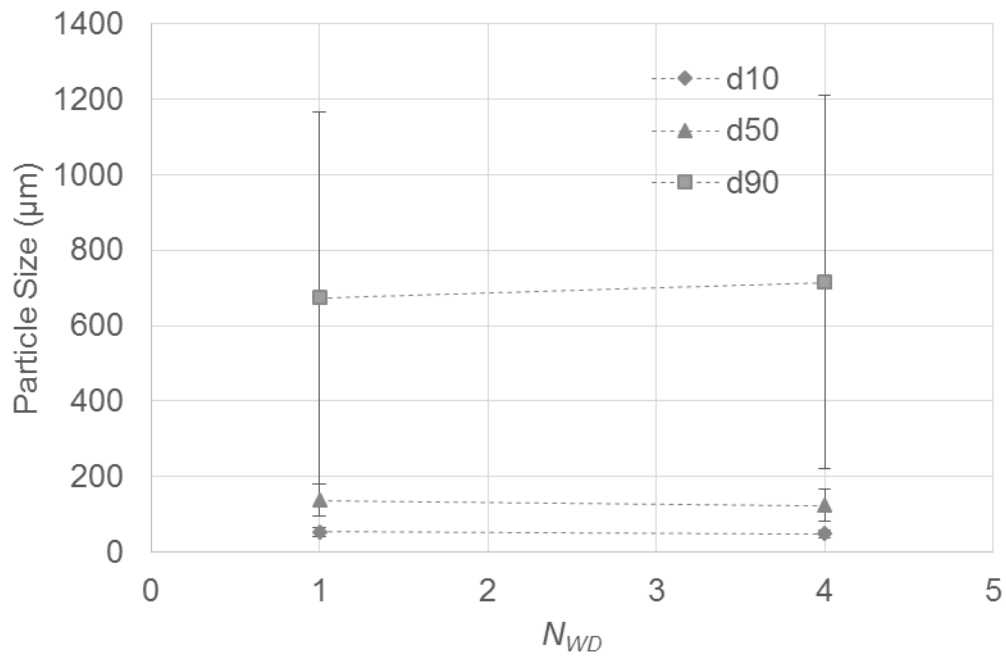

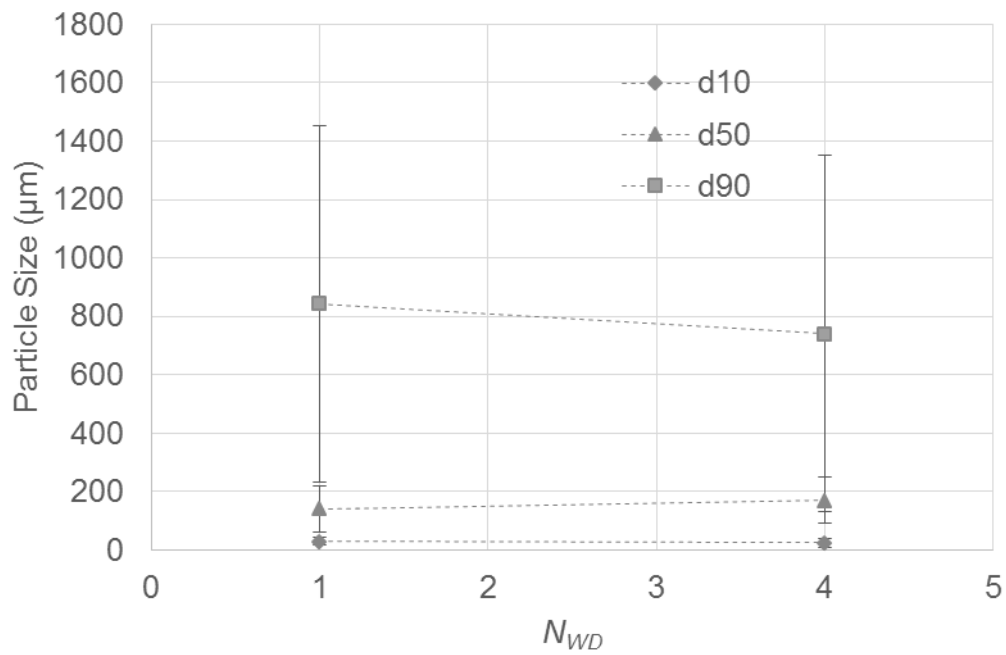Figure 47: Response of C_{AA} for *DF-Red* screening partial factorial set
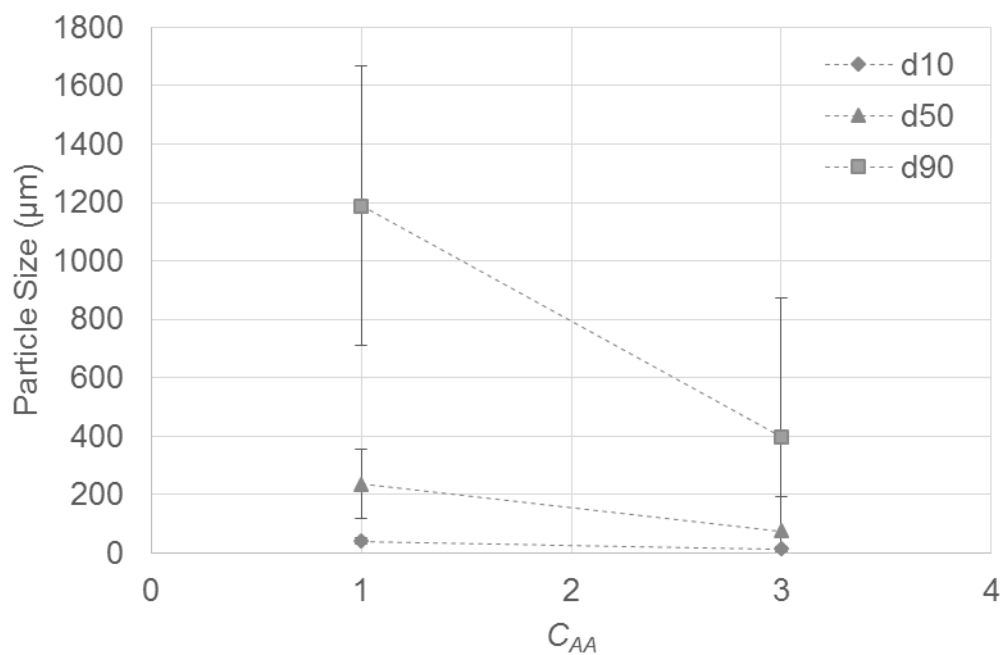
Figure 48: Response of C_{AA} for *NDF-Red* screening partial factorial set
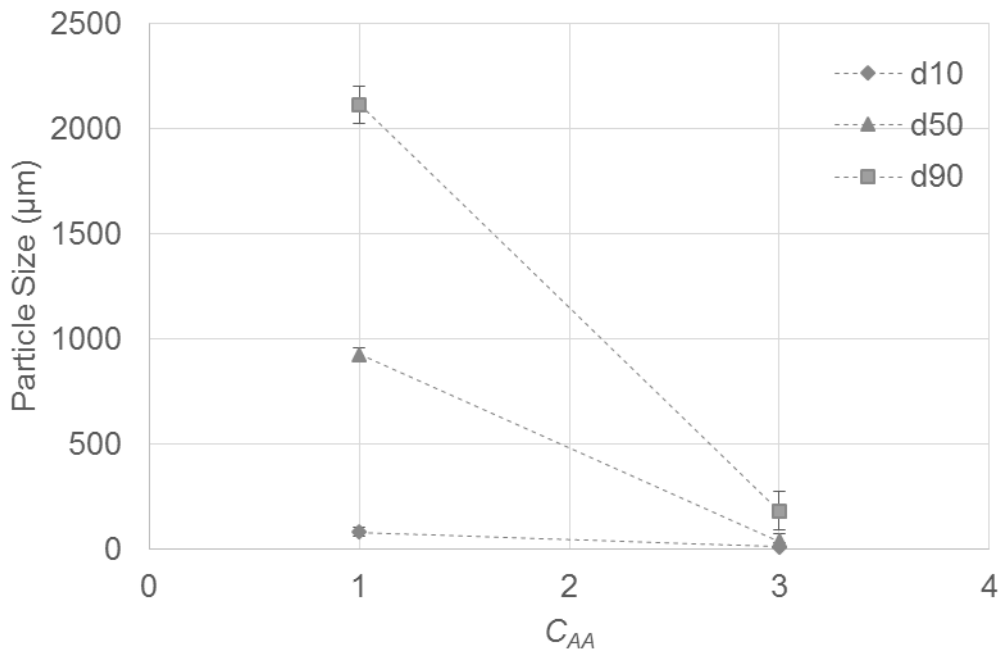
Figure 49: Response of C_{AA} for *DF-White* screening partial factorial set
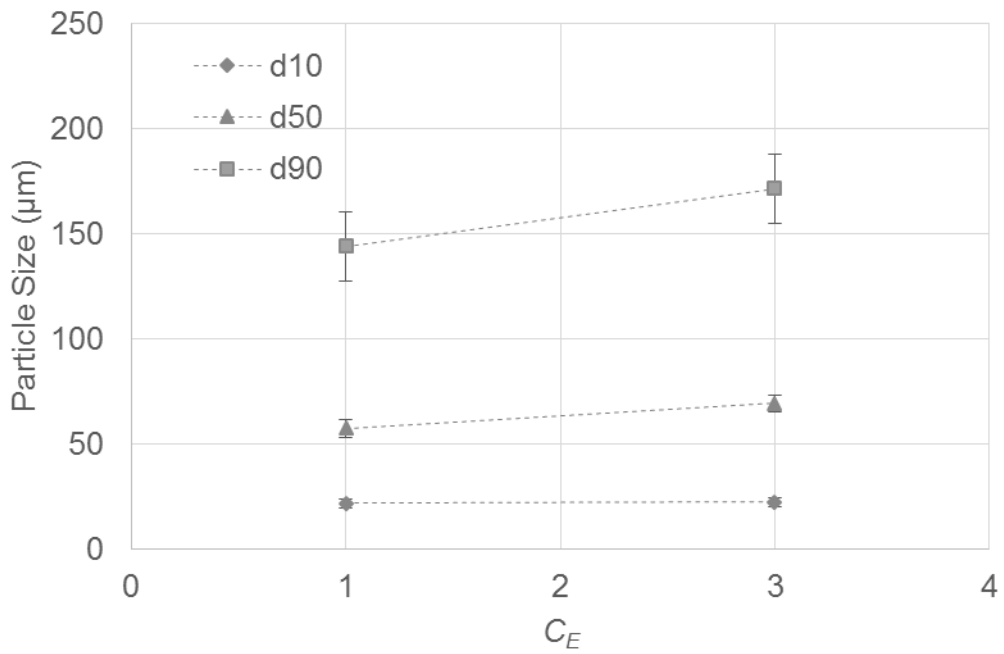
Figure 50: Response of C_E for *DF-Red* (ethanol) screening partial factorial set

D.3.2. Stirring speed (V$_{SS}$) responses for experimental screening sets
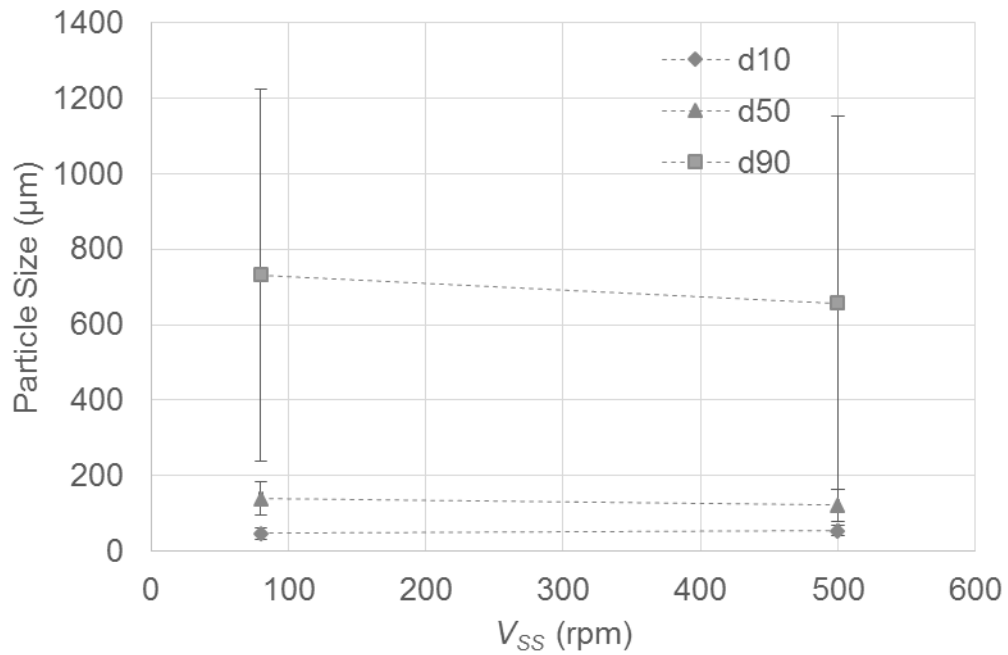
Figure 51: Response of V$_{SS}$ for *DF-Red* screening partial factorial set
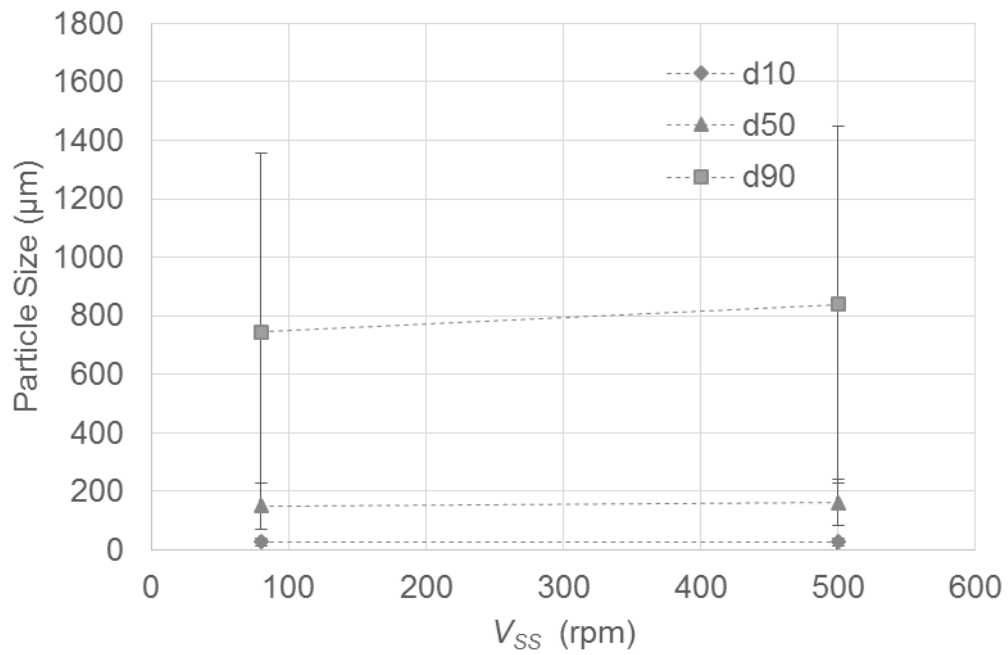
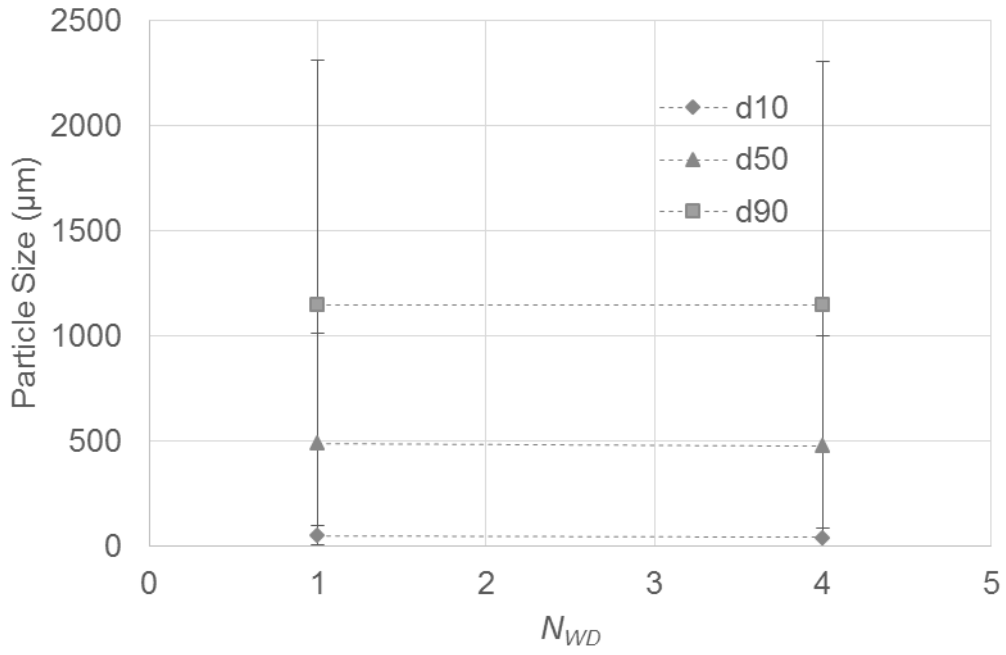Figure 52: Response of V$_{SS}$ for *NDF-Red* screening partial factorial set
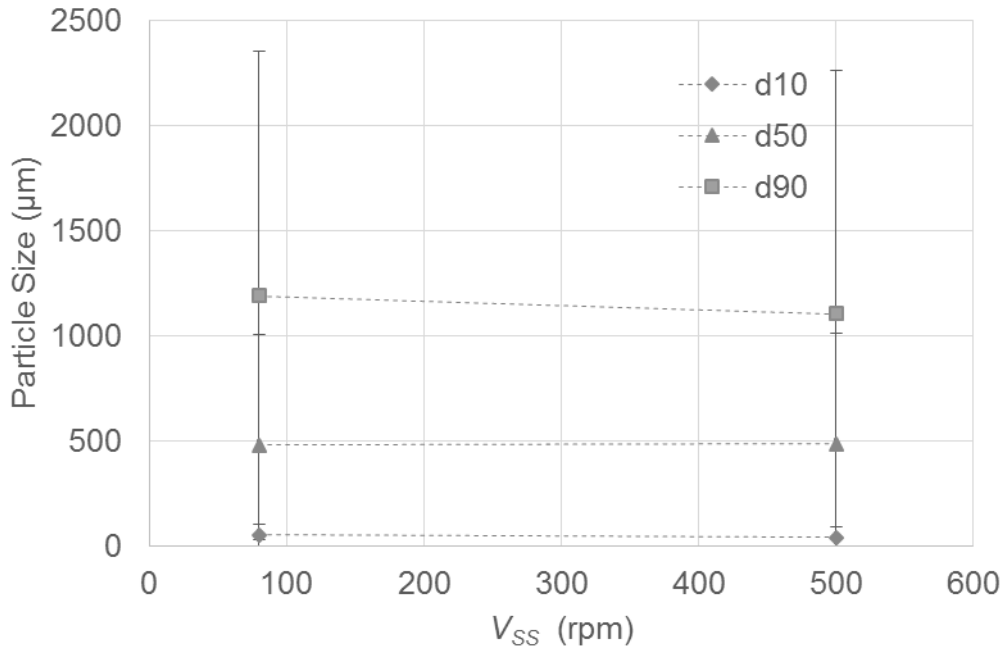
Figure 53: Response of V_{SS} for *DF-White* screening partial factorial set
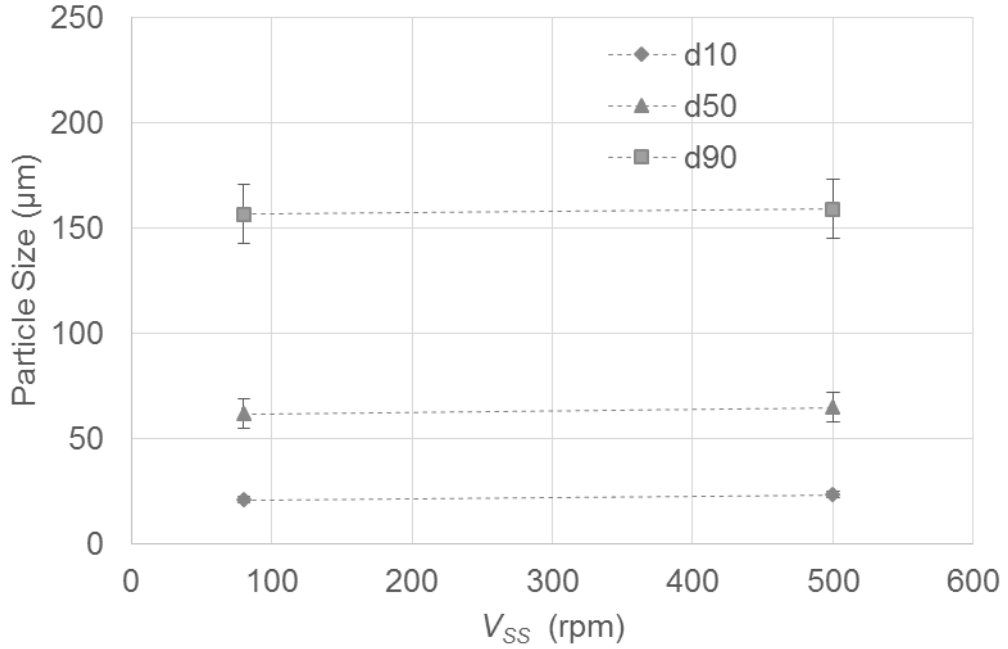
Figure 54: Response of V_{SS} for *DF-Red* (ethanol) screening partial factorial set

D.3.3. Water addition rate (R_{WA}) responses for experimental screening sets
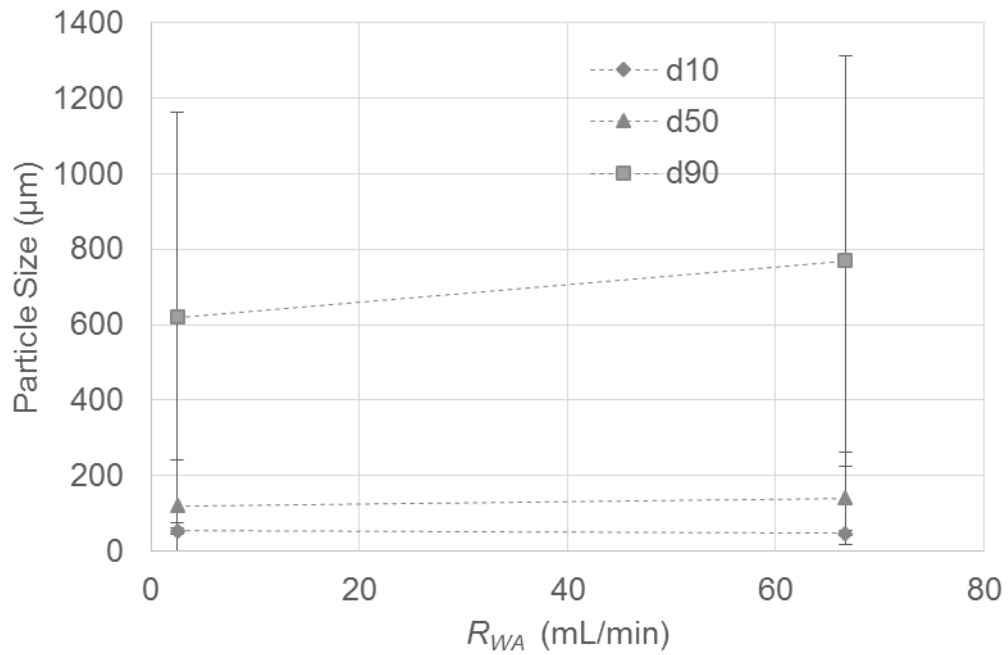
Figure 55: Response of R_{WA} for *DF-Red* screening partial factorial set
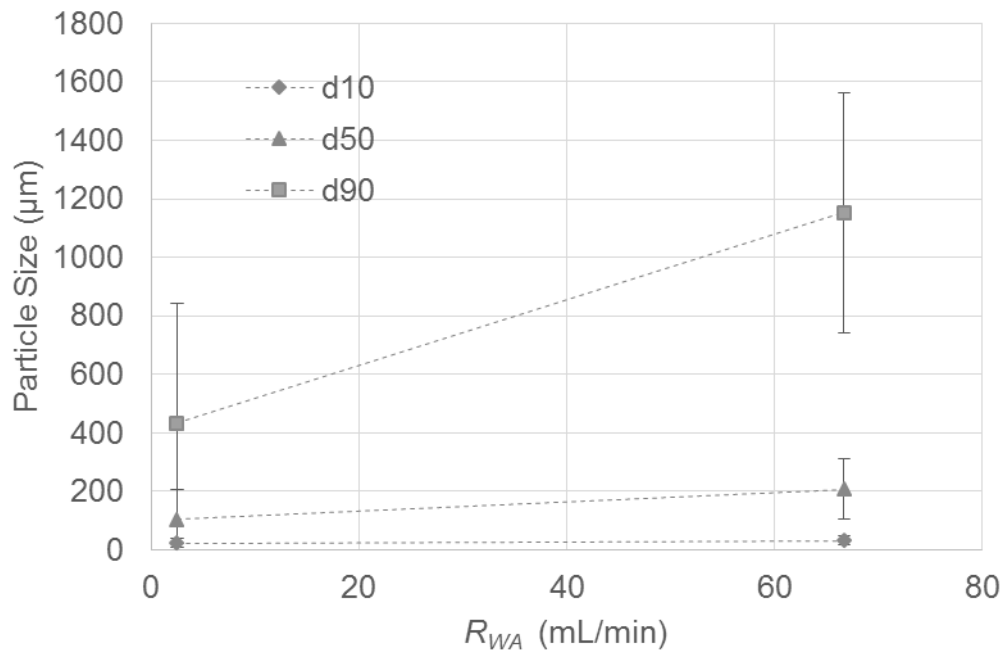
Figure 56: Response of R_{WA} for *NDF-Red* screening partial factorial set
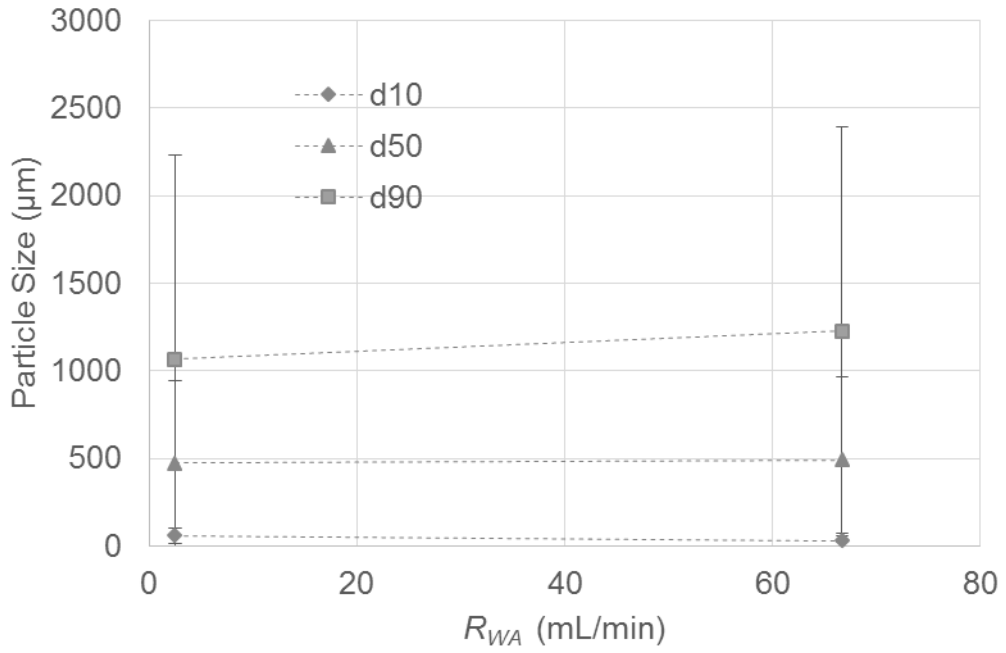
Figure 57: Response of R_{WA} for *DF-White* screening partial factorial set
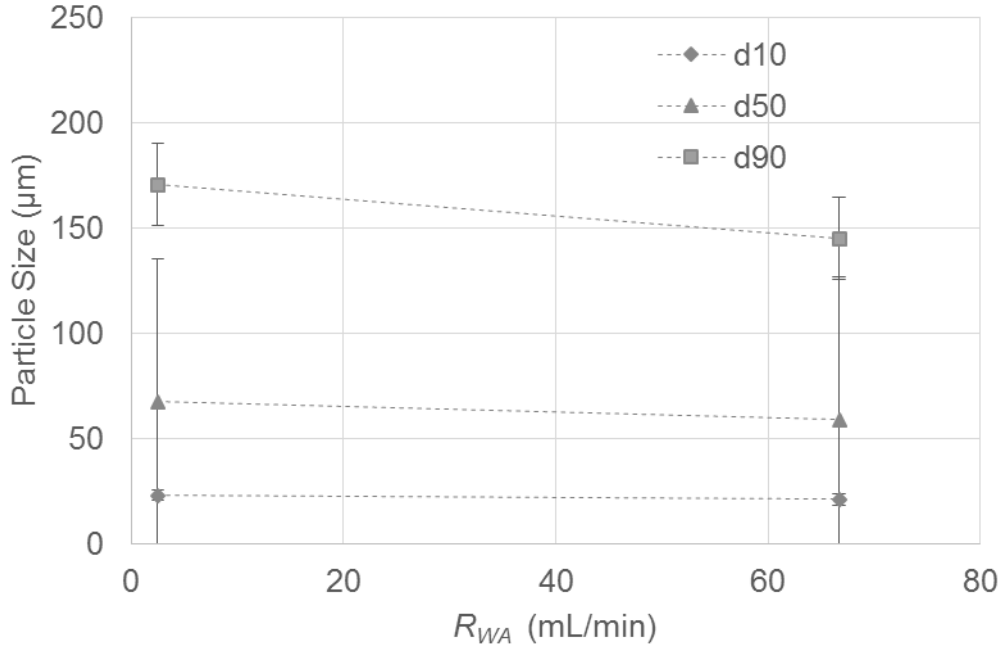
Figure 58: Response of R_{WA} for *DF-Red* (ethanol) screening partial factorial set

D.3.4. Number of water droplet (N$_{WD}$) responses for experimental screening sets

Figure 59: Response of N_{WD} for *DF-Red* screening partial factorial set

Figure 60: Response of N_{WD} for *NDF-Red* screening partial factorial set

Figure 61: Response of N_{WD} for *DF-White* screening partial factorial set
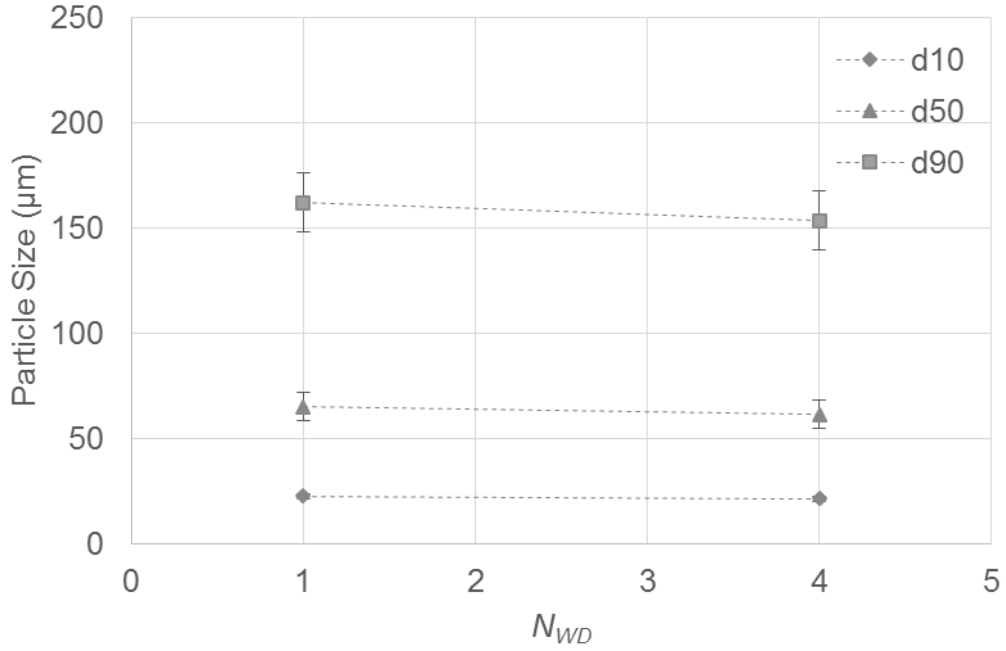
Figure 62: Response of N_{WD} for *DF-Red* (ethanol) screening partial factorial set

D.4. Raw material PSA comparison for screening partial factorial experiments
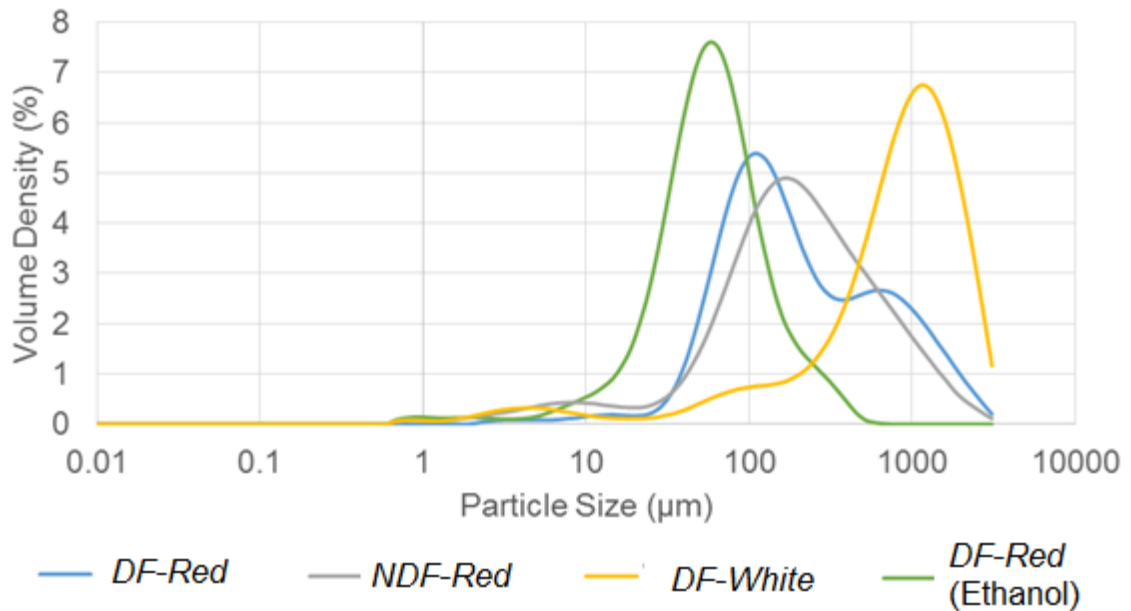
Figure 63: Combined PSA screening partial factorial experiment 1
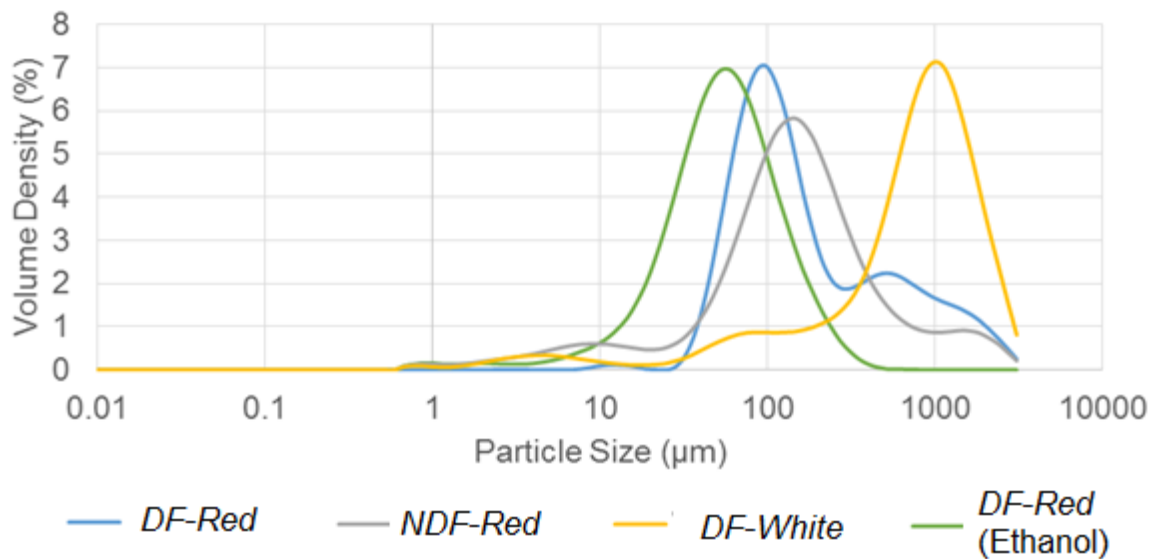
Figure 64: Combined PSA screening partial factorial experiment 2
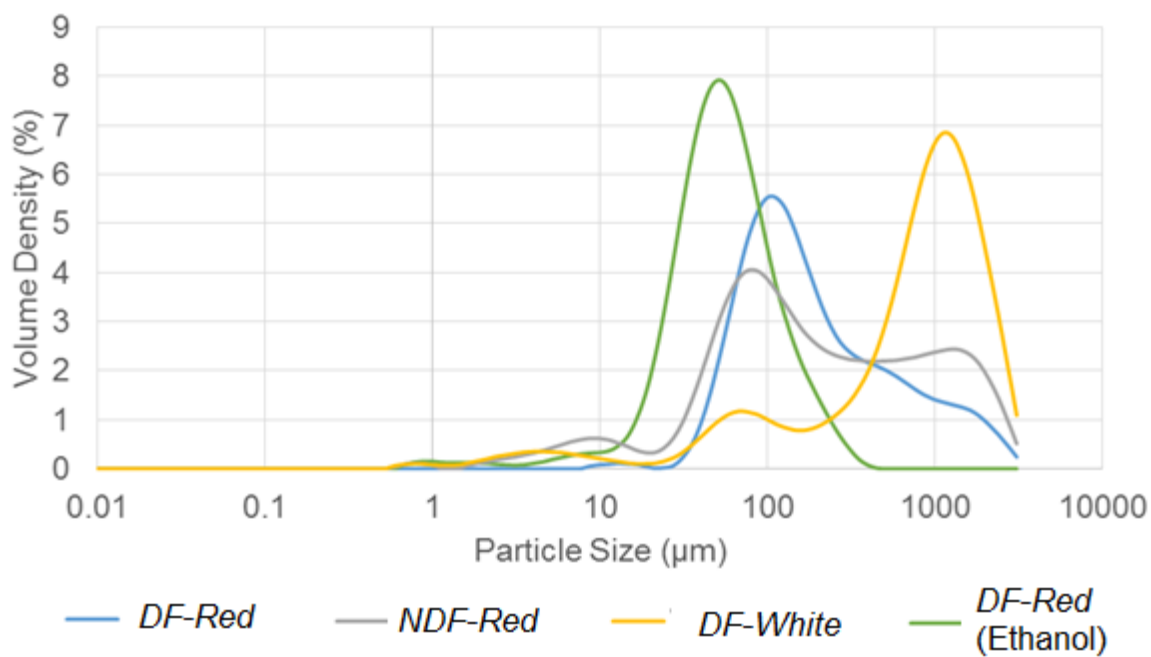
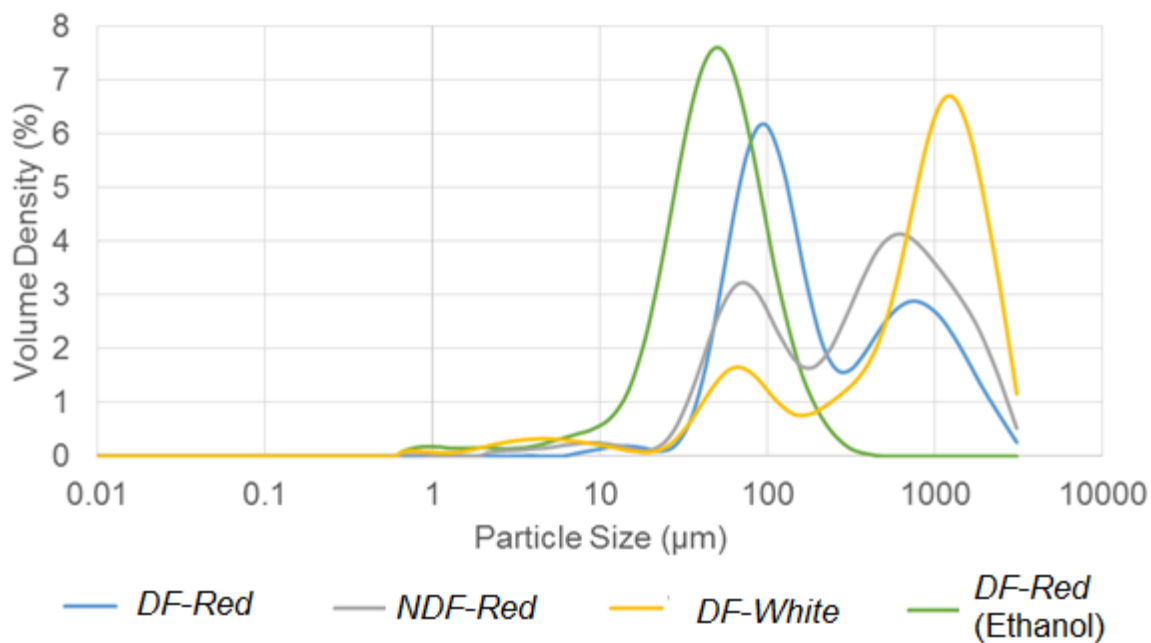Figure 65: Combined PSA screening partial factorial experiment 3

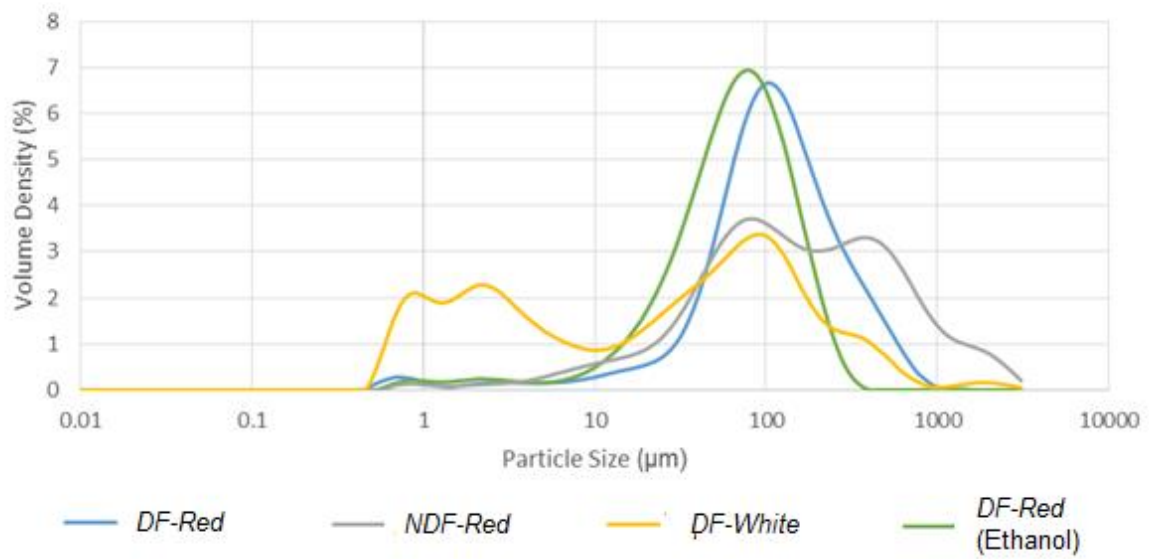Figure 66: Combined PSA screening partial factorial experiment 4

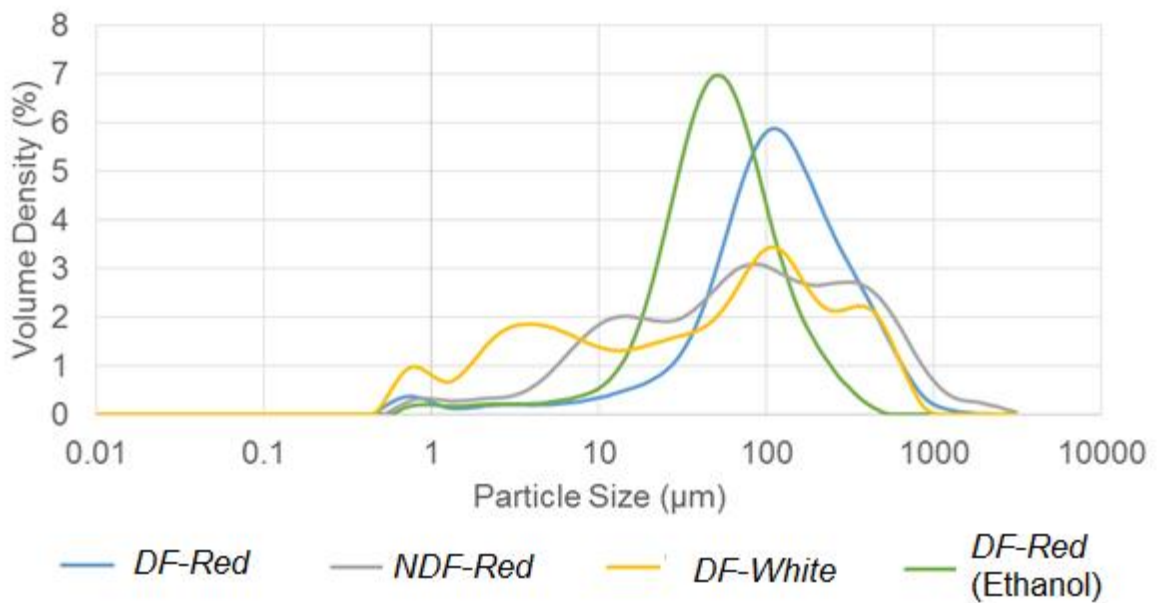Figure 67: Combined PSA screening partial factorial experiment 5

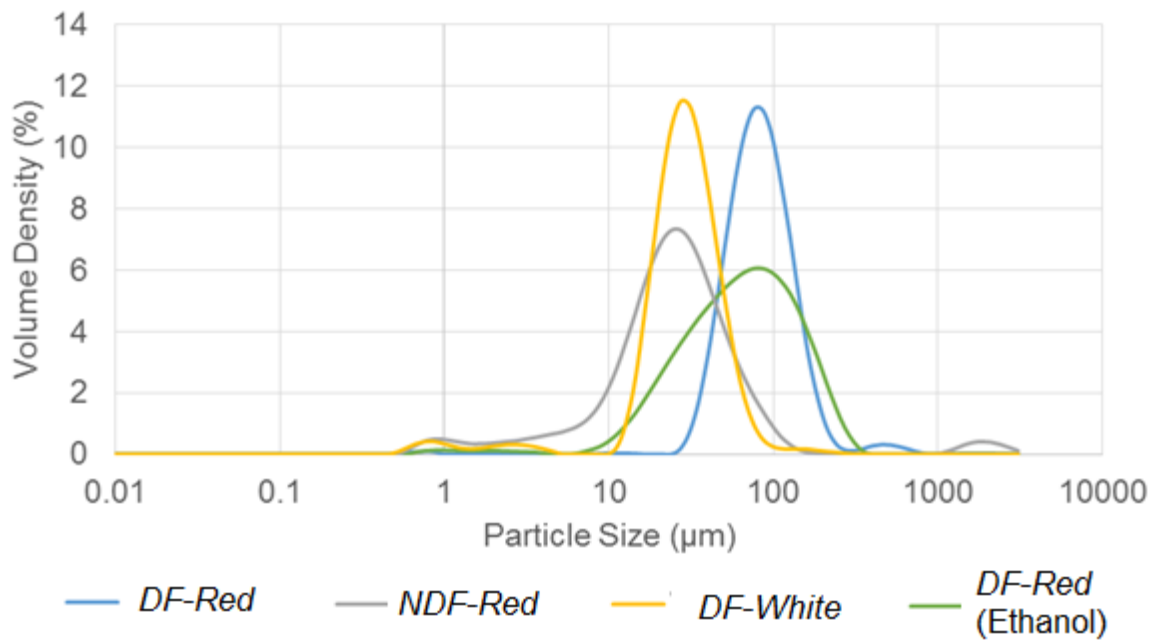Figure 68: Combined PSA screening partial factorial experiment 6

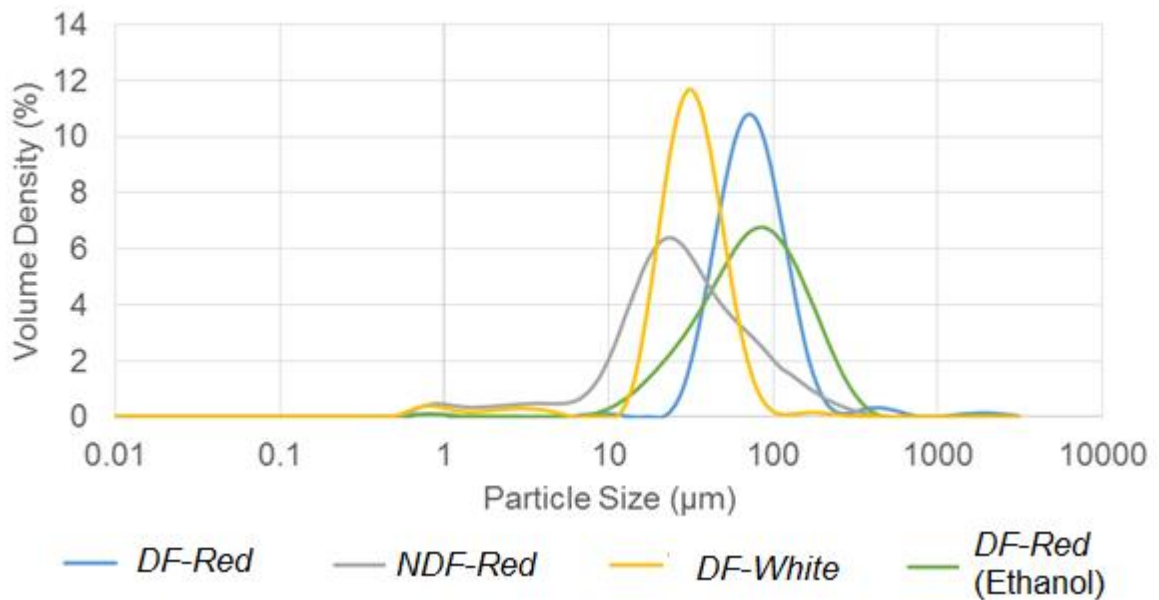Figure 69: Combined PSA screening partial factorial experiment 7

Figure 70: Combined PSA screening partial factorial experiment 8
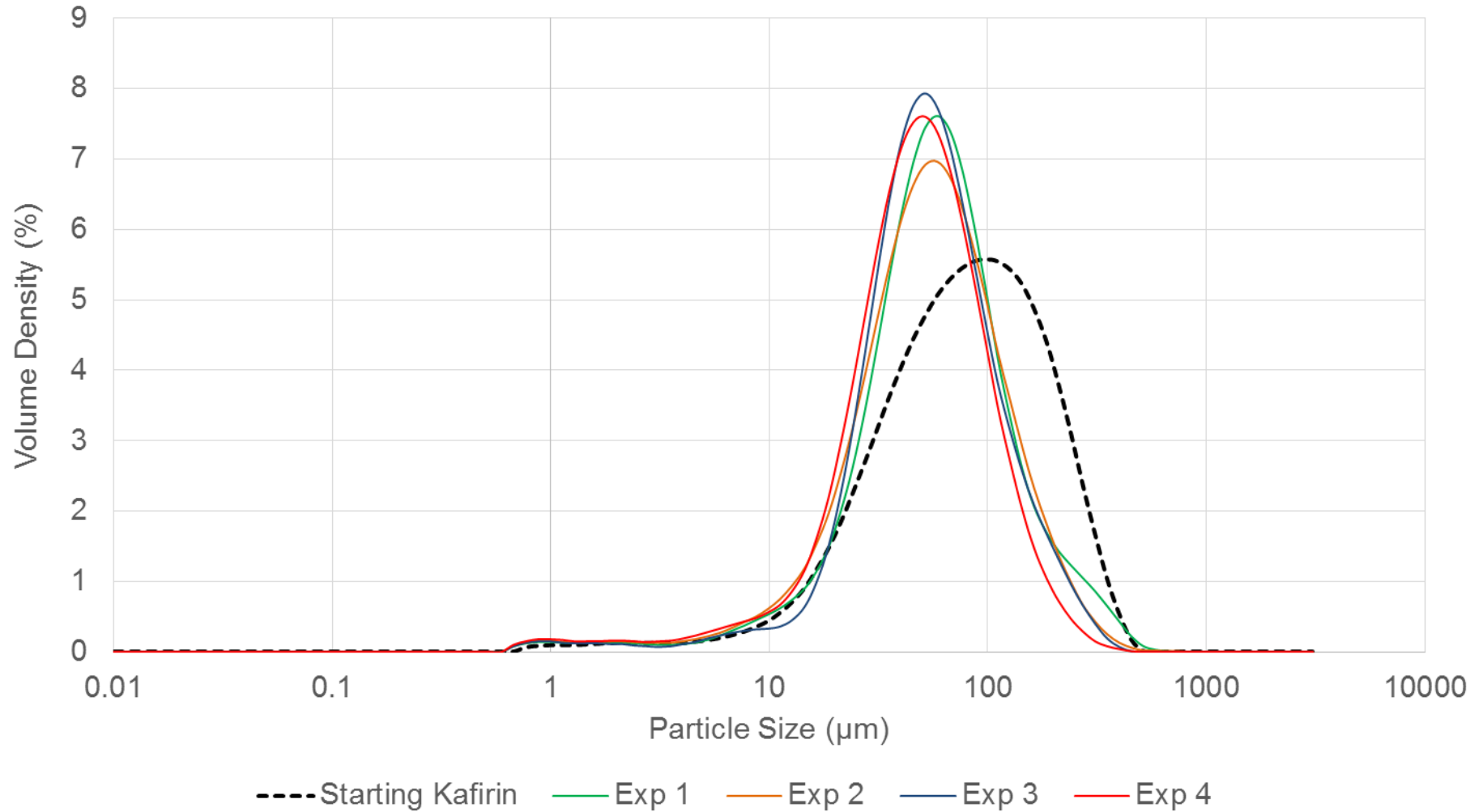
D.5. Ethanol based solubilisations PSA

Figure 71: Selected PSA of *DF-Red* kafirin in ethanol solvent screening partial factorial experiments

Appendix E. Complete FTIR Analysis for protein secondary structure
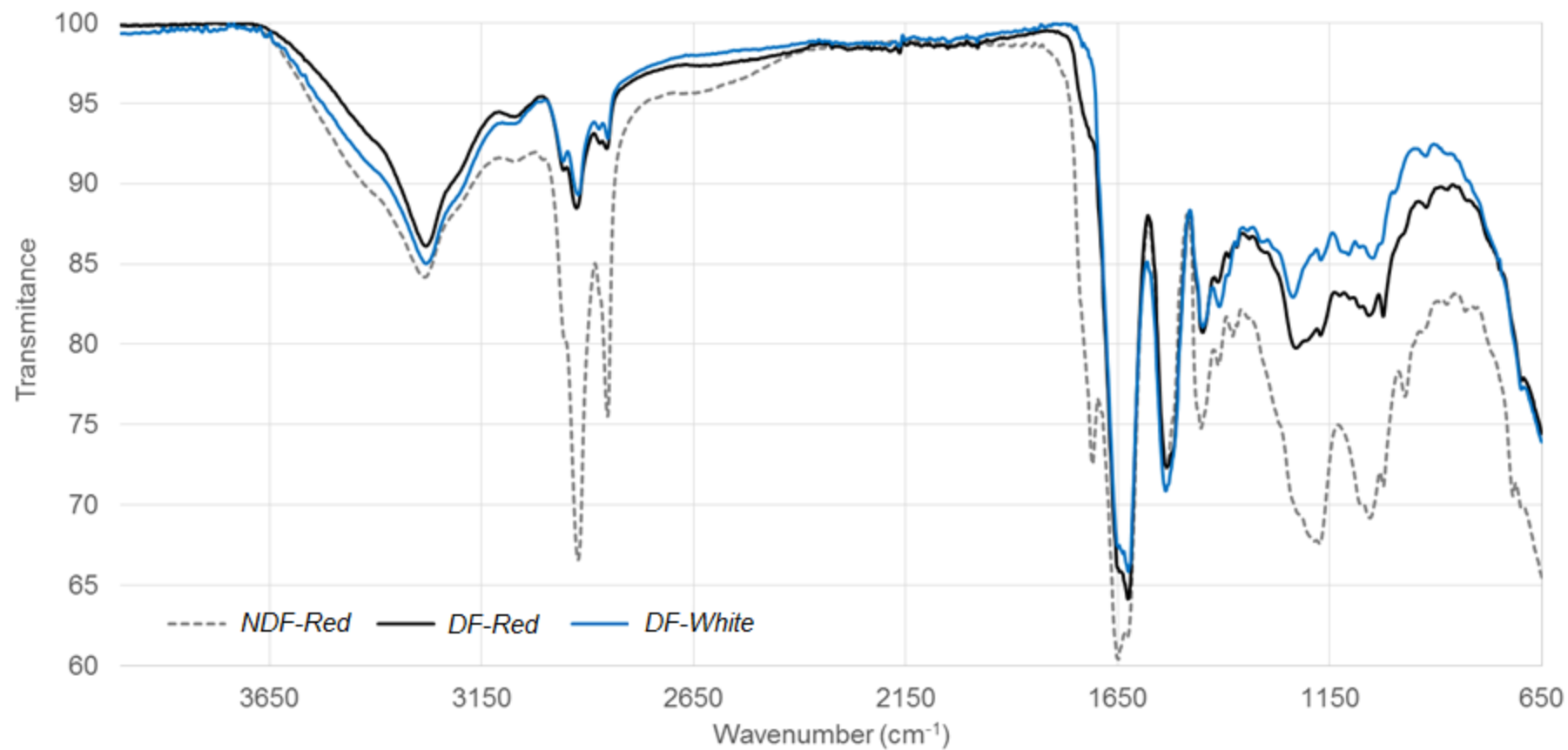
E.1. Complete FTIR scan of starting materials kafirin

Figure 72: Complete FTIR scan of starting material kafirin

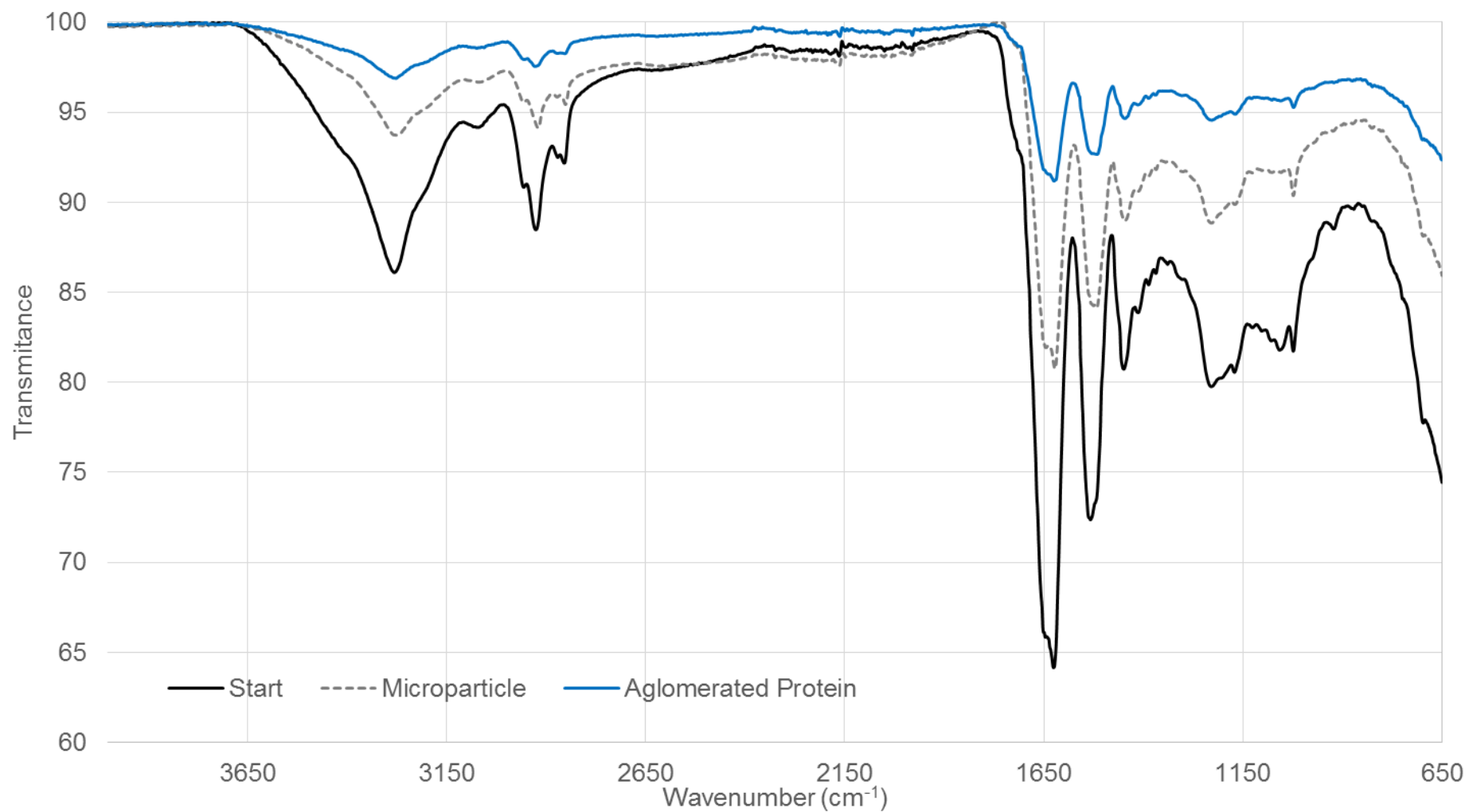**E.2. Complete FTIR scan of processed proteins produced from *DF-Red* kafirin**

Figure 73: Complete FTIR scan of the processed proteins made from *DF-Red* kafirin

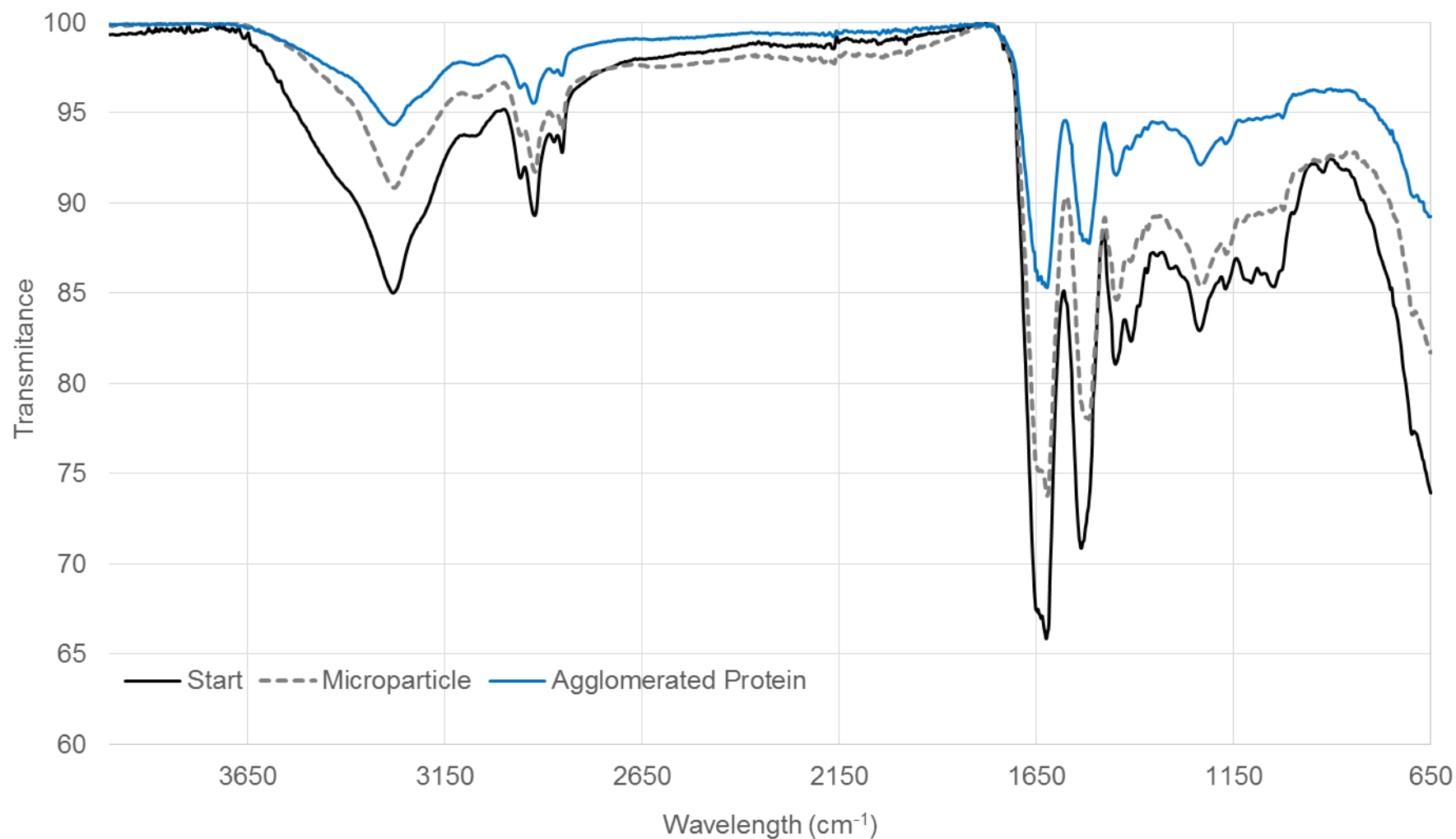## E.3. Complete FTIR scan of processed proteins produced from *DF-White* kafirin

Figure 74: Complete FTIR scan of the processed proteins made from *DF-White* kafirin

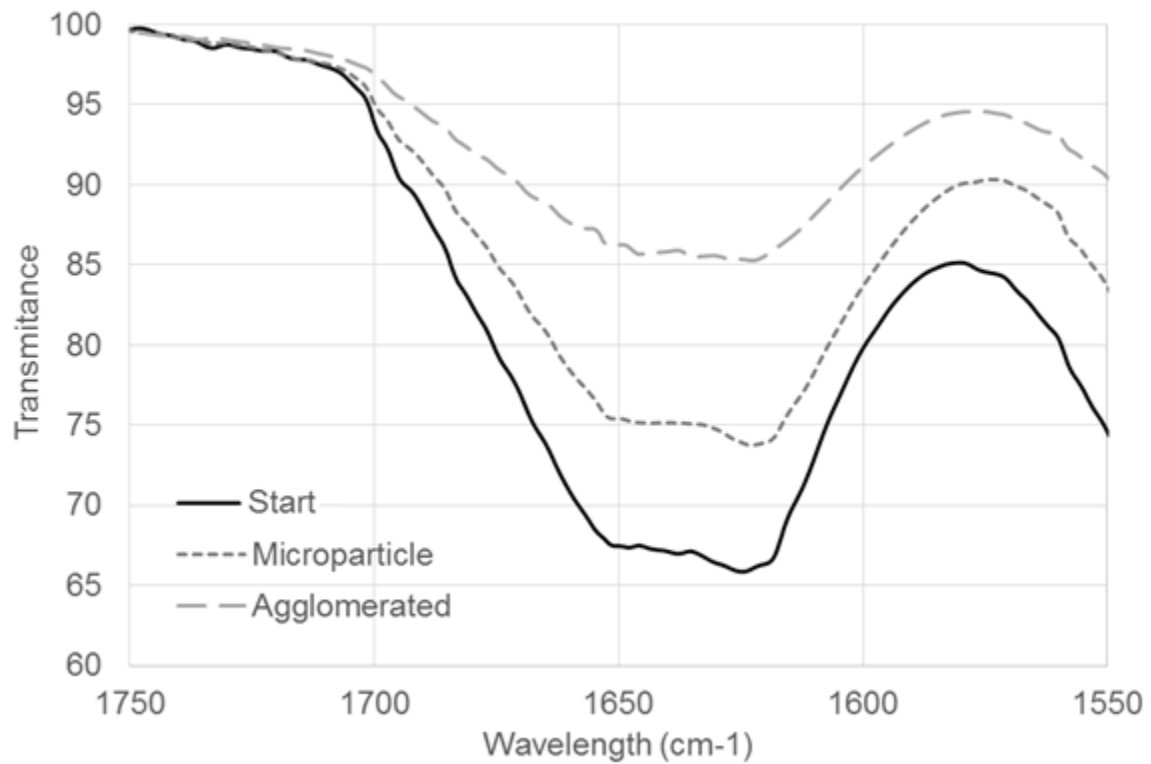**EF.4. FTIR scans of processed *DF-White* kafirin in the amide regions**

Figure 75: Processed *DF-White* kafirin FTIR scan in the amide I region
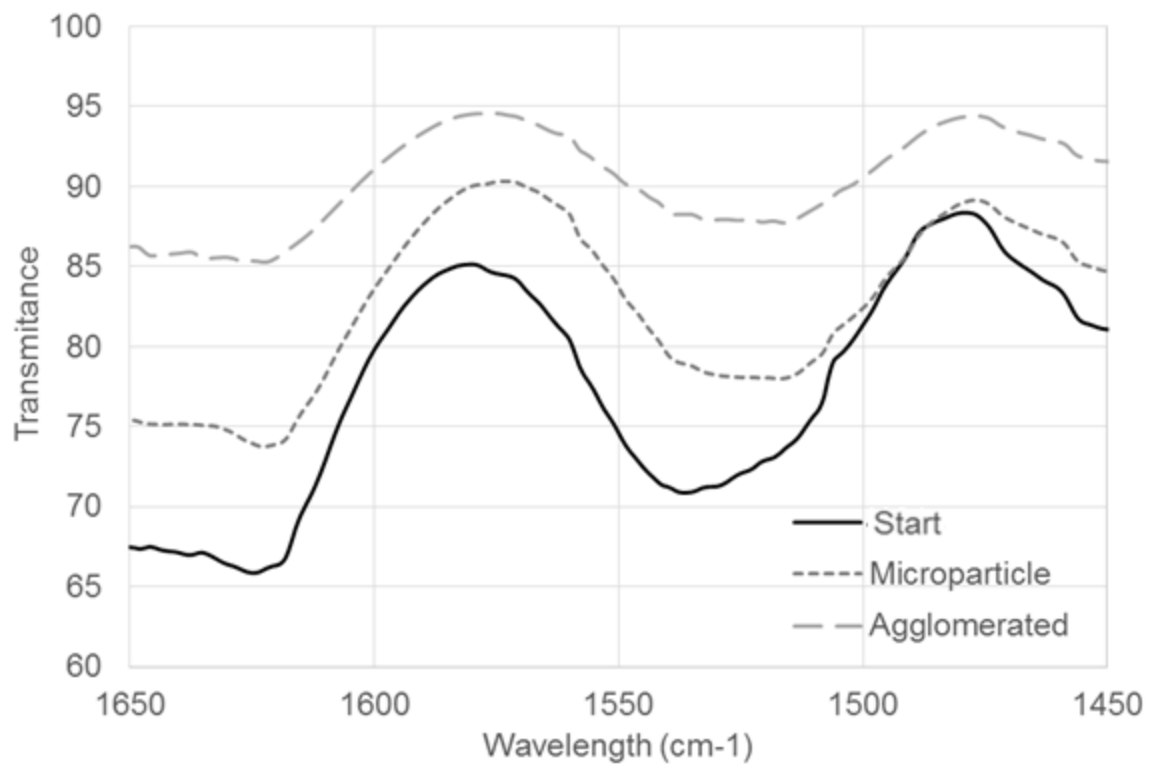
Figure 76: Processed *DF-White* kafirin FTIR scan in the amide II region

Appendix F. Model Curvature Determination

F.1. Mean particle size at constant V_{SS} while varying N_{PS}
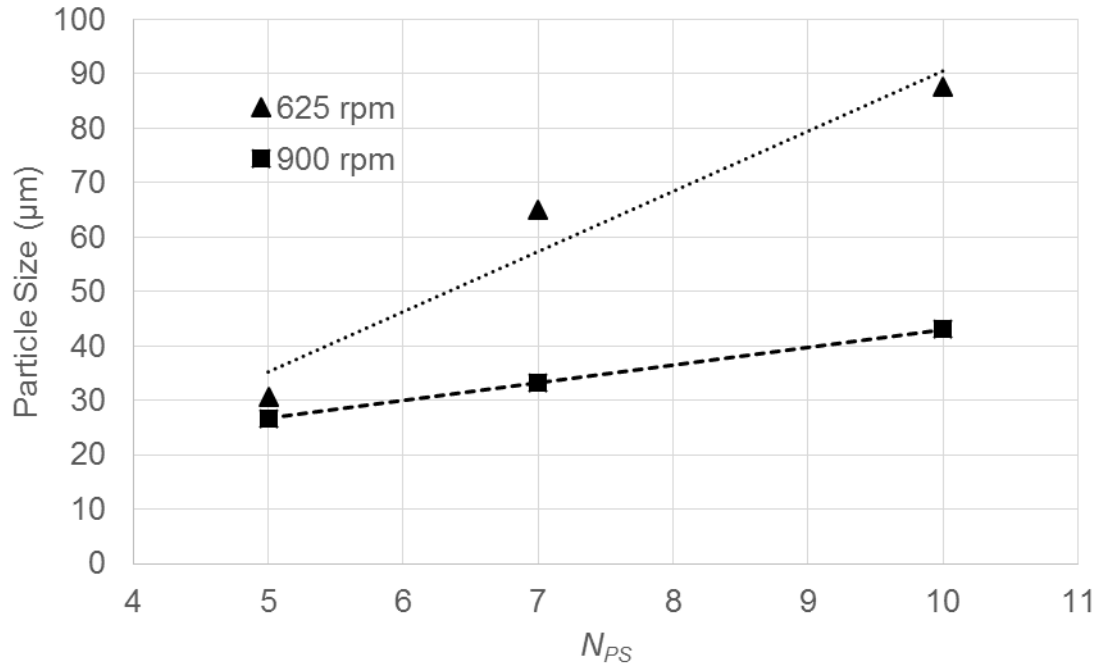
Figure 77: Resulting d_{50} at constant V_{SS} (350 rpm and 625 rpm) varying N_{PS}

F.2. Mean particle size at constant N_{PS} while varying V_{SS}

Figure 78: Resulting d_{50} at constant N_{PS} (7 and 10) varying V_{SS}

F.3. Comprehensive particle size distribution at constant V_{SS} while varying N_{PS}
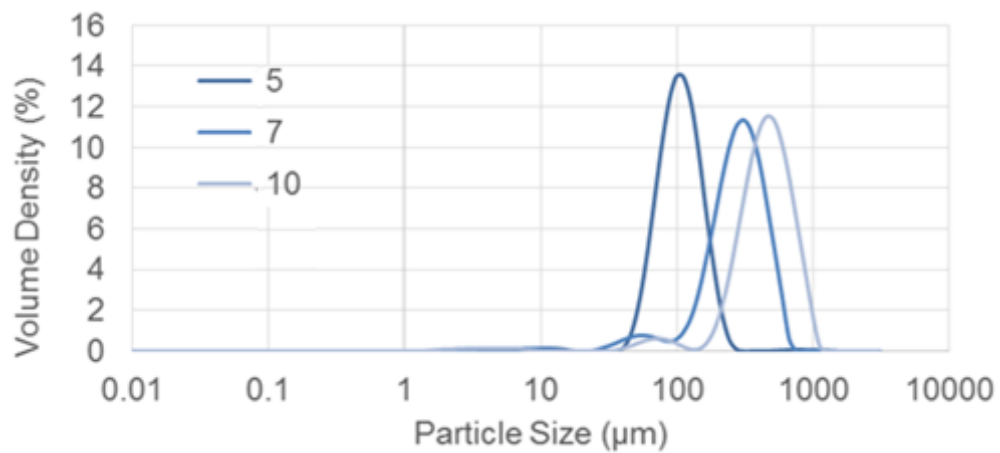
Figure 79: PSA analysis of KEMS formed varying N_{PS} (5, 7 and 10) at 350 rpm

Figure 80: PSA analysis of KEMS formed varying N_{PS} (5, 7 and 10) at 625 rpm

Figure 81: PSA analysis of KEMS formed varying N_{PS} (5, 7 and 10) at 900 rpm

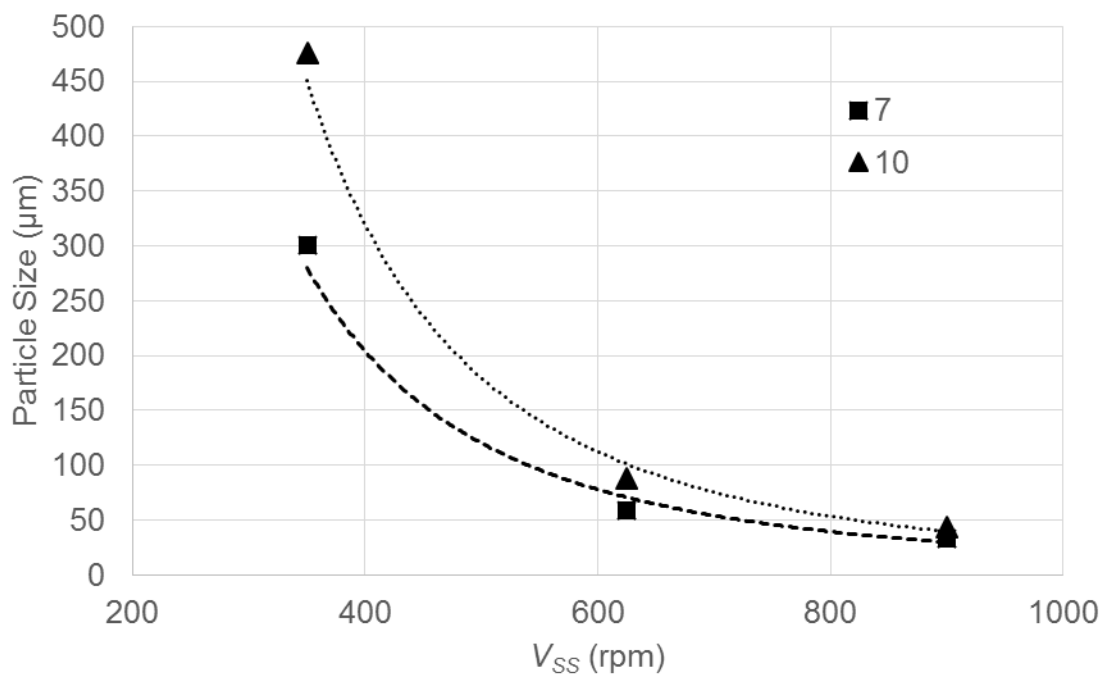**F.4. Comprehensive particle size distribution at constant N_{PS} while varying V_{SS}**

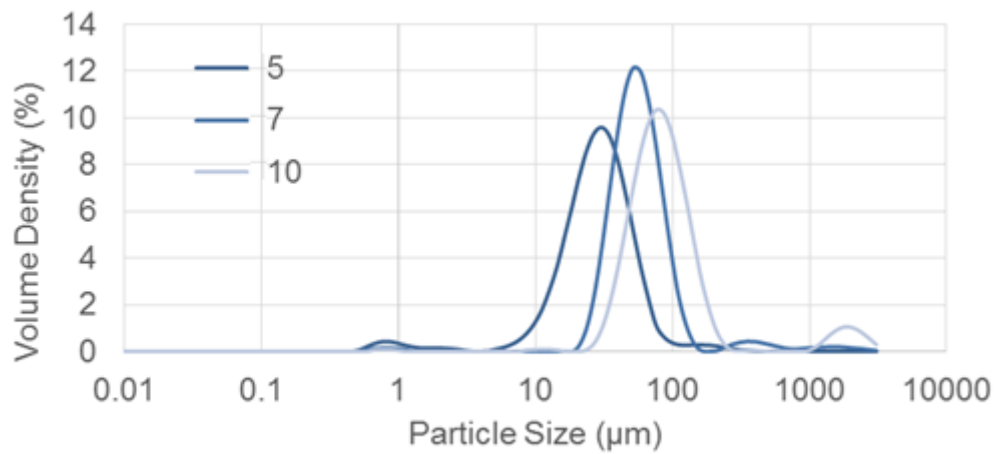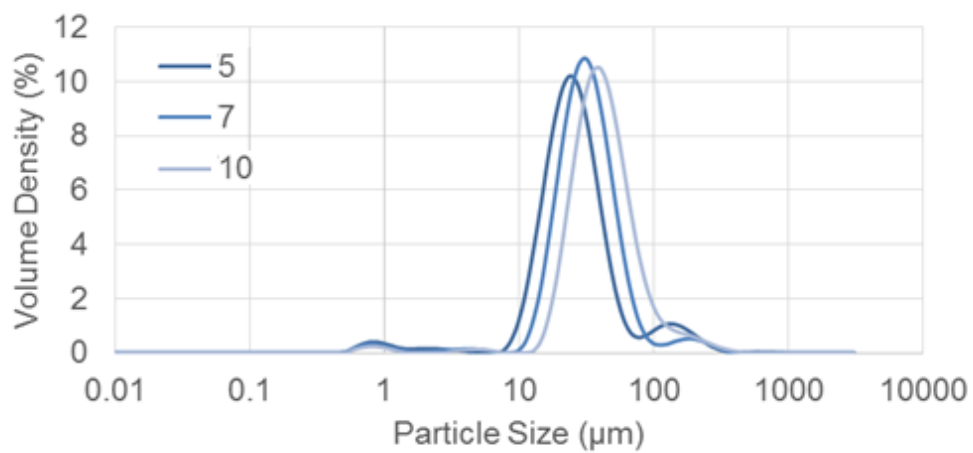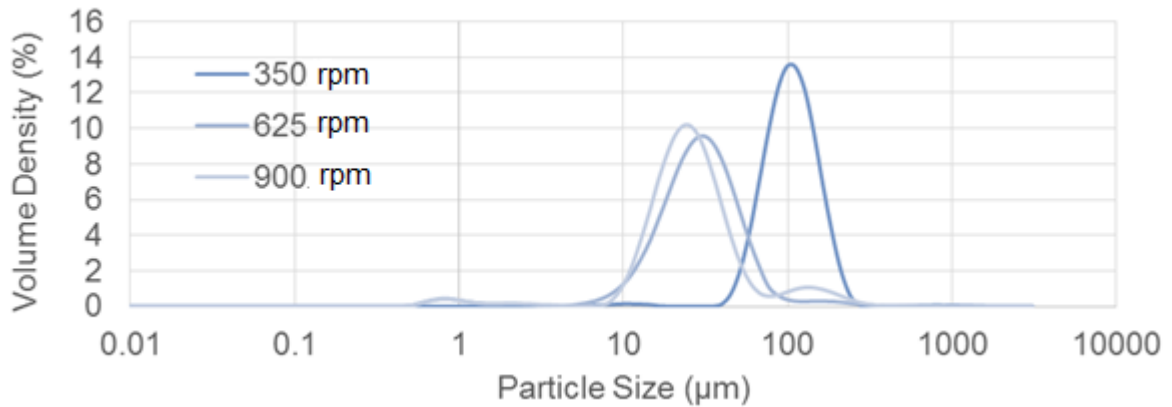Figure 82: PSA analysis of KEMS formed varying V_{SS} at 5 N_{PS}
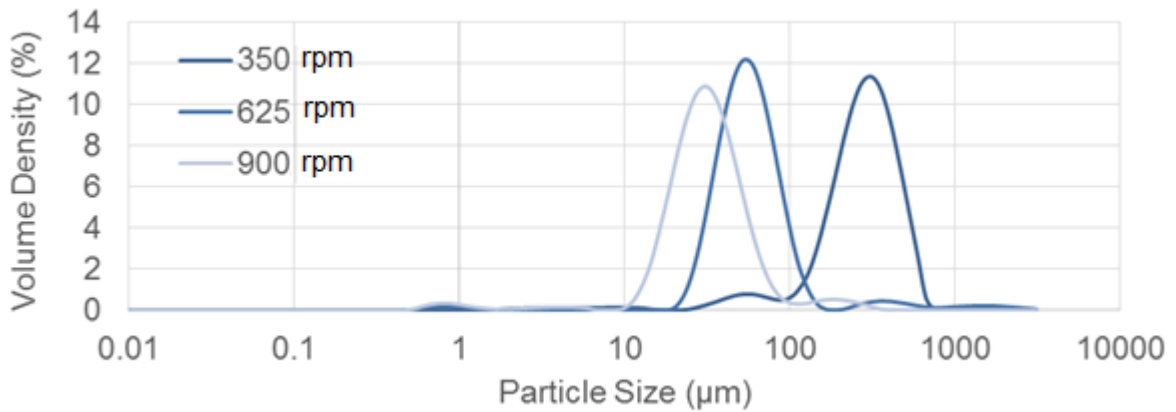
Figure 83: PSA analysis of KEMS formed varying V_{SS} at 7 N_{PS}
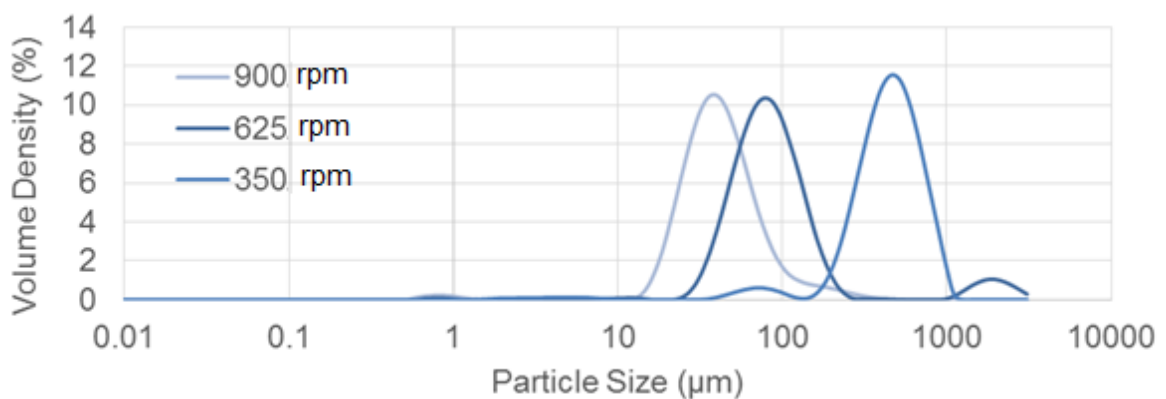
Figure 84: PSA analysis of KEMS formed varying V_{SS} at 10 N_{PS}

Appendix G. PSA Model Fitting Experimental Points

Table 21: Complete summary of particle size results for experimental fitting points

Exp	V_{SS}	N_{PS}	d_{10}	d_{50}	d_{90}
	RPM		µm	µm	µm
1	900	10	23.4	43	71.5
2	900	5	13.8	26.7	50.1
3	350	5	69.1	111	176
4	350	10	251	476	799
5	900	7	18.2	33.1	63.1
6	350	7	143.3	300	501.7
7	760	6	34.7	57.1	96.2
8	760	9	49.5	82.7	142
9	625	5	14	30.6	59
10	625	10	47.9	87.5	180
11	625	7	35.6	60.4	106
12	490	6	62	109	181
13	490	9	78.1	139	228
14	625	7	35.5	58.6	99.8
15	625	7	34.6	56.8	94.2

Figure 85: PSA for KEMS formed at 625 rpm and 7 N_{PS}

Figure 86: PSA for KEMS formed at 900 rpm and 5 N_{PS}

Figure 87: PSA for KEMS formed at 900 rpm and 10 N_{PS}

Figure 88: PSA for KEMS formed at 900 rpm and 7 N_{PS}

Figure 89: PSA for KEMS formed at 760 rpm and 9 N_{PS}
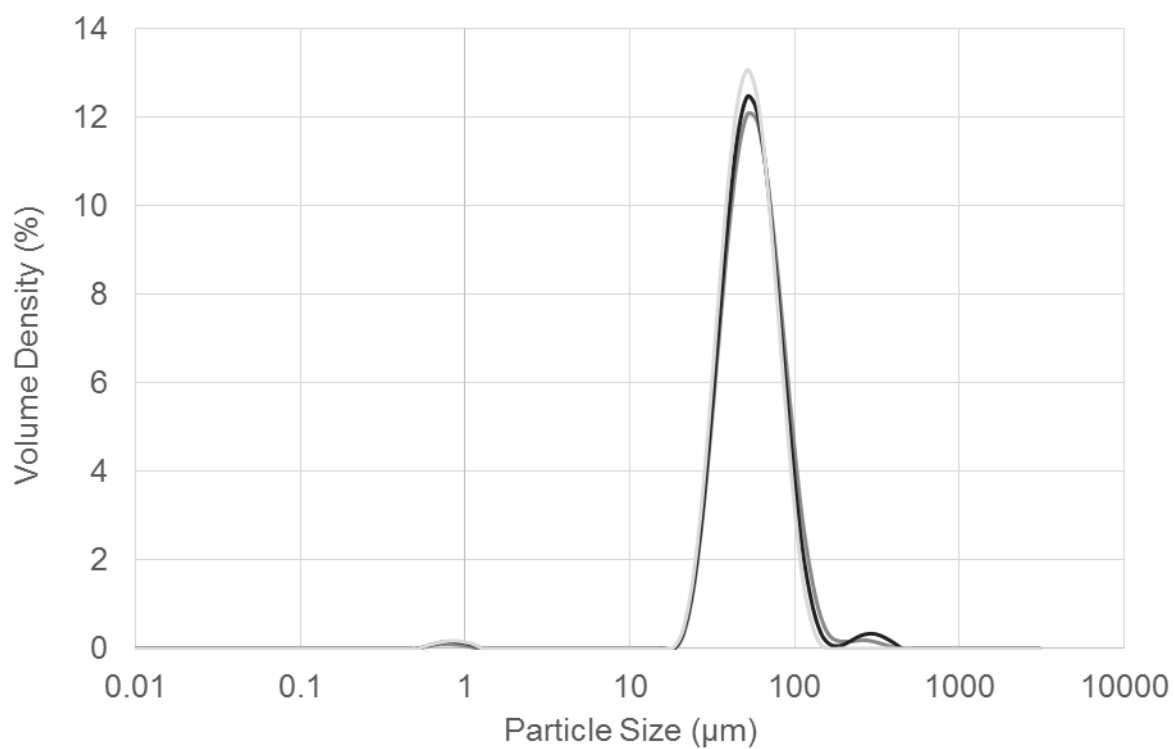
Figure 90: PSA for KEMS formed at 760 rpm and 6 N_{PS}
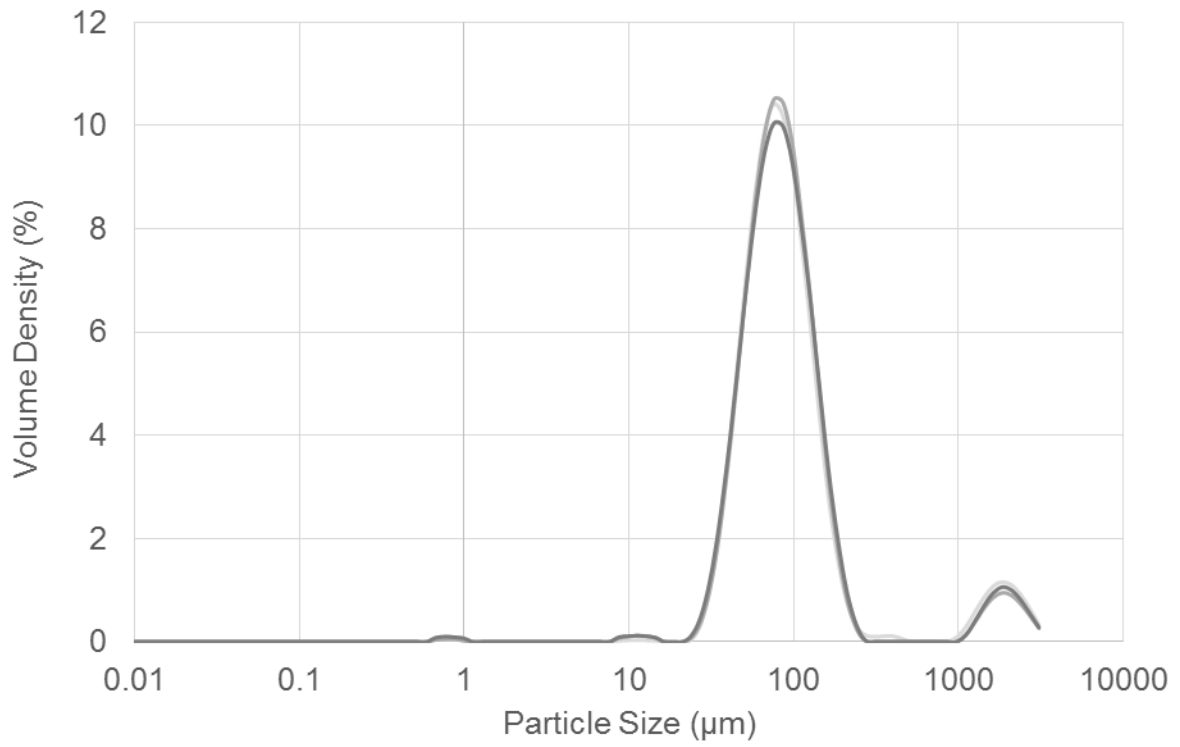
Figure 91: PSA for KEMS formed at 625 rpm and 10 N_{PS}
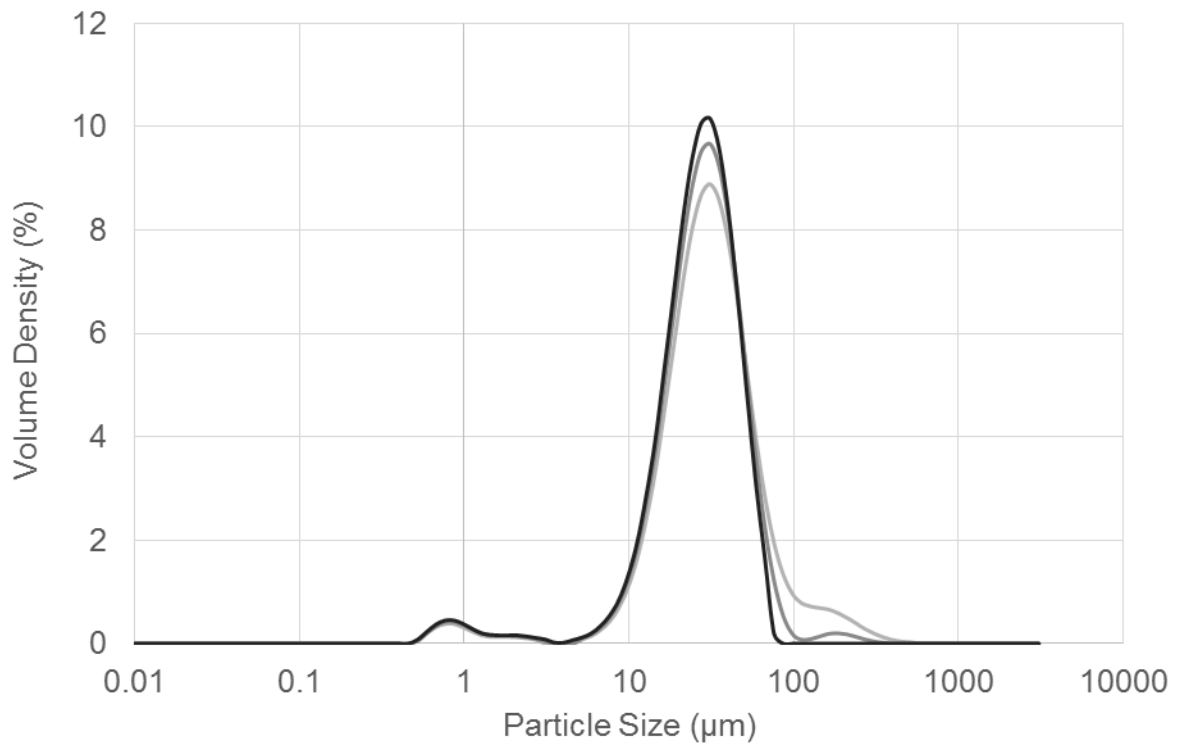
Figure 92: PSA for KEMS formed at 625 rpm and 5 N_{PS}
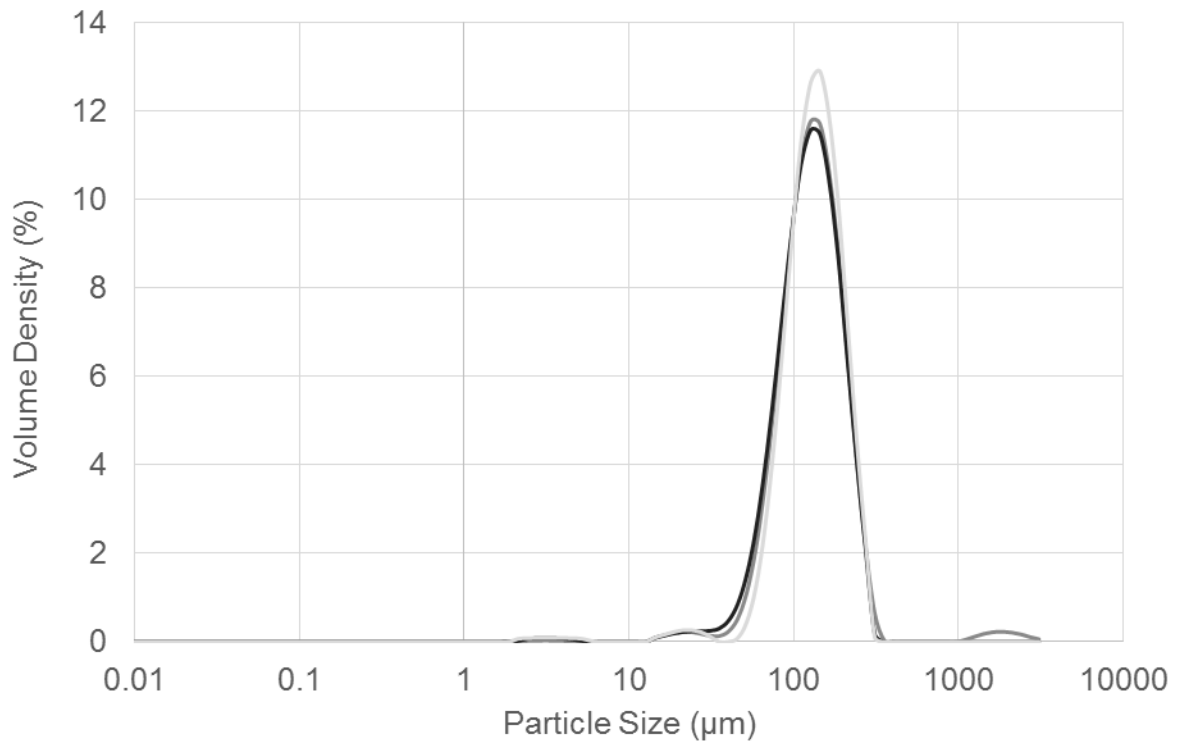
Figure 93: PSA for KEMS formed at 490 rpm and 9 N_{PS}
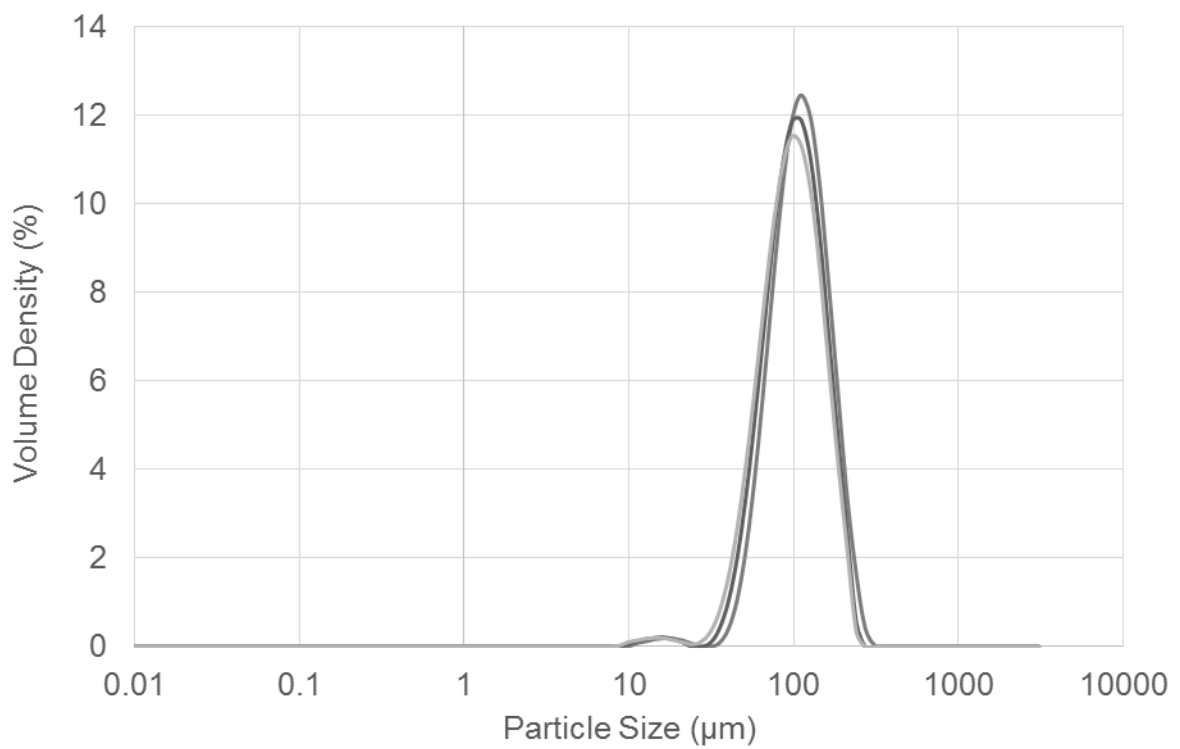
Figure 94: PSA for KEMS formed at 490 rpm and 6 N_{PS}
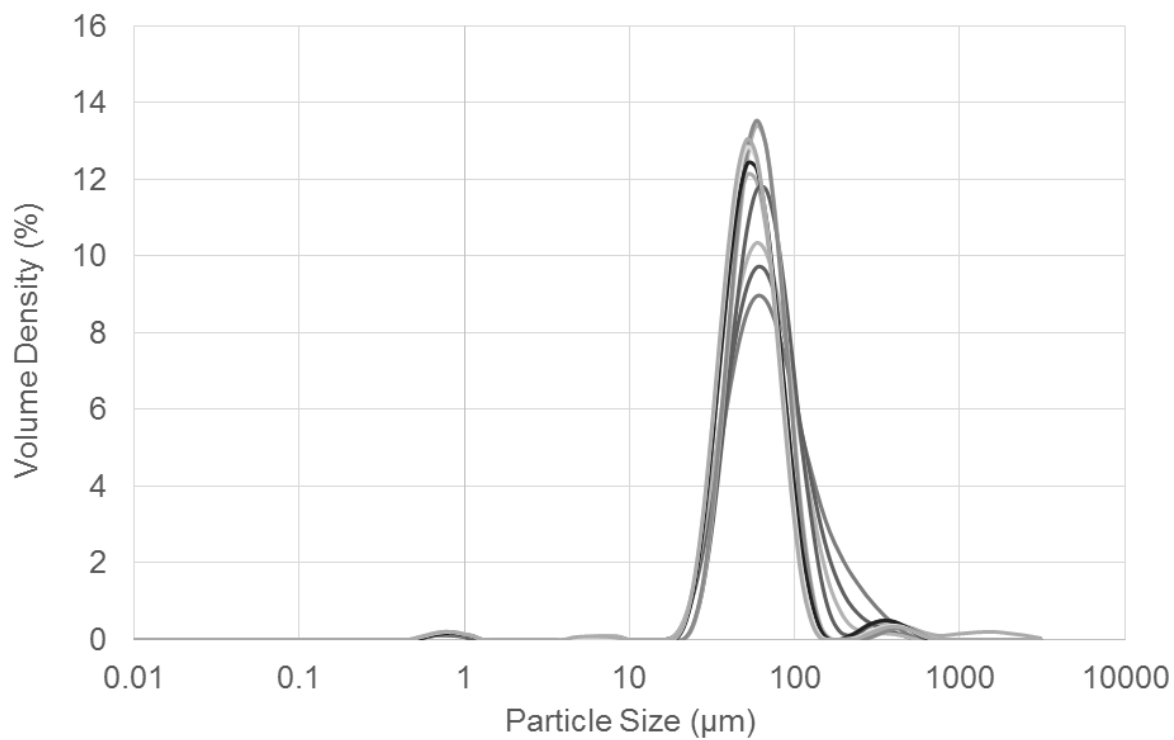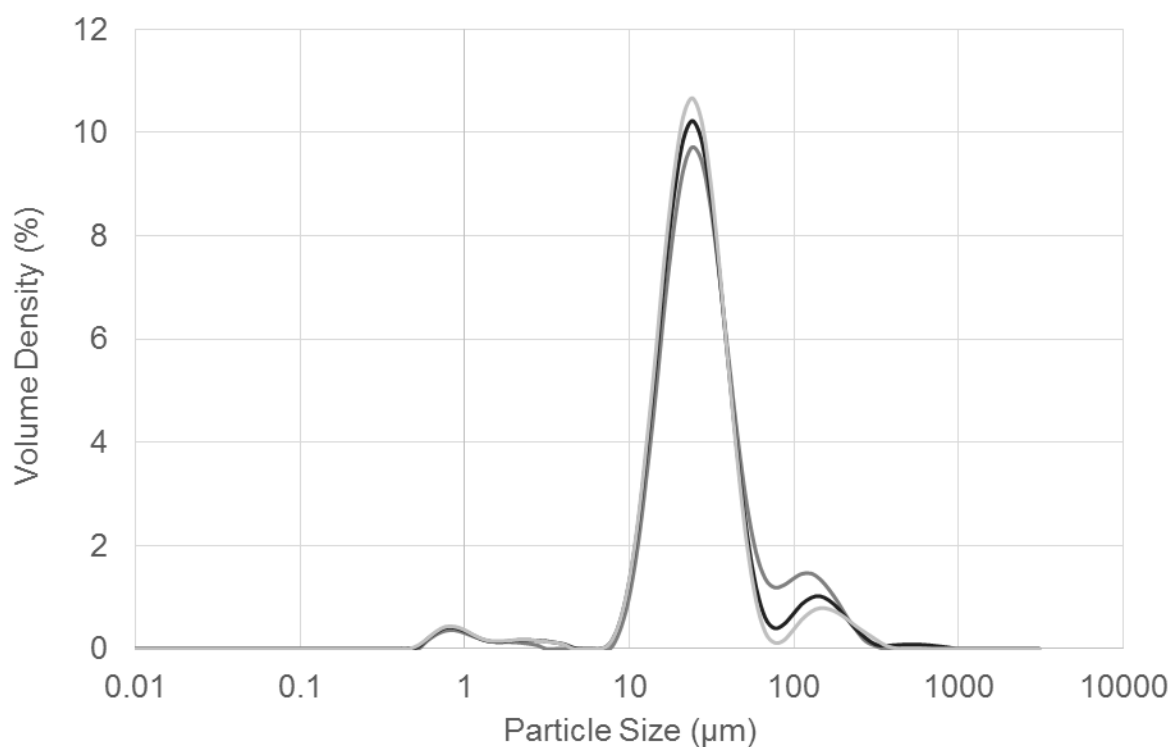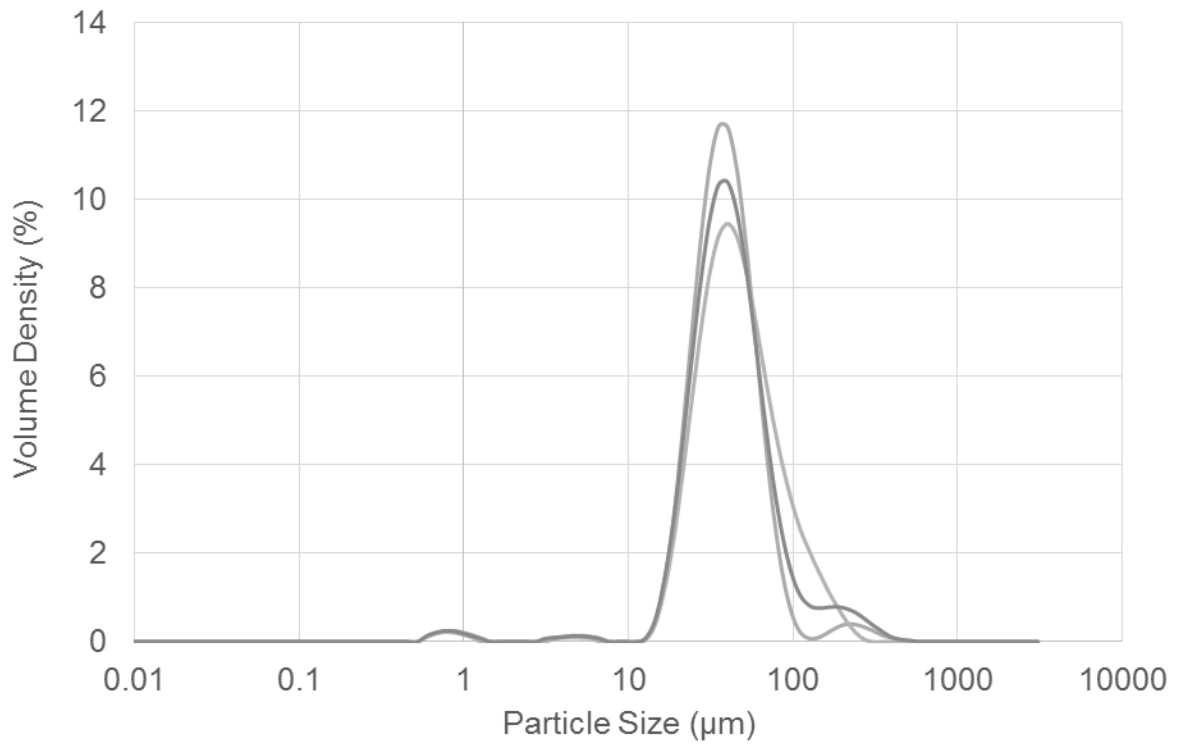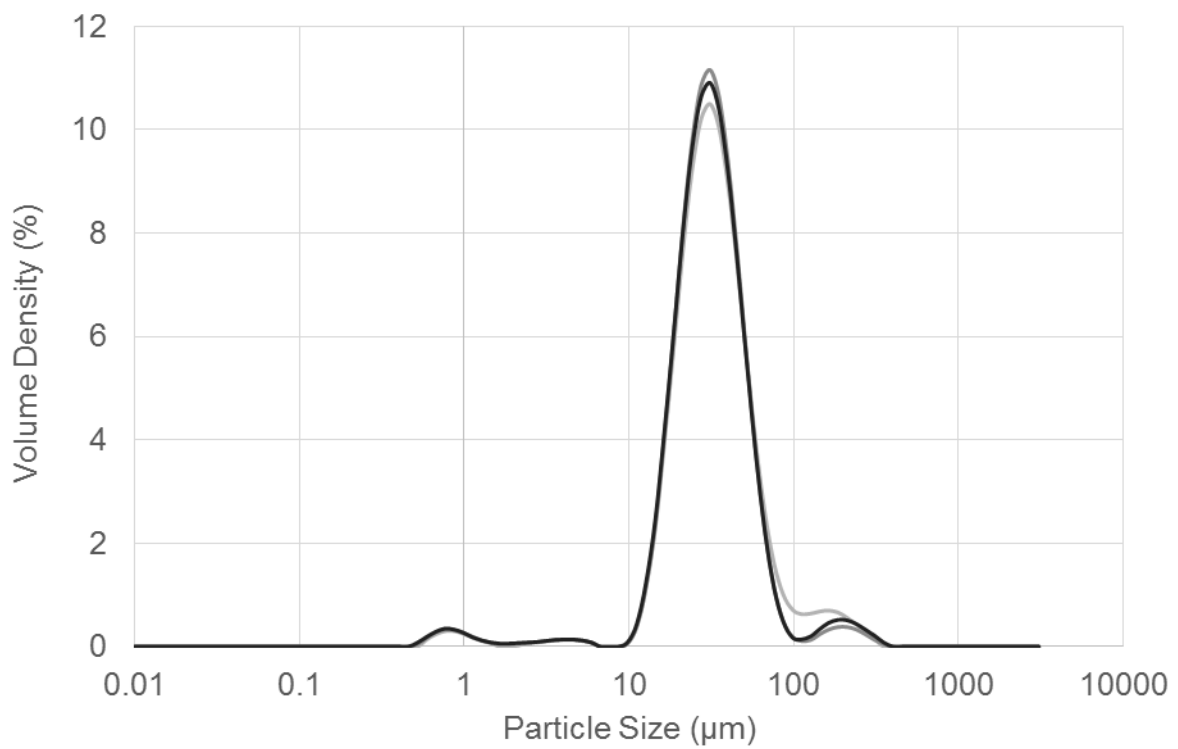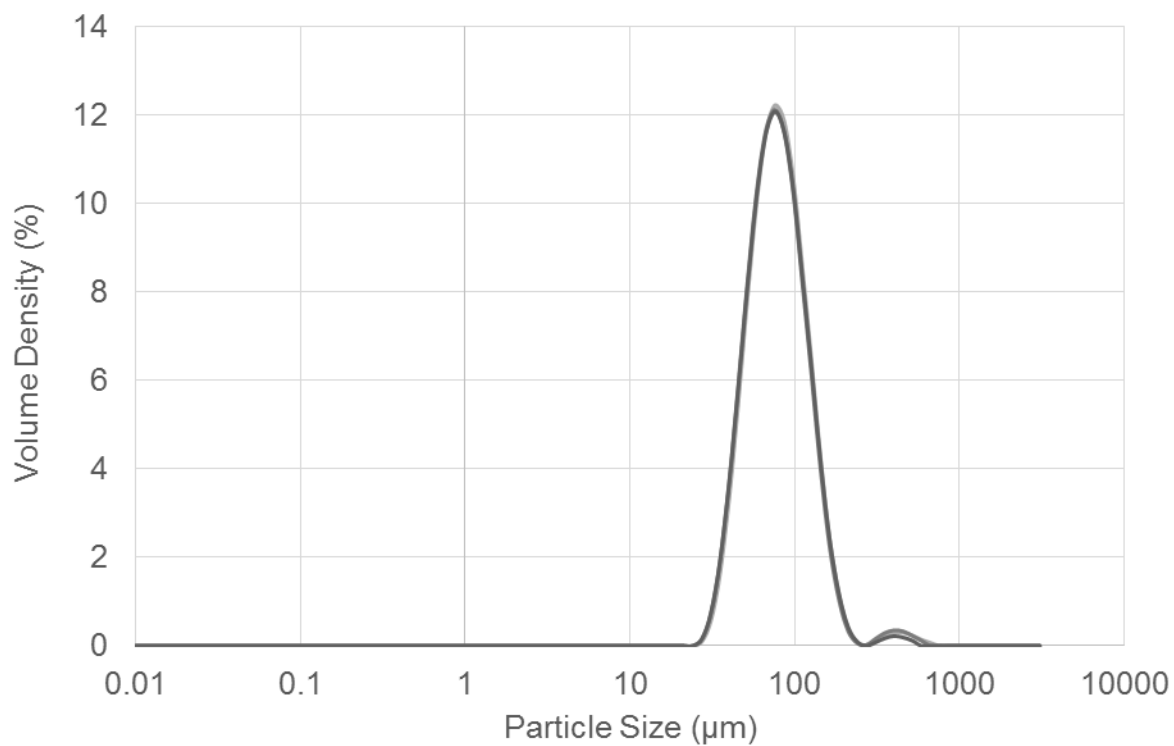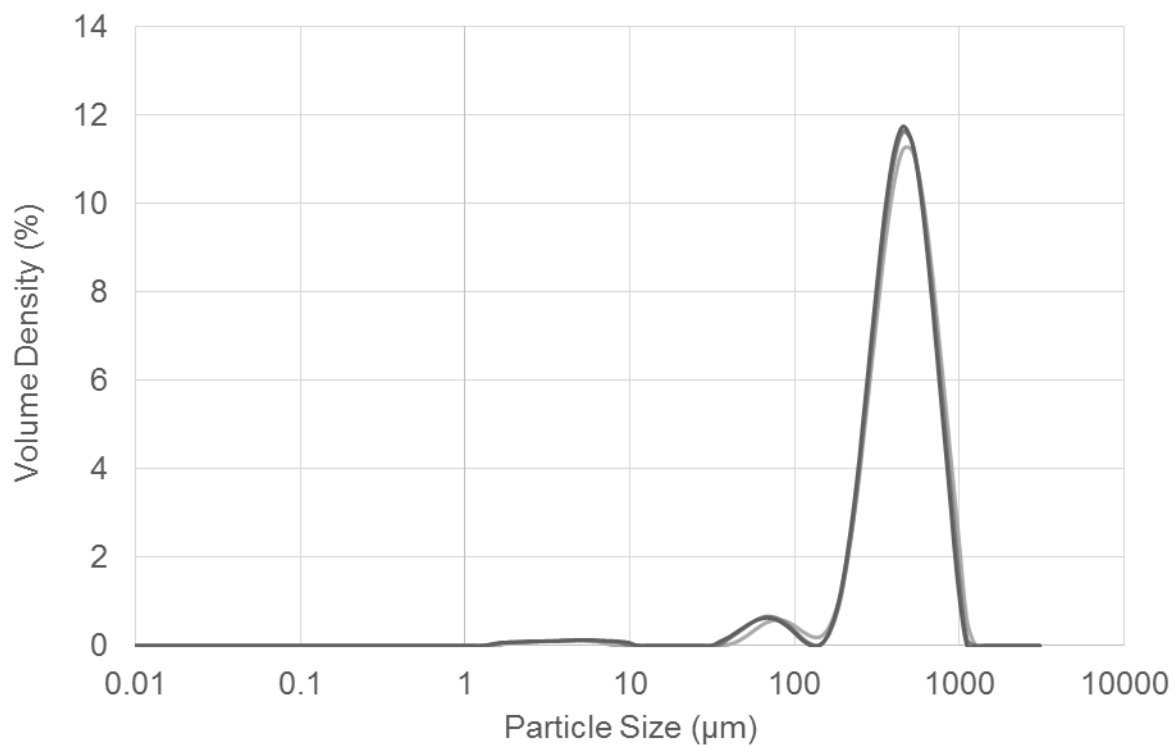
Figure 95: PSA for KEMS formed at 350 rpm and 10 N_{PS}
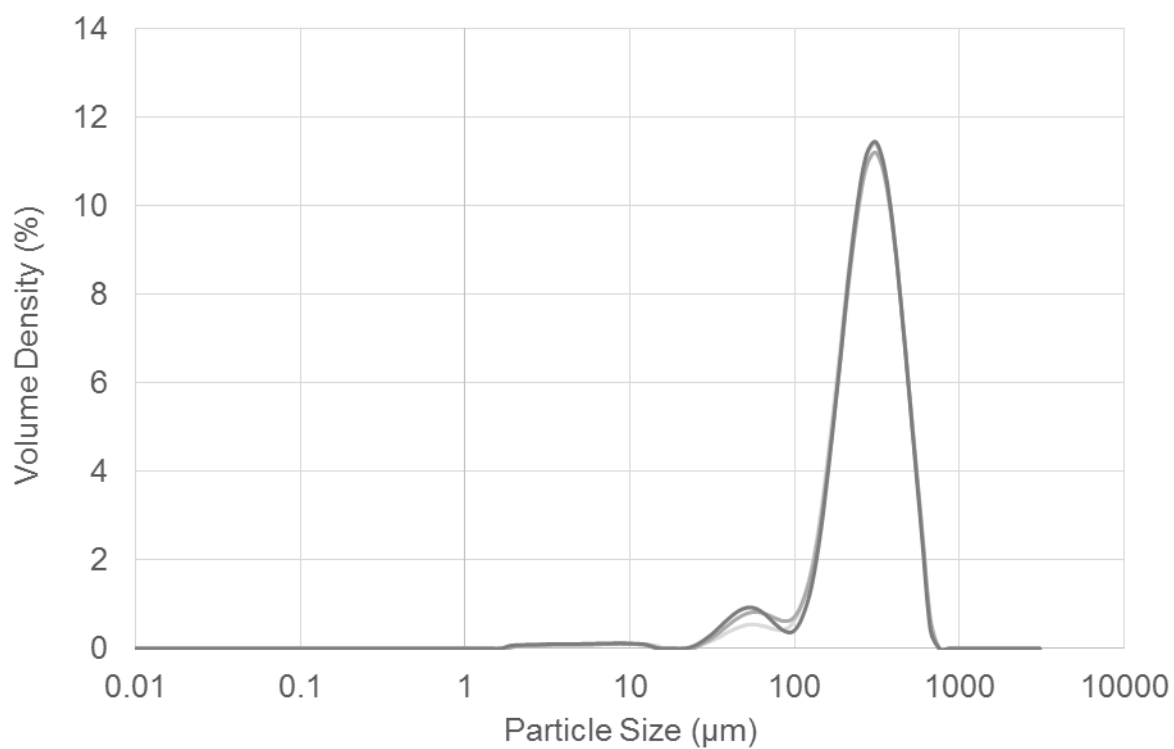
Figure 96: PSA for KEMS formed at 350 rpm and 7 N_{PS}
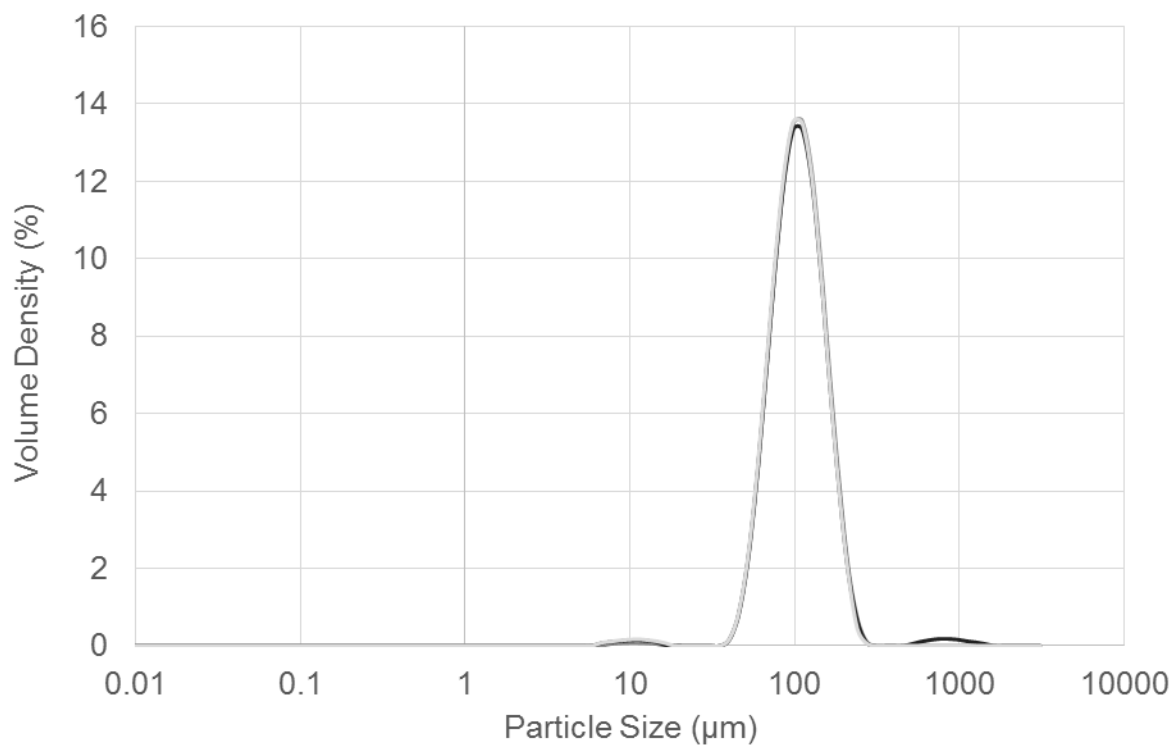
Figure 97: PSA for KEMS formed at 350 rpm and 5 N_{PS}

Appendix H. Statistical Analysis of Former Models

$$d_{50} = 139 - 1,25\,V_{SS} + 179N_{PS} + 0,0013\,V_{SS}^2 - 0,213\,V_{SS}\,N_{PS}$$

SUMMARY OUTPUT | with intercept

Regression Statistics	
Multiple R	0.956131746
R Square	0.914187916
Adjusted R	0.879863082
Standard E	42.04024864
Observatic	15

ANOVA

	df	SS	MS	F	ignificance F
Regressior	4	188285.8	47071.45	26.63343	2.59E-05
Residual	10	17673.83	1767.383		
Total	14	205959.6			

	Coefficients	andard Err	t Stat	P-value	Lower 95%	Upper 95%	ower 95.0%	lpper 95.0%
Intercept	139.5794348	187.3633	0.744967	0.473437	-277.892	557.0509	-277.892	557.0509
RPM (x)	-1.245401051	0.460006	-2.70736	0.022033	-2.27036	-0.22044	-2.27036	-0.22044
Pump (y)	179.7000375	35.88552	5.007592	0.000531	99.74212	259.658	99.74212	259.658
x2	0.001325799	0.000321	4.129903	0.002045	0.000611	0.002041	0.000611	0.002041
xy	-0.212682475	0.054434	-3.90717	0.002927	-0.33397	-0.0914	-0.33397	-0.0914

Figure 98: Summary of the statistical output for first iteration

$$d_{50} = -0,937\,V_{SS} + 200,2 N_{PS} + 0,0012\,V_{SS}^2 - 0,242\,V_{SS}\,N_{PS}$$

SUMMARY OUTPUT	without intercept							
Regression Statistics								
Multiple R	0.976004							
R Square	0.952584							
Adjusted R	0.848743							
Standard E	41.18106							
Observatic	15							
ANOVA								
	df	*SS*	*MS*	*F*	*ignificance F*			
Regressior	4	374771.2	93692.8	55.24731	8.79E-07			
Residual	11	18654.68	1695.88					
Total	15	393425.9						
	Coefficients	*andard Err*	*t Stat*	*P-value*	*Lower 95%*	*Upper 95%*	*ower 95.0%*	*pper 95.0%*
Intercept	0	#N/A	#N/A	#N/A	#N/A	#N/A	#N/A	#N/A
RPM (x)	-0.93664	0.195479	-4.79149	0.000561	-1.36689	-0.50639	-1.36689	-0.50639
Pump (y)	200.2044	22.55556	8.876056	2.4E-06	150.56	249.8489	150.56	249.8489
x2	0.001179	0.000249	4.743969	0.000606	0.000632	0.001727	0.000632	0.001727
xy	-0.24208	0.036731	-6.59057	3.91E-05	-0.32292	-0.16123	-0.32292	-0.16123

Figure 99: Summary of the statistical output for second iteration

$$d_{50} = -796 + 196\,V_{SS} + 228N_{PS} - 14\,V_{SS}^2 - 53,9\,V_{SS}\,N_{PS} + 3,8\,V_{SS}^2\,N_{PS}$$
$$- 0,34V_{SS}N_{PS}^2$$

Regression Statistics								
Multiple R	0.977789524							
R Square	0.956072352							
Adjusted R	0.923126617							
Standard E	33.62908341							
Observatic	15							

ANOVA

	df	SS	MS	F	ignificance F			
Regressior	6	196912.3	32818.72	29.01961	5.2E-05			
Residual	8	9047.322	1130.915					
Total	14	205959.6						

	Coefficients	andard Err	t Stat	P-value	Lower 95%	Upper 95%	ower 95.0%	pper 95.0%
Intercept	-796.3539304	388.83	-2.04808	0.074731	-1693	100.2896	-1693	100.2896
RPM (x)	196.8299919	139.877	1.407165	0.197022	-125.727	519.387	-125.727	519.387
Pump (y)	228.142466	51.47499	4.432103	0.002191	109.4409	346.844	109.4409	346.844
x2	-13.97899079	10.68162	-1.3087	0.22698	-38.6109	10.65287	-38.6109	10.65287
xy	-53.86120276	19.65132	-2.74084	0.025416	-99.1772	-8.54517	-99.1772	-8.54517
x2y	3.805801825	1.417307	2.685235	0.0277	0.537486	7.074117	0.537486	7.074117
xy2	-0.336711226	0.533721	-0.63087	0.545719	-1.56747	0.894052	-1.56747	0.894052

Figure 100: Summary of the statistical output for third iteration

$$d_{50} = -4586 + 1606\,V_{SS} + 1253 N_{PS} - 221\,V_{SS}^2 - 370\,V_{SS}\,N_{PS} + 48\,V_{SS}^2\,N_{PS}$$
$$+5,4V_{SS}N_{PS}^2 - 61\,N_{PS}^2 - 0,3\,V_{SS}^2 N_{PS}^2 + 10\,V_{SS}^3 + 1,8N_{PS}^3 - 2\,V_{SS}^3\,N_{PS}$$

Regression Statistics								
Multiple R	0.999349							
R Square	0.998698							
Adjusted R	0.993925							
Standard E	9.453611							
Observatic	15							
ANOVA								
	df	SS	MS	F	ignificance F			
Regressior	11	205691.5	18699.23	209.2321	0.000484			
Residual	3	268.1123	89.37076					
Total	14	205959.6						
	Coefficients	andard Err	t Stat	P-value	Lower 95%	Upper 95%	ower 95.0%	pper 95.0%
Intercept	-4586.3	882.9888	-5.19406	0.013862	-7396.36	-1776.23	-7396.36	-1776.23
RPM (x)	1606.867	401.9062	3.998116	0.028043	327.8226	2885.912	327.8226	2885.912
Pump (y)	1253.74	217.6471	5.760425	0.010397	561.0897	1946.39	561.0897	1946.39
x2	-221.727	62.52405	-3.54626	0.038192	-420.706	-22.7473	-420.706	-22.7473
xy	-370.339	69.42843	-5.33412	0.012879	-591.291	-149.387	-591.291	-149.387
x2y	48.14668	8.920755	5.397153	0.012467	19.75686	76.53651	19.75686	76.53651
xy2	5.42092	3.344173	1.621005	0.203463	-5.22173	16.06357	-5.22173	16.06357
y2	-61.0473	22.10334	-2.7619	0.070041	-131.39	9.295408	-131.39	9.295408
x2y2	-0.32914	0.264533	-1.24423	0.301768	-1.171	0.512721	-1.171	0.512721
x3	10.24547	3.240495	3.1617	0.050804	-0.06723	20.55818	-0.06723	20.55818
y3	1.759191	0.914342	1.923997	0.150048	-1.15065	4.669034	-1.15065	4.669034
x3y	-2.11442	0.423933	-4.98764	0.015497	-3.46357	-0.76528	-3.46357	-0.76528

Figure 101: Summary of the statistical output for fourth iteration

$$d_{50} = -3003 + 1361\,V_{SS} + 681 N_{PS} - 209\,V_{SS}^2 - 287\,V_{SS}\,N_{PS} + 42\,V_{SS}^2\,N_{PS}$$
$$- 2,4\,N_{PS}^2 + 10\,V_{SS}^3 - 2\,V_{SS}^3\,N_{PS}$$

Regression Statistics	
Multiple R	0.996671
R Square	0.993352
Adjusted R Squar	0.984489
Standard Error	15.10599
Observations	15

ANOVA

	df	SS	MS	F	ignificance F
Regression	8	204590.5	25573.81	112.072	5.79E-06
Residual	6	1369.146	228.191		
Total	14	205959.6			

	Coefficients	andard Err	t Stat	P-value	Lower 95%	Upper 95%	ower 95.0%	pper 95.0%
Intercept	-3003.07	1050.664	-2.85826	0.028867	-5573.95	-432.19	-5573.95	-432.19
RPM (x)	1361.757	573.0246	2.376436	0.055035	-40.3843	2763.897	-40.3843	2763.897
Pump (y)	681.13	139.2139	4.892687	0.002731	340.4859	1021.774	340.4859	1021.774
x2	-209.588	97.18147	-2.15666	0.074419	-447.382	28.2067	-447.382	28.2067
xy	-287.889	74.95902	-3.84062	0.008553	-471.307	-104.471	-471.307	-104.471
x2y	42.77648	12.71063	3.36541	0.015128	11.67469	73.87827	11.67469	73.87827
y2	-2.445	1.576657	-1.55075	0.171942	-6.30294	1.412944	-6.30294	1.412944
x3	10.43717	5.176686	2.016188	0.090376	-2.22972	23.10407	-2.22972	23.10407
x3y	-2.07848	0.677049	-3.06991	0.021945	-3.73516	-0.4218	-3.73516	-0.4218

Figure 102: Summary of the statistical output for fifth iteration

$$d_{50} = -2893 + 1369\,V_{SS} + 644 N_{PS} - 210\,V_{SS}^2 - 288\,V_{SS}\,N_{PS} + 43\,V_{SS}^2\,N_{PS}$$
$$+ 10\,V_{SS}^3 - 2\,V_{SS}^3\,N_{PS}$$

Regression Statistics								
Multiple R	0.995333							
R Square	0.990688							
Adjusted R Squar	0.981376							
Standard Error	16.55253							
Observations	15							
ANOVA								
	df	SS	MS	F	ignificance F			
Regression	7	204041.7	29148.82	106.3879	1.43E-06			
Residual	7	1917.904	273.9863					
Total	14	205959.6						
	Coefficients	andard Err	t Stat	P-value	Lower 95%	Upper 95%	ower 95.0%	pper 95.0%
Intercept	-2893.13	1148.651	-2.51872	0.039885	-5609.26	-177.002	-5609.26	-177.002
RPM (x)	1369.671	627.8722	2.181449	0.0655	-115.011	2854.353	-115.011	2854.353
Pump (y)	644.2951	150.3081	4.286497	0.003626	288.8729	999.7172	288.8729	999.7172
x2	-210.221	106.4866	-1.97415	0.088945	-462.022	41.57973	-462.022	41.57973
xy	-287.963	82.13702	-3.50588	0.009914	-482.186	-93.7396	-482.186	-93.7396
x2y	42.78236	13.92779	3.071726	0.018024	9.848367	75.71635	9.848367	75.71635
x3	10.43717	5.672402	1.839992	0.108346	-2.97593	23.85027	-2.97593	23.85027
x3y	-2.07848	0.741883	-2.80163	0.026462	-3.83275	-0.32421	-3.83275	-0.32421

Figure 103: Summary of the statistical output for sixth iteration

Appendix I. PSA Model Validation Experimental Points

Table 22: Complete summary of particle size results for experimental validation points

Exp	V_{SS}	N_{PS}	d_{10}	d_{50}	d_{90}
	RPM		μm	μm	μm
1	500	6	48.4	77.8	123
2	500	8	69	126	213
3	760	7	33.4	66.8	165
4	700	6	20.6	40.5	122
5	700	9	44.8	85.1	317
6	850	6	14.9	32.3	116
7	850	9	32.5	61.9	136
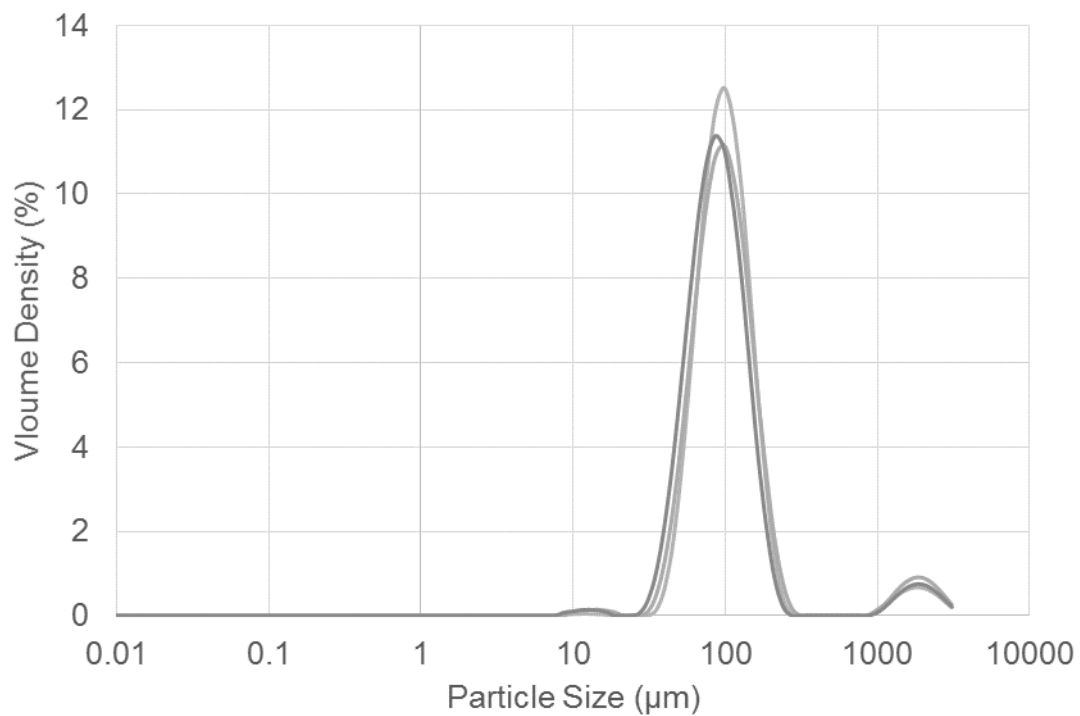
Figure 104: PSA for KEMS formed at 500 rpm and 6 N_{PS}
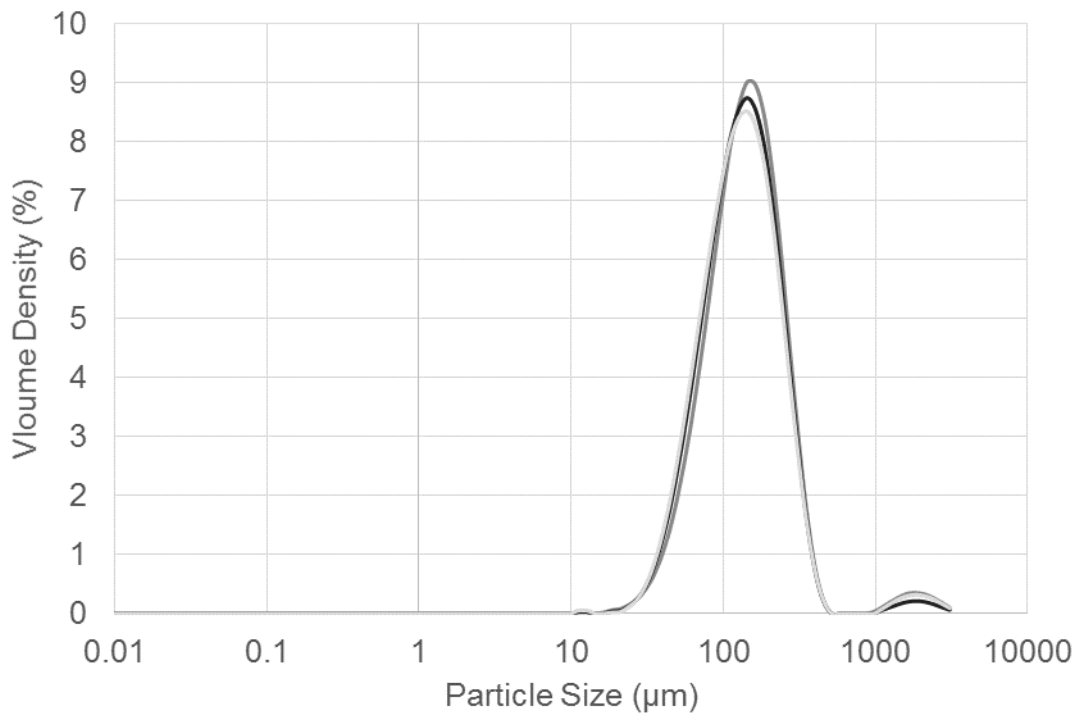
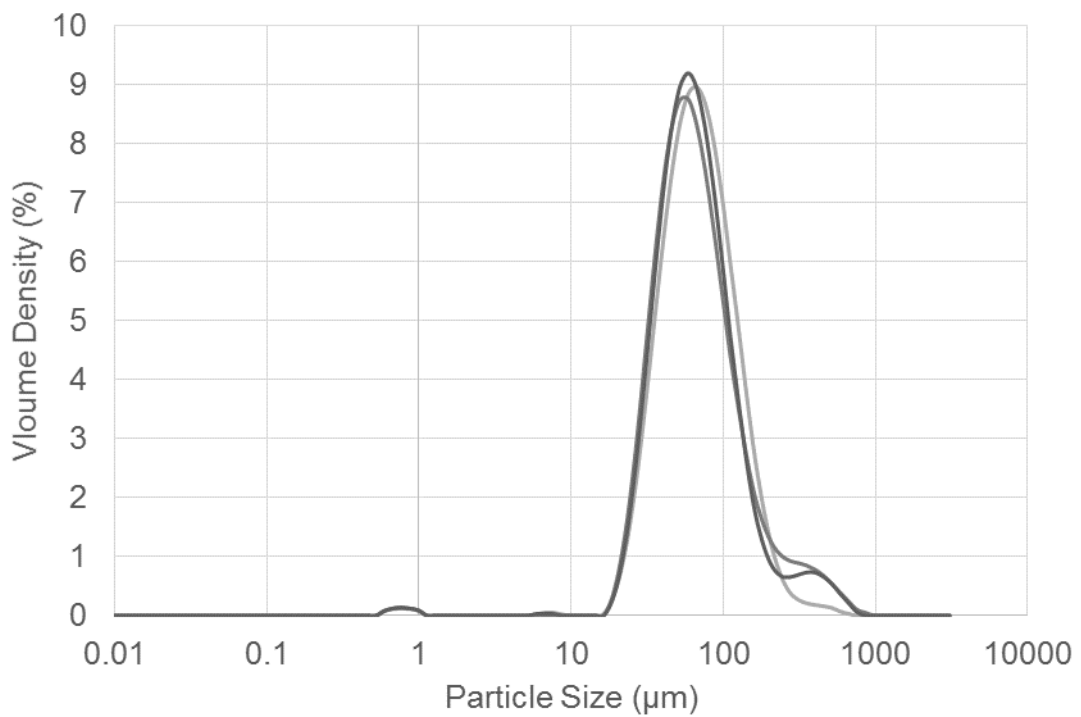Figure 105: PSA for KEMS formed at 500 rpm and 8 N_{PS}

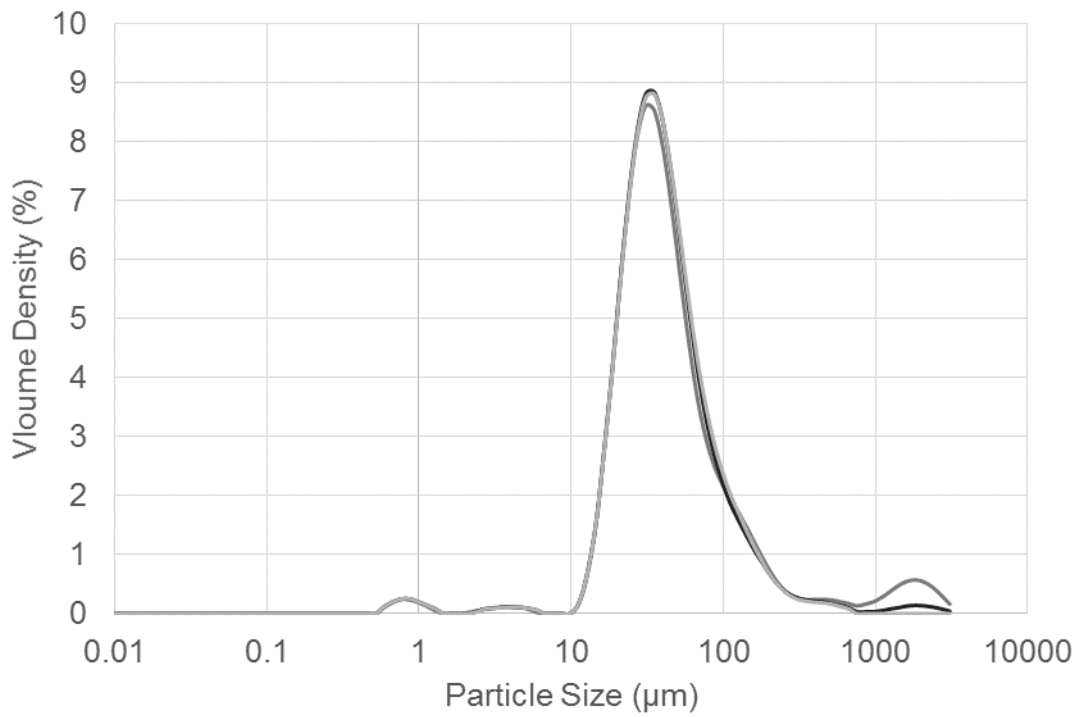Figure 106: PSA for KEMS formed at 760 rpm and 7 N_{PS}

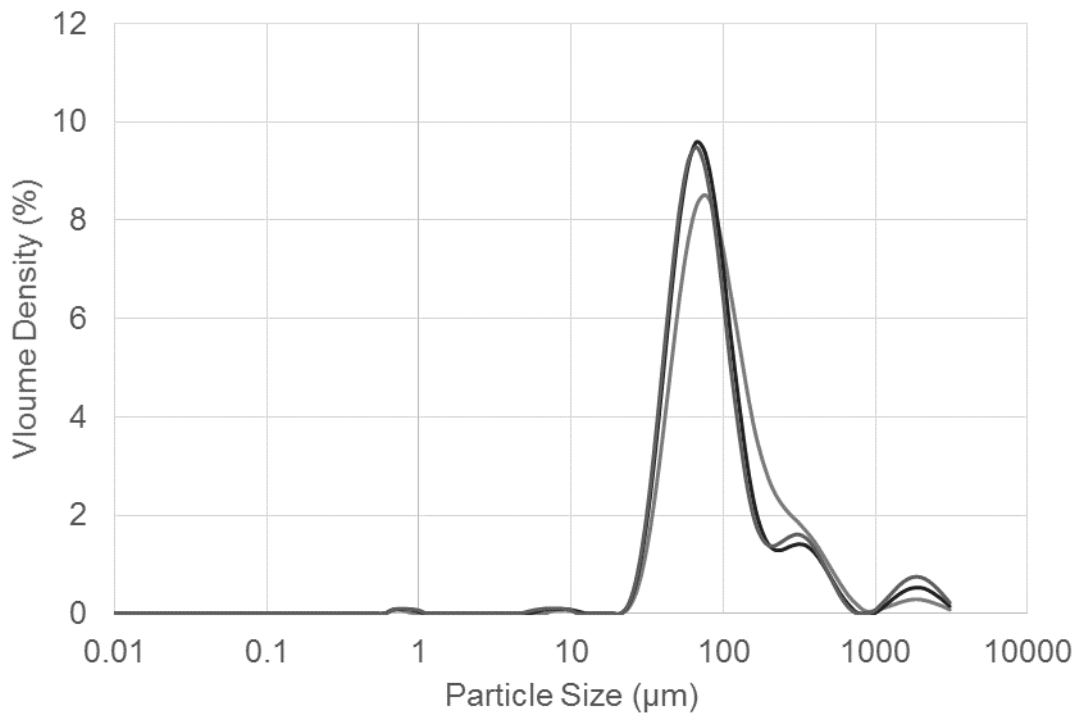Figure 107: PSA for KEMS formed at 700 rpm and 6 N_{PS}

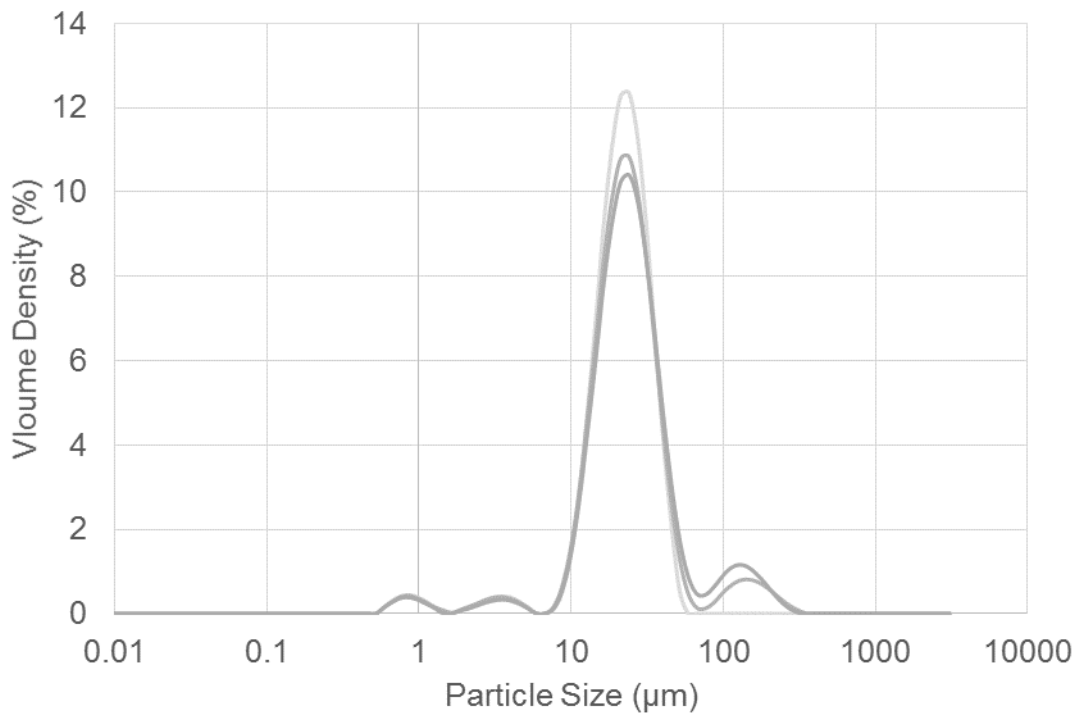Figure 108: PSA for KEMS formed at 700 rpm and 9 N_{PS}

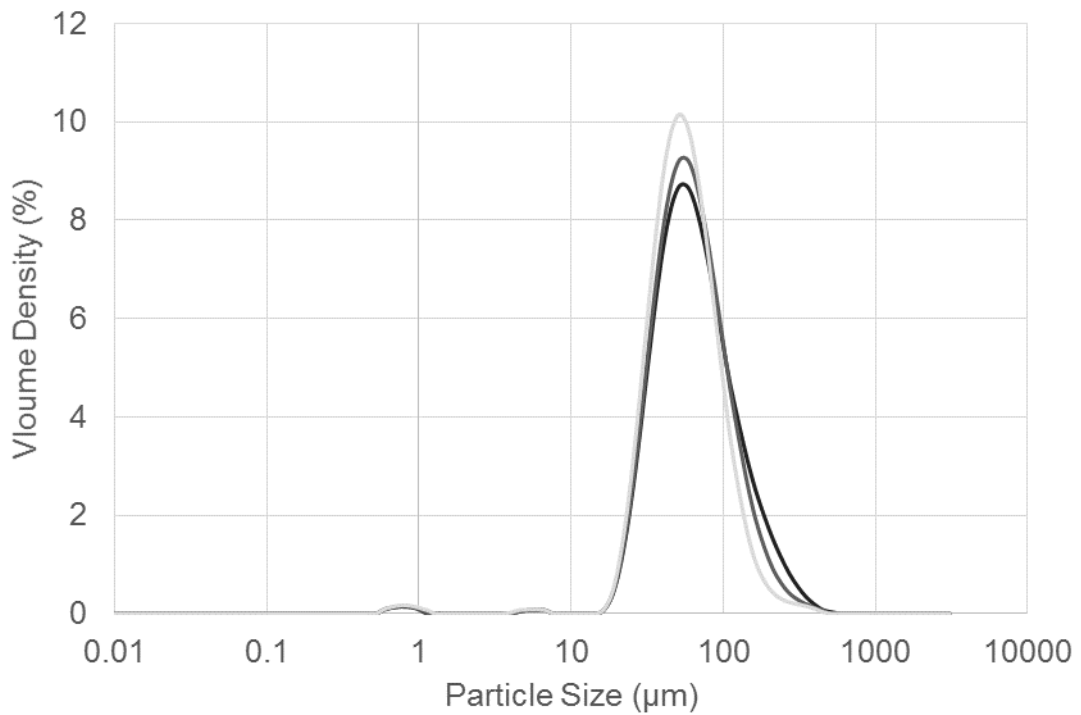Figure 109: PSA for KEMS formed at 850 rpm and 6 N_{PS}

Figure 110: PSA for KEMS formed at 850 rpm and 9 N_{PS}

Appendix J. Experimental qualitative films produced

Figure 111: A broken qualitative film produced without dewatering KEMS

Figure 112: A broken shard of thick film produced without dewatering KEMS

Figure 113: Another broken piece of thick film produced from KEMS

Figure 114: A broken qualitative film produced from agglomerated microparticles